THE UNIVERSITY OF MICHIGAN

COLLEGE OF ENGINEERING
Department of Electrical Engineering
Space Physics Research Laboratory

Scientific Report

THEORY AND DATA PROCESSING FOR THE PITOT TECHNIQUE OF UPPER ATMOSPHERE MEASUREMENT

Prepared on behalf of the project by

R. J. Cittadini
R. W. Simmons
G. T. Poole

ORA Project 03632

under contract with:

NATIONAL AERONAUTICS AND SPACE ADMINISTRATION
GODDARD SPACE FLIGHT CENTER
CONTRACT NO. NAS5-21147
GREENBELT, MARYLAND

administered through:

OFFICE OF RESEARCH ADMINISTRATION ANN ARBOR

April 1970

TABLE OF CONTENTS

LIST OF FIGURES

LIST OF SYMBOLS

a	local speed of sound in the undisturbed region of the gas flow
b	instrument sensitivity factor (a constant)
$\vec{B}$	geomagnetic field vector
$\vec{B}_D$	distorted geomagnetic field vector
B_M	component of $\vec{B}_D$ along the axis of the magnetometer sensor
c	output bias voltage (a constant)
d	characteristic dimension of the probe
g	gravitational acceleration
g_o	standard sea level gravitational acceleration
h	geometric altitude
H	geopotential altitude
k	Boltzmann's constant
K	transition number
$K(M)$	function of Mach number (defined in Equation (5))
Kn	Knudsen number
ℓ, m, n	direction cosines in the X, Y, Z directions, respectively
$\vec{L}$	angular momentum vector
$\vec{L}_1$	unit vector parallel to the angular momentum vector
m	molecular mass
M	Mach number of the probe
$\vec{M}$	magnetometer vector (a unit vector along the magnetometer sensor axis)
p	atmospheric pressure

P_i impact pressure behind the shock wave created by the blunt nose of the probe

r_o radius of the earth

R gas constant

$\vec{R}$ rocket vector (a unit vector along the longitudinal axis of the probe)

S speed ratio, $v_G/\bar{u}$

$\vec{S}$ sun (or moon) vector

S_o speed ratio, $v/\bar{u}$

T temperature of the gas in the undisturbed region of the flow, atmospheric temperature

T_i internal temperature of the gauge

$\bar{u}$ most probable thermal speed of a molecule

v speed of flight of the probe

$\vec{v}$ velocity vector

v_G velocity component along the gauge orifice axis

V magnetometer voltage output

X,Y,Z cartesian coordinate axes

α angle of attack of the probe

β projection of ϕ on the XY plane

γ ratio of specific heats of a gas

η correction factor which accounts for the effect of gas-wall collisions within the antechamber

θ angle between $\vec{B}$ and $\vec{M}$

λ molecular mean free path

μ_B angle between $\vec{R}$ and $\vec{B}$

$\mu_{B_{MIN}}$, $\mu_{B_{MAX}}$ minimum and maximum angles between $\vec{R}$ and $\vec{B}_D$

ξ precession cone half angle

ρ atmospheric density

ρ_1 atmospheric density calculated by using continuum flow theory

ρ_2 $\rho \cos\alpha$

ρ_{fmf} atmospheric density calculated by using free molecular flow theory

σ angle between $\vec{R}$ and $\vec{S}$

ϕ angle between $\vec{S}$ and $\vec{B}$

ω spin rate of the probe

1. INTRODUCTION

The pitot probe, as well as its predecessor the pitot static probe, is a rocket-borne instrumentation system designed for the purpose of measuring atmospheric density, temperature, and pressure in the region of the earth's atmosphere between 30 and 120 km (Ainsworth, Fox, and LaGow, 1961; Horvath, Simmons, and Brace, 1962). The technique utilizes a straightforward application of pressure sensing technology to obtain a measurement of the pressure at the stagnation point of a suitably designed rocket nose cone (Handy, 1970). The interpretation of this impact pressure data in terms of atmospheric density follows from basic aerodynamic theory (Simmons, 1964).

The following sections review the theory and present the procedures necessary for the reduction and presentation of data acquired through the implementation of the pitot technique by investigators at the Space Physics Research Laboratory (SPRL) of The University of Michigan. The theory which forms the basis of the pitot measurement is presented in terms of the equations used in the reduction of the data and is treated separately from the detailed processing of the actual numerical data. In the sections pertaining to the processing of the data, emphasis is placed upon the acquisition and application of auxiliary data necessary for obtaining the final atmospheric density profile. The design and implementation of the pitot probe system in conjunction with available analog to digital data conditioning equipment has resulted in the achievement of nearly 100% automatic processing of these data. A detailed account of the software and procedures used along with sample outputs from the various phases of the processing of a recent data set are given.

2. CALCULATION OF ATMOSPHERIC DENSITY

By measuring the impact pressure at the tip of a suitably designed rocket probe, atmospheric density can be calculated by means of equations appropriate to the fluid flow regime being encountered. A detailed discussion of the flow theories, the derivation of pertinent equations, and a statement of the involved assumptions is given by Simmons (1964).

Because of the wide range of atmospheric density covered by the pitot probe, there is a large variation in the mean free path of the atmospheric particles and in the characteristics of the flow field surrounding the probe. At low altitudes, compressible, nonviscous fluid flow theory adequately describes the flow field around the probe, and at high altitudes, particle theory or free molecular flow theory applies.

2.1. CONTINUUM FLOW REGION

In that portion of the atmosphere where the mean free path, λ, of the molecules is much smaller than a characteristic dimension, d, of the probe, the flow behaves as a continuum. With the Knudsen number defined as

$$Kn = \lambda/d \quad , \tag{1}$$

the condition for continuum flow is that $Kn \ll 1$. In the case of the pitot probe, the characteristic length, d, corresponds to the diameter of the blunt nose of the probe.

Atmospheric density is found from the impact pressure measurement by using the following equation, derived from the well-known Rayleigh supersonic pitot tube formula.

$$\rho_1 = \frac{P_i}{v^2 \left(\frac{\gamma + 1}{2\gamma}\right) \left[\frac{(\gamma + 1)^2 M^2}{4\gamma M^2 - 2\gamma + 2}\right]^{\frac{1}{(\gamma-1)}}} \tag{2}$$

where ρ_1 = atmospheric density for continuum flow,
P_i = impact pressure behind the shock wave created by the blunt nose of the probe,
v = speed of flight of the probe,

γ = ratio of specific heats of the gas, and
M = Mach number of the probe, defined as

$$M = \frac{v}{a} = \frac{v}{\sqrt{\gamma RT}} \tag{3}$$

where a = local speed of sound in the undisturbed region of the flow,
R = gas constant, k/m, where k = Boltzmann's constant and m = molecular mass of the specie considered,
T = temperature of the gas in the undisturbed region of the flow (atmospheric temperature).

To obtain ρ_1 in units of kg/m^3, Equation (2) can be written

$$\rho_1 = \frac{133.3218\ P_i}{K(M)\ v^2} \tag{4}$$

with the gauge pressure, P_i, given in torr and velocity from the trajectory in m/sec. The function of Mach number,

$$K(M) = \left(\frac{\gamma + 1}{2\gamma}\right)\left[\frac{(\gamma + 1)^2\ M^2}{4\gamma M^2 - 2\gamma + 2}\right]^{\frac{1}{\gamma - 1}} \tag{5}$$

cannot be evaluated exactly because M requires a knowledge of T (Equation (3)), which is one of the atmospheric parameters unknown at the time of measurement. However, in the region of measurement, because of the weak dependence of K(M) upon M, K(M) can be approximated to an uncertainty of less than 1% by $K(M_1)$, where M_1 is calculated by using the Standard Atmosphere speed of sound in Equation (3).

2.2. FREE MOLECULAR FLOW REGION

As the probe reaches higher altitudes, λ increases as the atmospheric density decreases. When the mean free path of the molecules is much larger than the characteristic length of the probe, the flow is free molecular flow. The condition for free molecular flow is that $Kn \gg 1$.

The equation linking atmospheric density, ρ, and impact pressure, P_i, in the free molecular flow region is

$$\rho = \frac{P_i}{R\sqrt{T}\sqrt{T_i}\,F(S)} \tag{6}$$

where T_i = internal temperature of the gauge,
S = speed ratio, $v_G/\bar{u}$, where v_G = velocity component along the gauge orifice axis, defined as

$$v_G = v \cos\alpha \tag{7}$$

where α = angle of attack of the probe (see the section on probe aspect),
$\bar{u}$ = most probable thermal speed of a molecule, and

$$\bar{u} = \sqrt{\frac{2kT}{m}} \quad . \tag{8}$$

The function F(S), defined as

$$F(S) = e^{-S^2} + S\sqrt{\pi}\,[1 + \text{erf } S] \tag{9}$$

can be approximated quite accurately for $S > 1.5$ by

$$F(S) \cong 2\sqrt{\pi}\, S \quad . \tag{10}$$

By substituting Equations (7) and (10) into Equation (6), we obtain

$$\rho = \frac{P_i}{\sqrt{2\pi R T_i}\, v \cos\alpha} \quad . \tag{11}$$

If we now let

$$\rho_2 = \rho \cos\alpha \quad , \tag{12}$$

we can write

$$\rho_2 = \frac{3.1263\, P_i}{\sqrt{T_i}\, v} \quad . \tag{13}$$

Equation (13) gives ρ_2 in kg/m^3 for air provided that P_i is given in torr, T_i in °K, and v in m/sec.

In the free molecular flow region, a correction for the geometry of the gauge and antechamber is necessary (Pearl, 1970). The correction factor, η, is a function of the angle of attack of the probe, α, and of the speed ratio, $S_o = v/\bar{u}$. Figure 1 shows $\eta(\alpha, S_o)$ versus α for the pitot probe geometry shown in Figure 2.

The speed ratio can be written as a function of Mach number:

$$S_o = \sqrt{\frac{\gamma}{2}} M \quad . \tag{14}$$

It was mentioned earlier that we do not know M, and therefore we approximate S by using M_1.

Atmospheric density in the free molecular flow region is then given by

$$\rho_{fmf} = \frac{\rho_2}{\eta \cos\alpha} \quad . \tag{15}$$

2.3. TRANSITION FLOW

Neither continuum nor free molecular flow exists in the region where Kn ~ 1, the transition flow region. To date, there is no satisfactory theoretical approach that would allow us to calculate atmospheric density easily in this region.

In looking for a means of using the impact pressures measured in the transition zone to calculate atmospheric density, a numerical model was derived by using actual pitot probe data and extrapolated experimental data from Wainwright and Rogers (1966). A transition number, K, has been obtained for the particular pitot probe geometry shown in Figure 2 and is presented in Figure 3. The atmospheric density in the transition region is approximated by using the following formula.

$$\rho = \rho_1 \left[1 + K \left(\frac{\rho_{fmf}}{\rho_1} - 1 \right) \right] \tag{16}$$

where ρ_1 = density according to the continuum flow theory (Equation (4)), and
ρ_{fmf} = density according to the free molecular flow theory, (Equation (15)).

An iterative procedure is necessary for the calculation of ρ since K is a strong function of ρ.

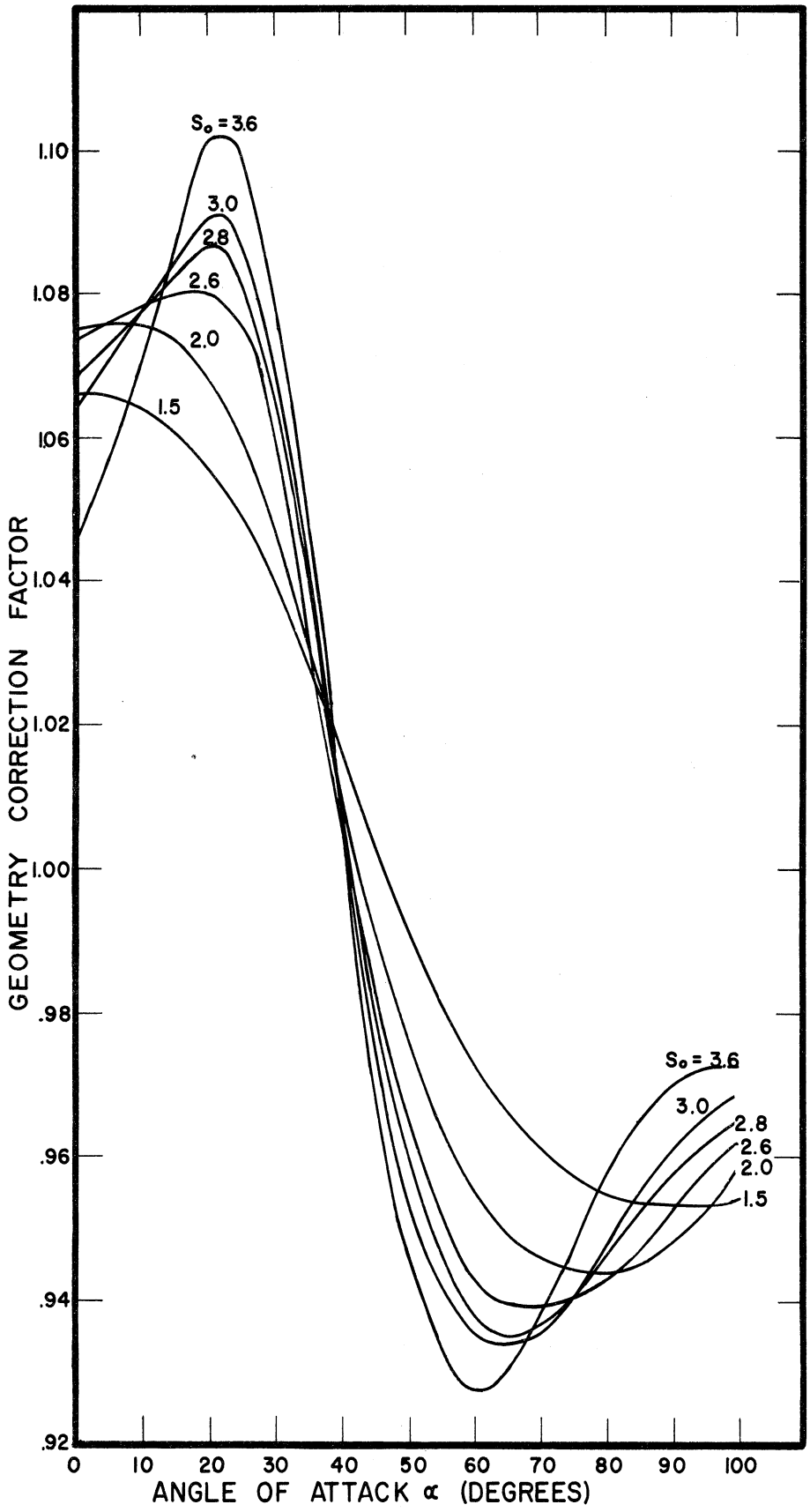

Figure 1. Correction factor which accounts for the effect of gas-wall collisions within the gauge antechamber versus angle of attack.

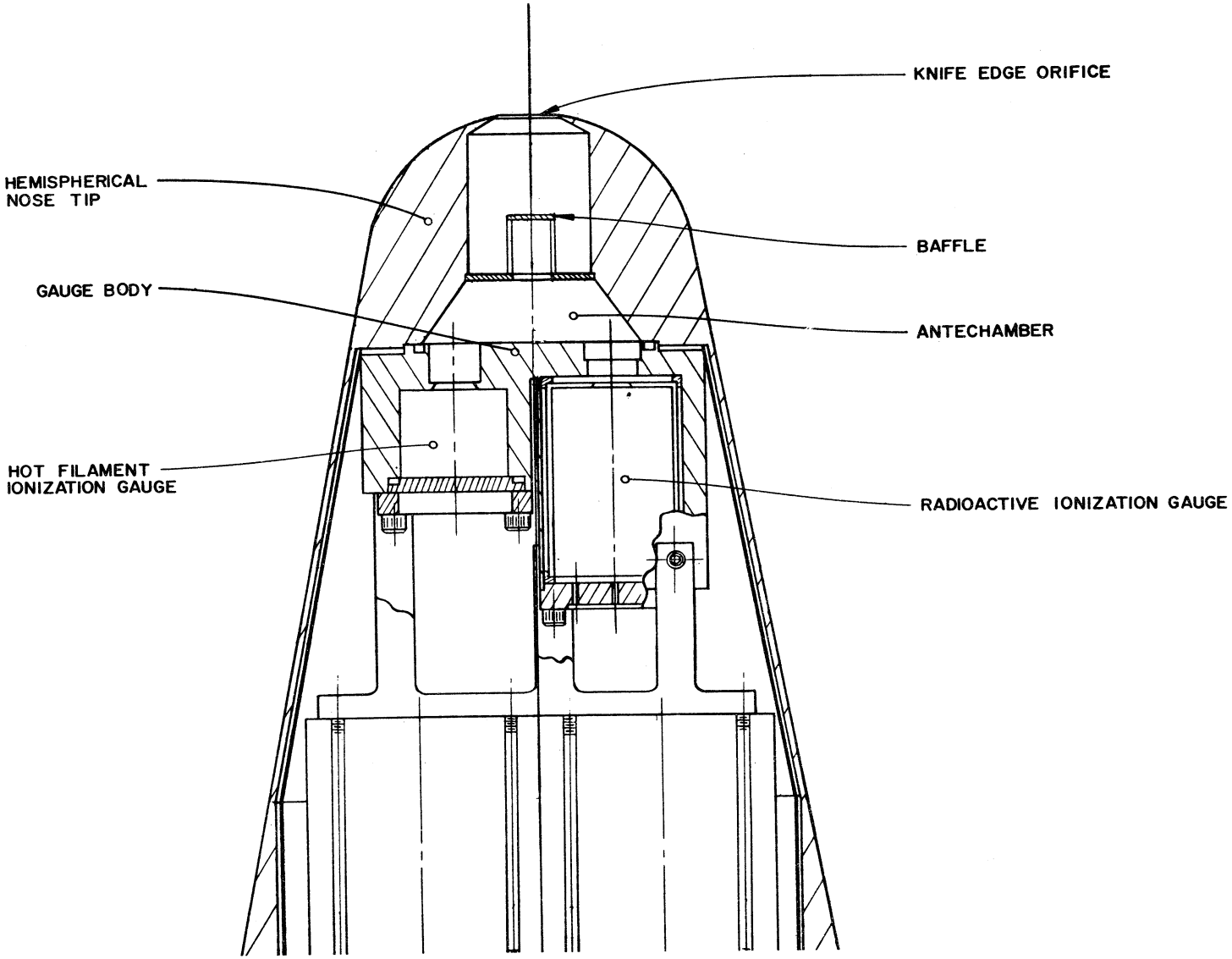

Figure 2. Pitot probe gauge and antechamber geometry.

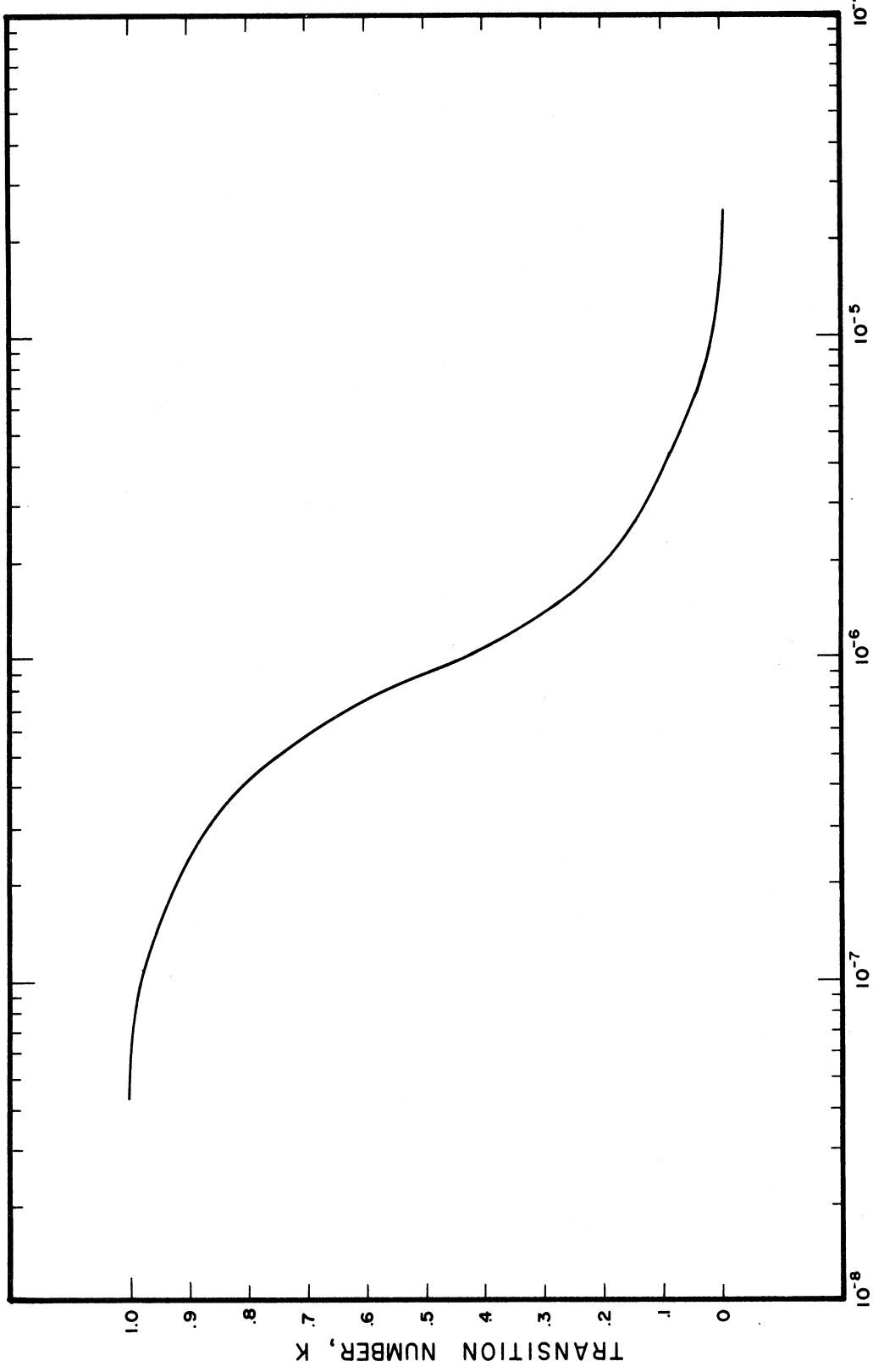

Figure 3. Transition number versus ρ.

3. ATMOSPHERIC PRESSURE AND TEMPERATURE CALCULATION

In the preceding section, the necessary equations for obtaining atmospheric density are given. From this density, atmospheric pressure and temperature may be obtained. The following paragraphs describe in detail the method used.

3.1. PRESSURE CALCULATION

Pressure is calculated by means of the hydrostatic equation:

$$\frac{dp}{dh} = -\rho g \tag{17}$$

where p = atmospheric pressure,
ρ = atmospheric density,
h = geometric altitude, and
g = gravitational acceleration.

We assume that the density can be represented locally as an exponential of geopotential altitude of the type

$$\rho(H_{i-1}) = \rho(H_i) \exp\{-C(H_{i-1} - H_i)\} \tag{18}$$

where H denotes geopotential altitude, i is a positive integer, and $H_{i-1} > H_i \geq H_n$. By rearranging Equation (18),

$$C = \frac{\ell n\, \rho(H_i) - \ell n\, \rho(H_{i-1})}{H_{i-1} - H_i} \quad . \tag{19}$$

By integrating Equation (17),

$$\Delta p_i = -\int_{h_i}^{h_{i-1}} \rho(h)\, g(h)\, dh \quad . \tag{20}$$

From the definition of geopotential altitude,

$$g\, dh = g_o\, dH \tag{21}$$

where g_o = standard sea level gravitational acceleration. If we use the approximation

$$\frac{g}{g_o} = \frac{r_o^2}{(r_o + h)^2} \tag{22}$$

where r_o = radius of the earth, we arrive at

$$H = \frac{r_o h}{r_o + h} \quad . \tag{23}$$

If we express Equation (20) in terms of geopotential altitude, we obtain

$$\Delta p_i = g_o \int_{H_i}^{H_{i-1}} \rho(H)\, dH \quad . \tag{24}$$

By substituting Equation (18) into Equation (24),

$$\Delta p_i = g_o\, \rho(H_i) \int_{H_{i-1}}^{H_i} \exp\{-C(H - H_i)\}\, dH = -\frac{g_o}{C} [\rho(H_{i-1}) - \rho(H_i)] \quad . \tag{25}$$

Then by substituting for C as given by Equation (19) and by reverting to geometric altitude,

$$H_{i-1} - H_i = \frac{r_o^2 (h_{i-1} - h_i)}{(r_o + h_{i-1})(r_o + h_i)} \quad , \tag{26}$$

we arrive at

$$\Delta p_i = g_o r_o^2 \frac{(h_{i-1} - h_i)}{(r_o + h_{i-1})(r_o + h_i)} \frac{\rho(h_{i-1}) - \rho(h_i)}{\ell n\, \rho(h_{i-1}) - \ell n\, \rho(h_i)} \tag{27}$$

Therefore, the change in atmospheric pressure between altitudes h_1 and h_n is given by

$$\sum_{i=1}^{n} \Delta p_i = g_o r_o^2 \sum_{i=1}^{n} \frac{(h_{i-1} - h_i)}{(r_o + h_{i-1})(r_o + h_i)} \frac{\rho(h_{i-1}) - \rho(h_i)}{\ell n\, \rho(h_{i-1}) - \ell n\, \rho(h_i)} \tag{28}$$

Thus,

$$p_n = p_1 + \sum_{i=1}^{n} \Delta p_i \tag{29}$$

where p_1 = atmospheric pressure at altitude h_1.

From Equation (29) and the equation of state of an ideal gas,

$$p = \rho RT \quad , \tag{30}$$

we obtain

$$p_n = \frac{\rho_1 k T_1}{m} + \sum_{i=1}^{n} \Delta p_i \tag{31}$$

where ρ_1 (determined from the impact measurement described previously) and T_1 are the density and temperature at a reference altitude h_1. Since T_1 is not available, it is approximated by using the Standard Atmosphere temperature at the reference altitude. The numerical integration for Δp_n, Equation (28), is carried from high altitude downward. As the integration proceeds, the summation term in Equation (31) increases rapidly and p_n quickly becomes insensitive to T_1, the assumed reference temperature.

3.2. TEMPERATURE CALCULATION

From Equations (30) and (31) we can write

$$T_n = \frac{1}{k\rho_n}\left[\rho_1 k T_1 + m \sum_{i=1}^{n} \Delta p_i\right] \quad . \tag{32}$$

4. ASPECT DETERMINATION

It is evident from Equation (7) (Section 2.2) that knowledge of the angle of attack of the probe is necessary for the calculation of atmospheric density.

The angle of attack of the probe changes with altitude. At low altitudes the main aerodynamic forces acting upon the probe are largely due to high atmospheric density and to the high speed of the probe. The angle of attack is essentially zero because of the influence of the restoring moments generated by aerodynamic forces acting on the fins. Throughout this portion of the flight, the spin rate is high and the angle of the precession cone is negligible. When the probe reaches an altitude at which the restoring moments become vanishingly small, the precession cone increases. How large this cone becomes depends on the flight configuration of the probe. In those cases in which the precession cone angle is very noticeable, the angle of attack can become significant long before the probe gets close to the peak of its trajectory.

The angle of attack is determined if the orientations in space of the pitot probe and of the velocity vector, $\vec{v}$, are known. Velocity vector orientation is readily obtained from the trajectory information. The orientation of the pitot probe is calculated from data supplied by a magnetic sensor (magnetometer) and an optical sensor (sun or moon sensor).

4.1. ANGLE BETWEEN THE PROBE AND THE EARTH'S MAGNETIC FIELD VECTOR

As part of its instrumentation the pitot probe carries a magnetometer whose output is used to determine the angle between the probe and the geomagnetic field vector. The cylindrical sensor of the magnetometer assembly is mounted with its axis normal to the longitudinal axis of the probe. Magnetometer output is a voltage proportional to the component of the geomagnetic field parallel to the axis of the sensor.

$$V = b(\vec{B}\cdot\vec{M}) + c = b(B\cos\theta) + c \qquad (33)$$

where V = magnetometer voltage output,
b = instrument sensitivity factor (a constant),
$\vec{B}$ = geomagnetic field vector,
$\vec{M}$ = magnetometer vector (a unit vector along the axis of the sensor of the magnetometer),
c = output bias voltage (a constant), and
θ = angle between $\vec{B}$ and $\vec{M}$.

3. ATMOSPHERIC PRESSURE AND TEMPERATURE CALCULATION

In the preceding section, the necessary equations for obtaining atmospheric density are given. From this density, atmospheric pressure and temperature may be obtained. The following paragraphs describe in detail the method used.

3.1. PRESSURE CALCULATION

Pressure is calculated by means of the hydrostatic equation:

$$\frac{dp}{dh} = -\rho g \tag{17}$$

where p = atmospheric pressure,
ρ = atmospheric density,
h = geometric altitude, and
g = gravitational acceleration.

We assume that the density can be represented locally as an exponential of geopotential altitude of the type

$$\rho(H_{i-1}) = \rho(H_i) \exp\{-C(H_{i-1} - H_i)\} \tag{18}$$

where H denotes geopotential altitude, i is a positive integer, and $H_{i-1} > H_i \geq H_n$. By rearranging Equation (18),

$$C = \frac{\ell n\, \rho(H_i) - \ell n\, \rho(H_{i-1})}{H_{i-1} - H_i} \quad . \tag{19}$$

By integrating Equation (17),

$$\Delta p_i = -\int_{h_i}^{h_{i-1}} \rho(h)\, g(h)\, dh \quad . \tag{20}$$

From the definition of geopotential altitude,

$$g\, dh = g_o\, dH \tag{21}$$

where g_o = standard sea level gravitational acceleration. If we use the approximation

$$\frac{g}{g_o} = \frac{r_o^2}{(r_o + h)^2} \tag{22}$$

where r_o = radius of the earth, we arrive at

$$H = \frac{r_o h}{r_o + h} \quad . \tag{23}$$

If we express Equation (20) in terms of geopotential altitude, we obtain

$$\Delta p_i = g_o \int_{H_i}^{H_{i-1}} \rho(H)\, dH \quad . \tag{24}$$

By substituting Equation (18) into Equation (24),

$$\Delta p_i = g_o\, \rho(H_i) \int_{H_{i-1}}^{H_i} \exp\{-C(H - H_i)\}\, dH = -\frac{g_o}{C} [\rho(H_{i-1}) - \rho(H_i)] \quad . \tag{25}$$

Then by substituting for C as given by Equation (19) and by reverting to geometric altitude,

$$H_{i-1} - H_i = \frac{r_o^2 (h_{i-1} - h_i)}{(r_o + h_{i-1})(r_o + h_i)} \quad , \tag{26}$$

we arrive at

$$\Delta p_i = g_o r_o^2 \frac{(h_{i-1} - h_i)}{(r_o + h_{i-1})(r_o + h_i)} \frac{\rho(h_{i-1}) - \rho(h_i)}{\ell n\, \rho(h_{i-1}) - \ell n\, \rho(h_i)} \tag{27}$$

Therefore, the change in atmospheric pressure between altitudes h_1 and h_n is given by

$$\sum_{i=1}^{n} \Delta p_i = g_o r_o^2 \sum_{i=1}^{n} \frac{(h_{i-1} - h_i)}{(r_o + h_{i-1})(r_o + h_i)} \frac{\rho(h_{i-1}) - \rho(h_i)}{\ell n\, \rho(h_{i-1}) - \ell n\, \rho(h_i)} \tag{28}$$

Let us now define a vector $\vec{R}$, called the rocket vector, a unit vector along the pitot probe longitudinal axis. We adopt a cartesian coordinate system defined by unit vectors $\hat{i}$, $\hat{j}$, and $\hat{k}$ such that $\hat{k}$ is parallel to $\vec{R}$, and impose the following restrictions:

(1) the probe's spin rate, ω, is much higher than its precession rate,

(2) the spin rate varies very slowly with time, that is, it is nearly constant during a spin period, and

(3) $\vec{B}$ stays constant during a spin period.

Let $t = 0$ be the instant at which $\hat{i}$ is parallel to $\vec{M}$, and we can now write

$$\vec{R} = \hat{k} \tag{34}$$

$$\vec{M} = (\cos\omega t)\,\hat{i} + (\sin\omega t)\,\hat{j} \quad , \text{ and} \tag{35}$$

$$\vec{B} = B_x\hat{i} + B_y\hat{j} + B_z\hat{k} \quad . \tag{36}$$

By substituting Equations (34), (35), and (36) into Equation (33), we obtain

$$V = b(B_x \cos\omega t + B_y \sin\omega t) + c \quad . \tag{37}$$

The magnetometer output is shown in Figure 17 in Section 5.3. At a maximum or minimum, $dV/dt = 0$, and

$$(\vec{R} \times \vec{M})\cdot\vec{B} = \frac{dV}{dt} = 0 \quad . \tag{38}$$

Since none of the three vectors is zero, they must be coplanar when $dV/dt = 0$. If we call μ_B the angle between the rocket vector and the magnetic field vector, we have the situation depicted in Figure 4 for $V = V_{MAX}$ and for $V = V_{MIN}$. Using Equation (33), we can write an equation for the voltage difference, ΔV, between maximum and minimum in magnetometer output.

$$\Delta V = V_{MAX} - V_{MIN} = \{b\,B[\cos(\frac{\pi}{2} - \mu_B)] + c\} - \{b\,B[\cos(\frac{\pi}{2} + \mu_B)] + c\}$$

$$= 2b\,B\sin\mu_B \quad . \tag{39}$$

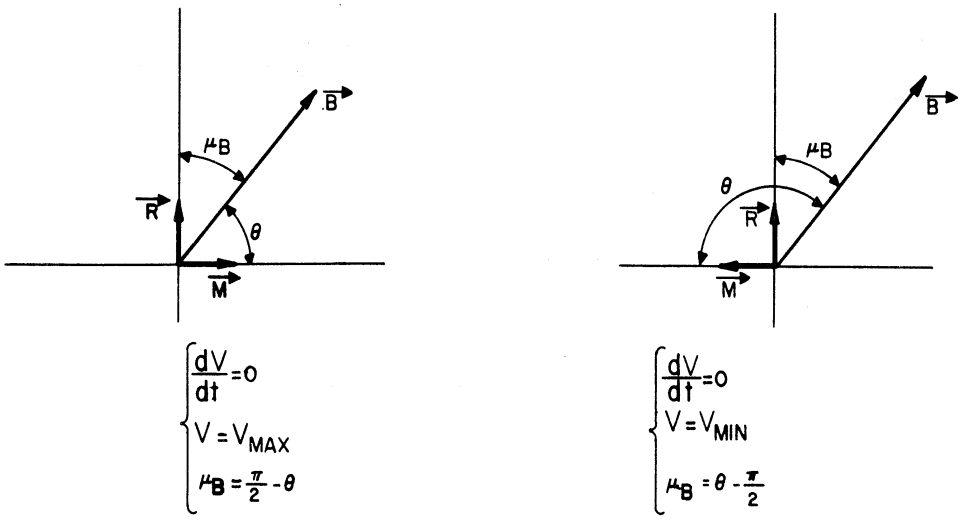

Figure 4. Relationship between μ_B and θ for $dV/dt = 0$.

By means of Equation (39), μ_B can be calculated from the measured ΔV provided that b and B are known. The quantity 2b represents a calibration constant. The value of B can be obtained from a geomagnetic field model. Assuming that the distortion caused by the probe in the magnetic field seen by the magnetometer sensor is negligible, we can say that $\vec{B}$ is known.

As mentioned before, at low altitudes the angle of attack of the probe is negligible and $\vec{R}$ and $\vec{v}$ can be considered to have the same orientation in space. Since the velocity vector and the magnetic field vector are known (Cain, Daniels, Hendricks, and Jensen, 1965), at low altitudes

$$\mu_B = \arccos \frac{\vec{v} \cdot \vec{B}}{v \cdot B} \quad . \tag{40}$$

From the value of μ_B calculated at low altitudes, the value of the calibration constant 2b can be determined,

$$2b = \frac{\Delta V}{B \sin \mu_B} \tag{41}$$

where μ_B is given by Equation (40) and ΔV is taken at the same altitude at which μ_B was calculated. Equation (39) is used to calculate μ_B for that portion of the flight which is of interest.

4.2. ANGLE BETWEEN THE PROBE AND THE SUN (MOON) VECTOR

Let us define a vector $\vec{S}$, called the sun (moon) vector, as a unit vector

having the direction of the line joining the center of the probe and the center of the sun (moon). The angle σ between the rocket vector and the sun (moon) vector is given by the output of the optical sensor. The measurement is direct and will not be treated in detail. The position of the sun (moon) can be obtained from the ephemeris.

4.3. ORIENTATION OF THE PROBE IN SPACE

Once the angle μ_B between the rocket vector and the geomagnetic field vector, and the angle σ between the rocket vector and the sun (moon) vector are known, the orientation of the probe can be calculated.

The angle ϕ between the sun vector and the geomagnetic field vector is given by

$$\cos\phi = \frac{\vec{S}\cdot\vec{B}}{B} \quad . \tag{42}$$

Now we introduce, for the sake of simplicity, a right-handed cartesian coordinate system in which the Z axis is defined by a unit vector $\hat{k}$ parallel to the sun (moon) vector $\vec{S}$, and the X axis is contained in the plane determined by the vectors $\vec{B}$ and $\vec{S}$ (see Figure 5). This coordinate system is called the sun-axis coordinate system.

The loci of possible positions of $\vec{R}$ with respect to $\vec{B}$ determine a cone with its axis parallel to $\vec{B}$ and with a cone angle of $2\mu_B$. The loci of possible positions of $\vec{R}$ with respect to $\vec{S}$ determine another cone with its axis parallel to $\vec{S}$ and a cone angle of 2σ. The intersection of the two cones gives the possible positions of the $\vec{R}$ vector in space.

The following equations can be written in the sun-axis coordinate system:

$$\vec{S} = \hat{k} \quad . \tag{43}$$

$$\frac{\vec{B}}{B} = \sin\phi\,\hat{i} + \cos\phi\,\hat{k} \quad . \tag{44}$$

$$\vec{R} = R_x\hat{i} + R_y\hat{j} + R_z\hat{k} \quad . \tag{45}$$

$$\left.\begin{aligned} \vec{R}\cdot\vec{S} &= \cos\sigma = R_z \\ \frac{\vec{R}\cdot\vec{B}}{B} &= \cos\mu_B = \sin\phi\, R_x + \cos\phi\, R_z \\ R_x^2 + R_y^2 + R_z^2 &= 1 \quad . \end{aligned}\right\} \tag{46}$$

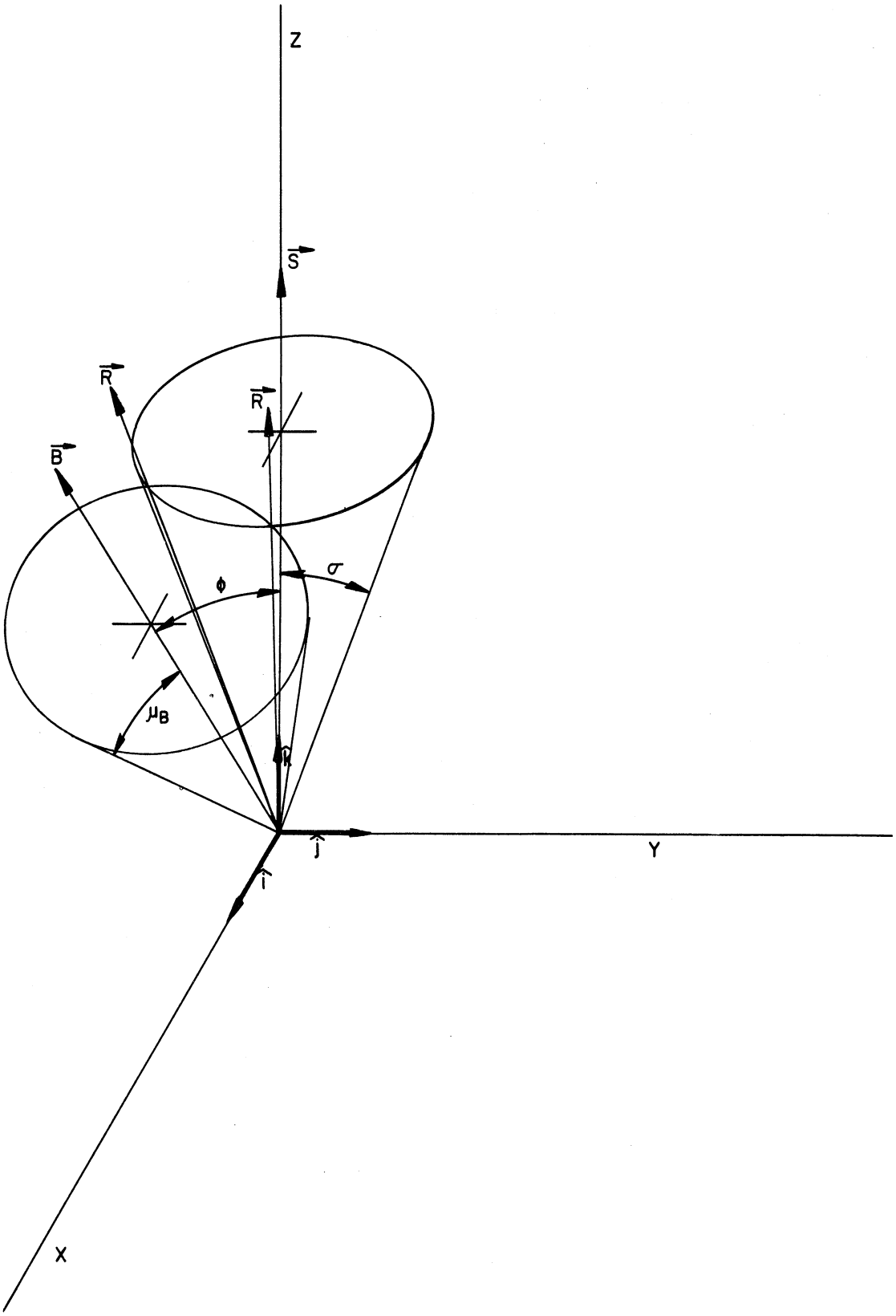

Figure 5. Sun-axis coordinate system.

From the system of equations numbered (46), the following solutions are obtained:

$$R_x = \frac{\cos\mu_B - \cos\phi \cos\sigma}{\sin\phi} , \tag{47}$$

$$R_y = \pm \sqrt{1 - (R_x^2 + R_z^2)} , \text{ and} \tag{48}$$

$$R_z = \cos\sigma . \tag{49}$$

Equations (47), (48), and (49) give the direction cosines of the rocket vector $\vec{R}$. In the most general case, there are two solutions for the vector $\vec{R}$. The choice of one of the solutions should be based on the physics of the problem.

4.4. ANGLE OF ATTACK

The rocket vector is then converted from the sun-axis coordinate system to the launch pad coordinate system, a cartesian coordinate system with positive Y north, positive X east, and positive Z perpendicular to the earth's tangent plane at the site. Calculation of the angle of attack is straightforward.

$$\cos\alpha = \frac{\vec{v} \cdot \vec{R}}{v} . \tag{50}$$

4.5. SPECIAL CASE: PRECESSION CONE METHOD

When the flight configuration of the probe is such that significant precession takes place, another method can be used to solve the aspect problem and to determine the angle of attack. It is believed that, in general, the probe causes some distortion in the geomagnetic field; hence, the magnetometer sensor does not sense the geomagnetic field vector $\vec{B}$, but rather a somewhat distorted geomagnetic field vector, $\vec{B}_D$. The alternate method has the advantage of obtaining the geomagnetic field vector from flight data without having to resort to geomagnetic field models, thereby resulting in what is believed to be improved accuracy.

The probe precesses about the total angular momentum vector $\vec{L}$ which remains unchanged when there are no exterior moments acting on the probe. For the sake of simplicity, we use a unit vector $\vec{L}_1$ parallel to $\vec{L}$. We then define a right-handed cartesian coordinate system which we call the angular-momentum-axis coordinate system. The Z axis is defined by a unit vector $\hat{k}$ parallel to the angular momentum vector $\vec{L}$ of the probe. The Y axis, defined by a vector $\hat{j}$,

is such that the YZ plane contains the sun vector $\vec{S}$. The X axis completes the right-handed system (see Figure 6).

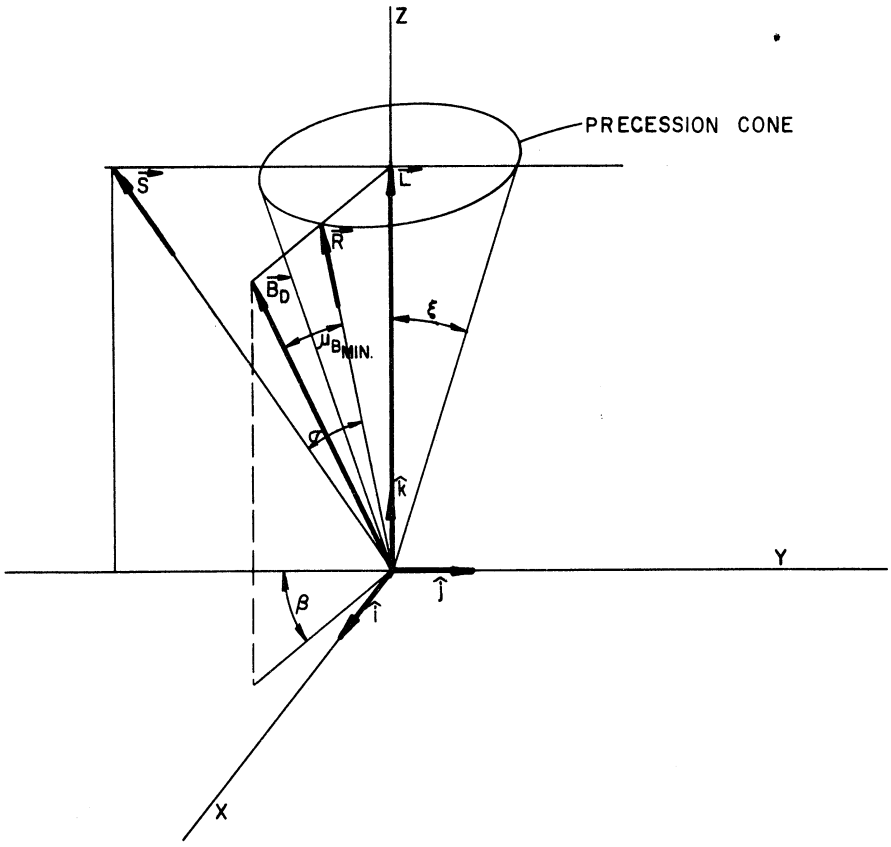

Figure 6. Angular-momentum-axis coordinate system.

Consider a precession period at the apogee of the trajectory for a given probe. A precession period is easily distinguished in the magnetometer output or by plotting the optical sensor output (see Figure 7). Let 2ξ be the angle of the precession cone. The rocket vector $\vec{R}$ describes in time a cone with its axis parallel to $\vec{L}_1$ and a cone half angle ξ. The angle ξ can be calculated easily from optical (sun or moon) sensor data (see Figure 7).

$$2\xi = \sigma_{MAX} - \sigma_{MIN} \quad . \tag{51}$$

The angle between the rocket vector $\vec{R}$ and the distorted geomagnetic field vector $\vec{B}_D$ varies during a precession period from a minimum, $\mu_{B_{MIN}}$, to a maximum, $\mu_{B_{MAX}}$, such that

$$\mu_{B_{MAX}} = \mu_{B_{MIN}} + 2\xi \quad . \tag{52}$$

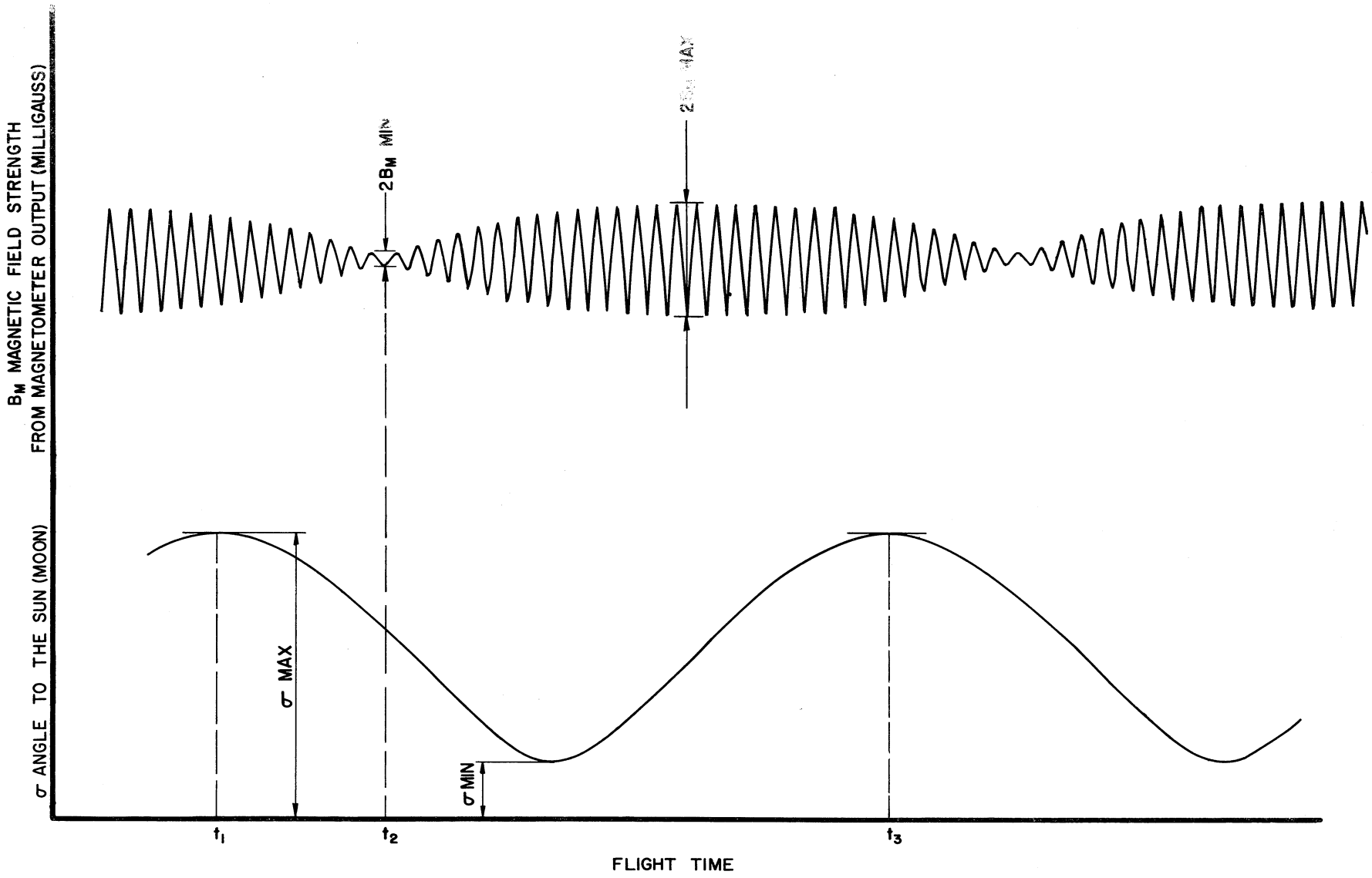

Figure 7. Determination of precession period.

The component of $\vec{B}_D$ along the axis of the magnetometer sensor is denoted as B_M. Magnetometer output given in volts can be converted to magnetic flux density in milligauss through the calibration data supplied by the manufacturer.

$$\begin{cases} B_D \sin \mu_{B_{MIN}} = B_{M_{MIN}} , \text{ and} & (53) \\ B_D \sin \mu_{B_{MAX}} = B_{M_{MAX}} . & (54) \end{cases}$$

Solving the system of Equations (52), (53), and (54) for B_D and $\mu_{B_{MIN}}$ yields

$$\mu_{B_{MIN}} = \arcsin \frac{B_{M_{MIN}}}{B_D} , \text{ and} \quad (55)$$

$$B_D = \pm \sqrt{\left(\frac{B_{M_{MAX}} - B_{M_{MIN}} \cos 2\xi}{\sin 2\xi} \right)^2 + B^2_{M_{MIN}}} . \quad (56)$$

The quantity B_D is determined quite accurately at apogee where all the intervening quantities can be measured without much error because of the large precession half cone angle ξ. Because the geomagnetic field strength varies with altitude above the earth's surface, the values of B_D at different altitudes can be approximated by applying to B_D, as calculated by Equation (56), the same percentage variation with altitude suffered by B as given in the geomagnetic field model. In this case, we have used only the rate of decay in the field from the geomagnetic field model, as opposed to using the geomagnetic field vector (direction, magnitude, and their rates of change) from the model as required in the method described in Section 4.1.

At apogee the following equations can be written (see Figure 6):

$$\vec{L}_1 \cdot \vec{S} = \cos(\sigma_{MIN} + \xi) \quad (57)$$

$$\vec{B}_D \cdot \vec{L}_1 = \cos(\mu_{B_{MIN}} + \xi) B_D , \quad (58)$$

$$(\vec{L}_1 \times \vec{S}) \cdot (\vec{L}_1 \times \vec{B}_D) = B_D \{\cos\gamma [\sin(\sigma_{MIN} + \xi)][\sin(\mu_{B_{MIN}} + \xi)]\}$$

$$= (\vec{L}_1 \cdot \vec{L}_1)(\vec{S} \cdot \vec{B}_D) - (\vec{B}_D \cdot \vec{L}_1)(\vec{S} \cdot \vec{L}_1) . \quad (59)$$

The angle γ (see Figure 6) is the projection on the XY plane of the angle ϕ between the sun vector $\vec{S}$ and the distorted geomagnetic field vector $\vec{B}_D$. The angle γ can be calculated (see Figure 7) by means of the following relationship:

$$\gamma = \frac{t_2 - t_1}{t_3 - t_1} 2\pi \quad . \tag{60}$$

Combining Equations (57), (58), and (59), we obtain

$$\vec{S}\cdot\vec{B}_D = B_D\{\cos\gamma[\sin(\sigma_{MIN} + \xi)][\sin(\mu_{B_{MIN}} + \xi)]\} + \{[\cos(\mu_{B_{MIN}} + \xi)]\cos(\sigma_{MIN} + \xi)]\}. \tag{61}$$

The general equation

$$\vec{R}\cdot\vec{B}_D = B_D \cos\mu_B = \pm B_D\left[1 - \left(\frac{B_M}{B_D}\right)^2\right]^{1/2} \tag{62}$$

can be written in a different form when the probe is in the low-altitude region. At low altitudes, where the aerodynamic restoring moments are the controlling factor in the orientation of the probe, the velocity vector $\vec{v}$ and the rocket vector $\vec{R}$ can be considered to be coincident. Equation (62) then becomes

$$\vec{v}\cdot\vec{B}_D = vB_D \cos\mu_B = \pm vB_D\left[1 - \left(\frac{B_M}{B_D}\right)^2\right]^{1/2} \quad . \tag{63}$$

The previous equations can then be grouped into systems of equations that would allow us to obtain the orientation of the rocket vector $\vec{R}$.

In order to find the orientation of $\vec{B}_D$ we use Equations (61) and (63) and add the condition which must be satisfied by the direction cosines of a vector in a cartesian coordinate system. The following system results.

$$\frac{\vec{S}\cdot\vec{B}}{B_D} = S_\ell B_{D\ell} + S_m B_{Dm} + S_n B_{Dn} = \{\cos\gamma[\sin(\sigma_{MIN} + \xi)][\sin(\mu_{B_{MIN}} + \xi)]\}$$

$$+ \{[\cos(\mu_{B_{MIN}} + \xi)][\cos(\sigma_{MIN} + \xi)]\} \quad , \tag{64}$$

$$\frac{\vec{v}\cdot\vec{B}_D}{vB_D} = v_\ell B_{D\ell} + v_m B_{Dm} + v_n B_{Dn} = \pm\left[1 - \left(\frac{B_M}{B_D}\right)^2\right]^{1/2} \quad , \text{ and} \tag{65}$$

$$B_{D\ell}^2 + B_{Dm}^2 + B_{Dn}^2 = 1 \quad . \tag{66}$$

The subscripts ℓ, m, and n denote direction cosines of the subscripted quantity in the X, Y, and Z directions, respectively.

The solution of the system of Equations (64), (65), and (66) gives the direction cosines $B_{D\ell}$, B_{Dm}, and B_{Dn} of the distorted geomagnetic field vector $\vec{B}_D$. In Equation (65), B_M and B_D should be given for the same low altitude at which v_ℓ, v_m, and v_n are taken. Although the orientation of the geomagnetic field vector changes with altitude, the change in the region of interest (between 70 and 140 km) is so small that it can be neglected. On these grounds we disregard any variation in $B_{D\ell}$, B_{Dm}, and B_{Dn} with altitude.

In order to find the orientation of the rocket vector, we resort to the following system of equations. Notice that the following equations apply to any point along the trajectory. They are not restricted to near apogee conditions like Equations (61) and (64) or to low altitudes like Equations (63) and (65).

$$\left\{ \begin{aligned} \vec{R}\cdot\vec{S} &= R_\ell S_\ell + R_m S_m + R_n S_n = \cos\sigma \quad , && (67) \\ \frac{\vec{R}\cdot\vec{B}_D}{B_D} &= R_\ell B_{D\ell} + R_m B_{Dm} + R_n B_{Dn} = \pm\left[1 - \left(\frac{B_M}{B_D}\right)^2\right]^{1/2} \quad , \text{ and} && (68) \\ R_\ell^2 + R_m^2 + R_n^2 &= 1 \quad . && (69) \end{aligned} \right.$$

Solution of the system constituted by Equations (67), (68), and (69) provides the direction cosines R_ℓ, R_m, and R_n of the rocket vector for the time and altitude corresponding to the values of σ, B_M, and B_D used in Equations (67) and (68).

Once the rocket vector $\vec{R}$ is known along the trajectory, the angle of attack can be calculated by means of Equation (50). Note that although the equations were derived for the sake of simplicity by using the angular-momentum-axis coordinate system, any other coordinate system can be used, for example, the launch pad coordinate system.

The systems of Equations (64), (65), and (66), and (67), (68), and (69) are of the following type:

$$\left. \begin{aligned} a_x X + a_y Y + a_z Z &= K_1 \quad , \\ b_x X + b_y Y + b_z Z &= K_2 \quad , \\ X^2 + Y^2 + Z^2 &= 1 \quad , \end{aligned} \right\} \tag{70}$$

and the general solution is of the following form:

$$X = \frac{-(C_{zx}K_z - C_{xy}K_y) \pm \{(C_{zx}K_z - C_{zy}K_y)^2 - [(C_{xy}^2 + C_{yz}^2 + C_{zx}^2)(K_z^2 + K_y^2 - C_{yz}^2)]\}^{1/2}}{C_{xy}^2 + C_{yz}^2 + C_{zx}^2}, \tag{71}$$

$$Y = \frac{(C_{yz}K_z - C_{xy}K_x) \pm \{(C_{yz}K_z - C_{xy}K_x)^2 - [(C_{xy}^2 + C_{yz}^2 + C_{zx}^2)(K_z^2 + K_x^2 - C_{zx}^2)]\}^{1/2}}{(C_{xy}^2 + C_{yz}^2 + C_{zx}^2)}, \tag{72}$$

$$Z = \pm (1 - X^2 - Y^2)^{1/2}, \tag{73}$$

where

$$\left.\begin{aligned} K_x &= K_1 b_x - K_2 a_x , \\ K_y &= K_1 b_y - K_2 a_y , \\ K_z &= K_1 b_z - K_2 a_z , \end{aligned}\right\}$$

and

$$\left.\begin{aligned} C_{xy} &= a_x b_y - a_y b_x , \\ C_{yz} &= a_y b_z - a_z b_y , \\ C_{zx} &= a_z b_x - a_x b_z . \end{aligned}\right\}$$

5. PROCESSING OF FLIGHT DATA

5.1. GROUND SUPPORT REQUIREMENTS

Because of the automated data processing techniques used in the reduction of pitot data, the following modest ground support requirements must be met for each flight. Failure to fulfill these requirements can result in a degradation of the overall quality of the final data as well as jeopardize the automatic data processing procedures.

5.1.1. Tracking

The complete time history of the position and velocity of the probe during flight may be obtained from either radar or DOVAP (Doppler Velocity and Position) tracking. The fully processed tracking (trajectory) data may be supplied in the form of either a digital magnetic tape or punched tape decks along with a formatted listing of the contents of either. These data should be presented in either common metric or English units and should include the geometric position and velocity of the probe referred to a launch pad coordinate system versus time. Figure 8 illustrates the required punched card format (two decks: one for velocity data and one for position data).

The required magnetic tape format is 7-track, BCD mode recorded at 556 BPI with even longitudinal parity. The information contained must include, at least, that which is shown in Figure 8. It is common, however, to provide more information than that specified for the card decks. Upon receipt, this information is read into and stored on a disc file at The University of Michigan Computing Center for future use as input to the main processing programs.

5.1.2. Telemetry

Since the pitot probe utilizes an IRIG FM/FM telemetry system, the range must provide an appropriate telemetry receiving station for acquiring and recording the data from the probe in flight. In addition, the station must provide a source of range timing suitable for both magnetic and strip chart or oscillograph recording, and a source of 100 kHz to be used for magnetic tape wow and flutter compensations. Range timing should be a modulated carrier BCD type. Usable codes are: NASA 36 Bit, AMR D5, IRIG A and IRIG B for both tape and oscillograph recording; and NASA 28 Bit for oscillograph recordings only. Figure 9 shows a typical telemetry format for the pitot probe.

As stated previously, the pitot probe data are processed automatically using the SPRL Data Conditioning System (Caldwell, 1966), and The University of

Michigan Computing Center's IBM 360/67. For this reason, the quality and format of the analog magnetic tape is of primary importance and a few words regarding this format are in order.

The SPRL Data Conditioning System is primarily an FM/FM Analog to Digital conversion facility. Included in the equipment of this system is an analog instrumentation recorder which is used to play back the analog tape. The data output of the recorder is then demodulated and the individual data channels are digitized and recorded in digital form on an IBM compatible magnetic tape. The analog recorder is of the low band direct record type and is capable of processing 7-track, 1/2 in. wide direct recorded magnetic tapes at speeds of 60 or 30 ips. The tape drive is capable of the other standard lower tape speeds, but proper equalization electronics are not available. For this low band recorder (Range Commanders Council, 1966) the frequency response at 60 ips is 100-120,000 Hz while at 30 ips it is 50-60,000 Hz. At 30 ips the maximum "flat" frequency response (-3 db) is 60 kHz; above 60 kHz the nonlinearity in response can introduce severe cross-talk and distortion in the telemetry signals of higher frequency. In addition, the tape speed (wow and flutter) compensation hardware of the Data Conditioning System will accept only 100 kHz reference signals. If only VCO frequencies lower than 60 kHz are used in a telemetry video, it is still desirable to record a 100 kHz reference signal, for it has been found that if the signal is strong, enough of it can be recovered at 30 ips for use by the compensation discriminator. However, when maximum VCO frequencies exceed 60 kHz, as is the general case with the pitot probe, a tape speed of 60 ips is mandatory. Recording levels should be adjusted to give 1% (or less) third-harmonic distortion. Tracks 2 and 4 of the magnetic tape should not carry signals with strong 100-500 Hz components (such as voice) because of the cross-talk characteristics of magnetic tape recorders. A suggested use for tracks 2 and 4 is that of back-up data. Tracks 1, 3, 5, and 7 should carry the most valuable signals and those with the most critical time relationships because these tracks are all in the same head stack, and at 60 ips the time delay between head stacks is 25 msec.

Taking into consideration the preceding observations, the following magnetic tape format should be requested. This format insures high data quality and compatibility with automatic processing procedures.

Recording Mode:	Direct
Tape Speed:	60 ips
Tape Width:	1/2 in.
Tape Thickness:	At least 1 mil
Head Format:	IRIG
Recording Levels:	Normal (see above)

TRACK	INFORMATION	REMARKS
1	NASA 36 Bit Time Code	100 pps/1 kHz
2	Rx #A Video	Backup
3	Diversity Combiner #A Video	Primary Data Track
4	Diversity Combiner #B Video	Backup
5	100 kHz Ref. ONLY	
6	Station Multiplex	
	Reference	100 kHz
	NASA 36 Bit	70 kHz ± 7.5%
	NASA 28 Bit	40 kHz ± 7.5%
	Voice	52.5 kHz ± 7.5%
	AGC A	10.5 kHz
	AGC B	7.35 kHz
	AGC C	5.4 kHz
	AGC D	3.9 kHz
7	Rx #D Video	Backup

Note: Record 100 kHz and time code at maximum level.

The paper oscillograph record requirements are straightforward and are of secondary importance to the data processing techniques used for the pitot probe. Figures 10, 11, and 12 show typical oscillograph record formats required for visual analysis.

GMT TIME				V_x	V_y	V_z	V_t
Day	Hr	Min	Sec	(m/sec)	(m/sec)	(m/sec)	(m/sec)
324	20	5	50.019	247.7	-145.8	1362.1	1392.1

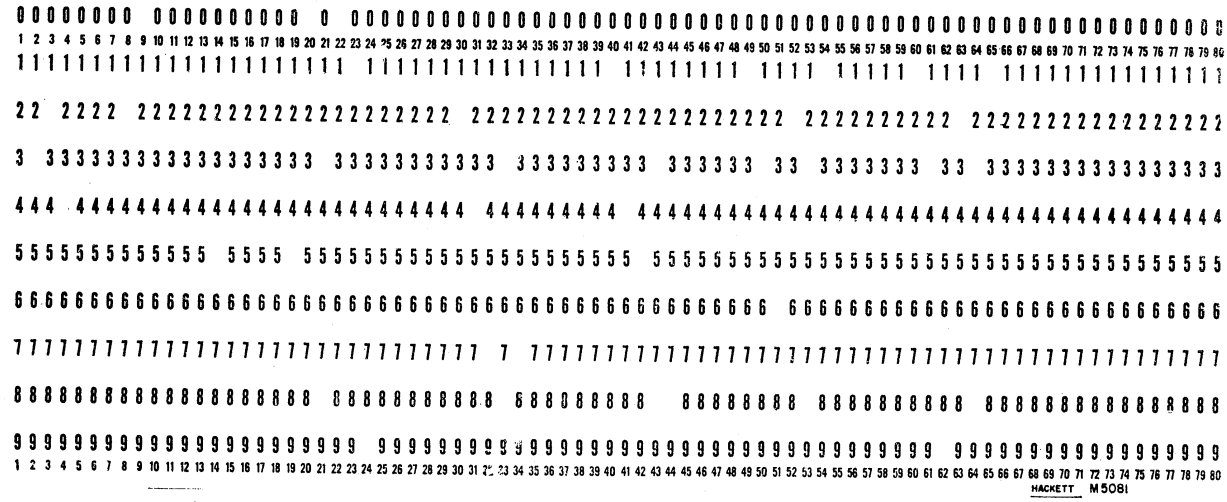

GMT TIME				X	Y	Z	Lat	Long	Alt
Day	Hr	Min	Sec	(meters)	(meters)	(meters)	(deg)	(deg)	(meters)
324	20	5	50.019	8560.9	-4115.2	50243.7	37.80049	75.38747	50254.7

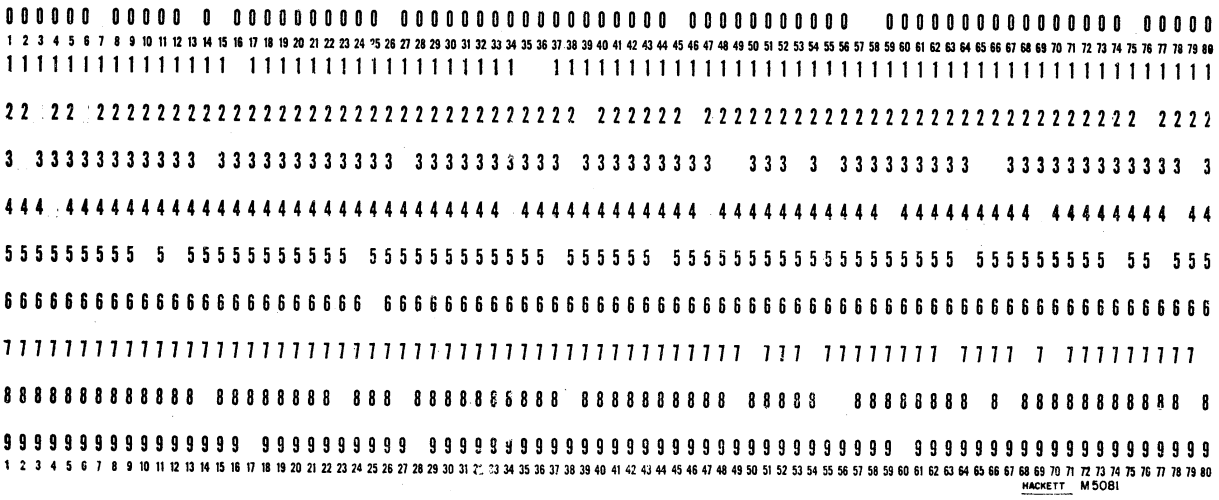

Figure 8. DOVAP trajectory information format.

NOSE CONE PRIMARY TM 244.3 RF LINK TOTAL DEVIATION 135 KHZ

DESCRIPTION	IRIG CHANNEL NO.	CENTER FREQ	FREQ DEV	LP FILTER FREQ	FILTER TYPE
GAGE I DUAL COLLECTOR RADIOACTIVE IONIZATION GAGE	18	70 kHz	7-1/2 %	1050	CD

COMMUTATOR	FREE RUN SAMPLE TIME 15.2 SEC OR RANGE CHANGE FORCED SAMPLE	SEGMENT WIDTH msec 70

SEG NO	INFORM & PURPOSE	LAUNCH COND'S	SUPPLY	R_{S1}	R_{S2}	THERM
1	G 1 GAGE THERM	3.7 V	5.003	10 K		30 K
2	0 VOLT REF	+.004				
3	5 VOLT REF	5.003				
4	2.5 VOLT REF	2.503				
5	RANGE INDICATE	4.5 V				
DATA	GAGE OUTPUT					

DESCRIPTION	IRIG CHANNEL NO.	CENTER FREQ	FREQ DEV	LP FILTER FREQ	FILTER TYPE
GAGE II HOT FILAMENT IONIZATION GAGE	17	52.5 kHz	7-1/2 %	790	CD

COMMUTATOR	FREE RUN SAMPLE TIME 15 SEC OR RANGE CHANGE FORCED SAMPLE	SEGMENT WIDTH msec 70

SEG NO	INFORM & PURPOSE	LAUNCH COND'S	SUPPLY	R_{S1}	R_{S2}	THERM
1	+28 BAT. REF.	4.3 V	BATT.-.8	33 K	5.1 K	
2	0 VOLT REF	+.004				
3	5 VOLT REF.	5.003				
4	2.5 VOLT REF.	2.503				
5	RANGE INDICATE	3.5 V				
DATA	GAGE OUTPUT					

DESCRIPTION	IRIG CHANNEL NO.	CENTER FREQ	FREQ DEV	LP FILTER FREQ	FILTER TYPE
MAGNETOMETER	13	14.5 kHz	7-1/2 %	220	CD

COMMUTATOR	FREE RUN SAMPLE TIME 14.5 SEC	SEGMENT WIDTH msec 70

SEG NO	INFORM & PURPOSE	LAUNCH COND'S	SUPPLY	R_{S1}	R_{S2}	THERM
1	4 THERM	4.9 V	5.003	1.8K		1 MEG
2	0 VOLT REF	+.004				
3	5 VOLT REF	5.003				
4	3 THERM	4.9 V	5.003	3.3 K		300 K
5	2 THERM	4.9 V	5.003	3.3 K		300 K
DATA	MAG. OUTPUT	—				

DESCRIPTION	IRIG CHANNEL NO.	CENTER FREQ	FREQ DEV	LP FILTER FREQ	FILTER TYPE
SOLAR ASPECT	15	30 kHz	7-1/2 %	450	CD

Figure 9. Telemetry format.

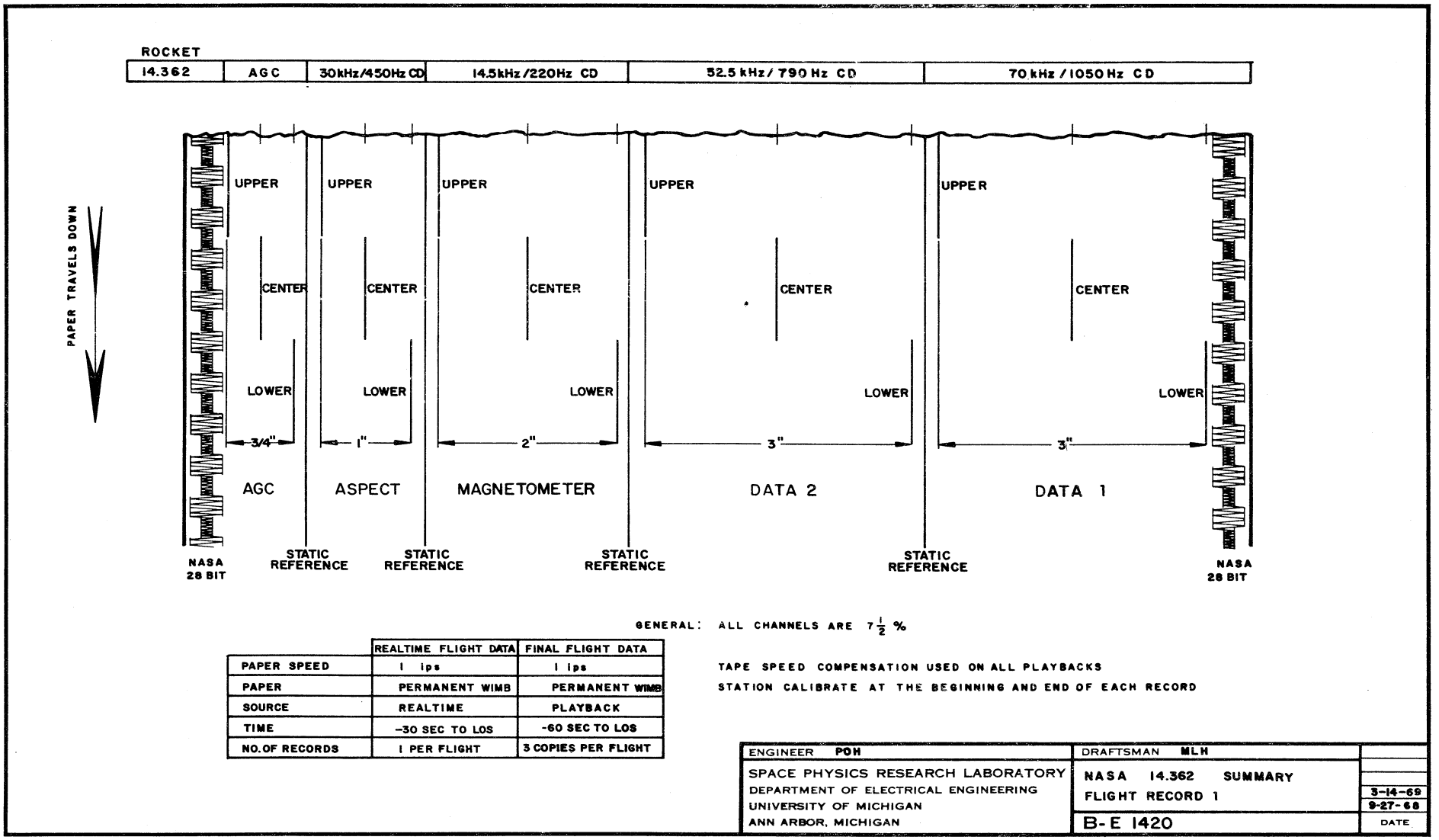

	REALTIME FLIGHT DATA	FINAL FLIGHT DATA
PAPER SPEED	1 ips	1 ips
PAPER	PERMANENT WIMB	PERMANENT WIMB
SOURCE	REALTIME	PLAYBACK
TIME	-30 SEC TO LOS	-60 SEC TO LOS
NO.OF RECORDS	1 PER FLIGHT	3 COPIES PER FLIGHT

Figure 10. Oscillograph record format, summary.

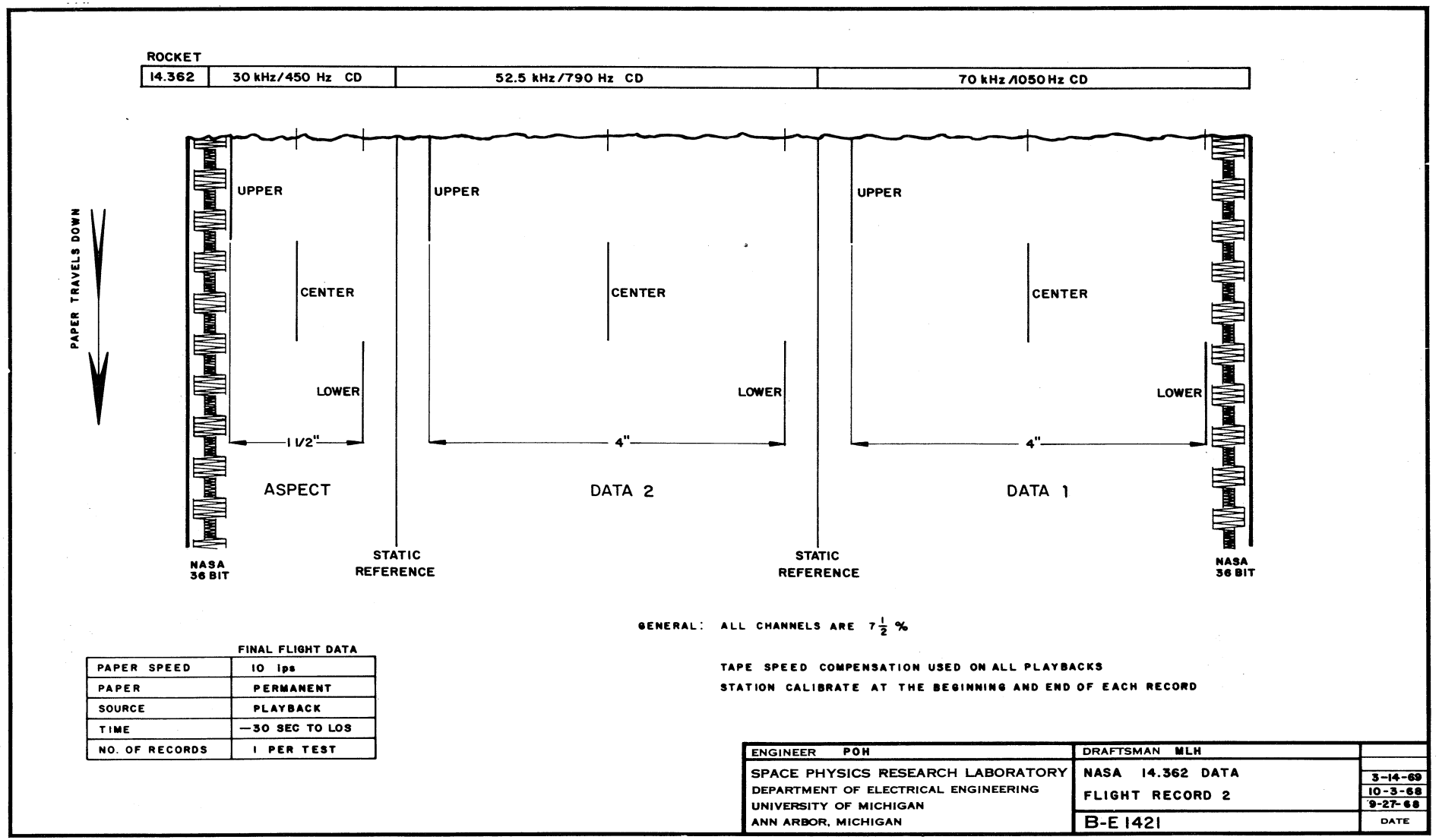

Figure 11. Oscillograph record format, data.

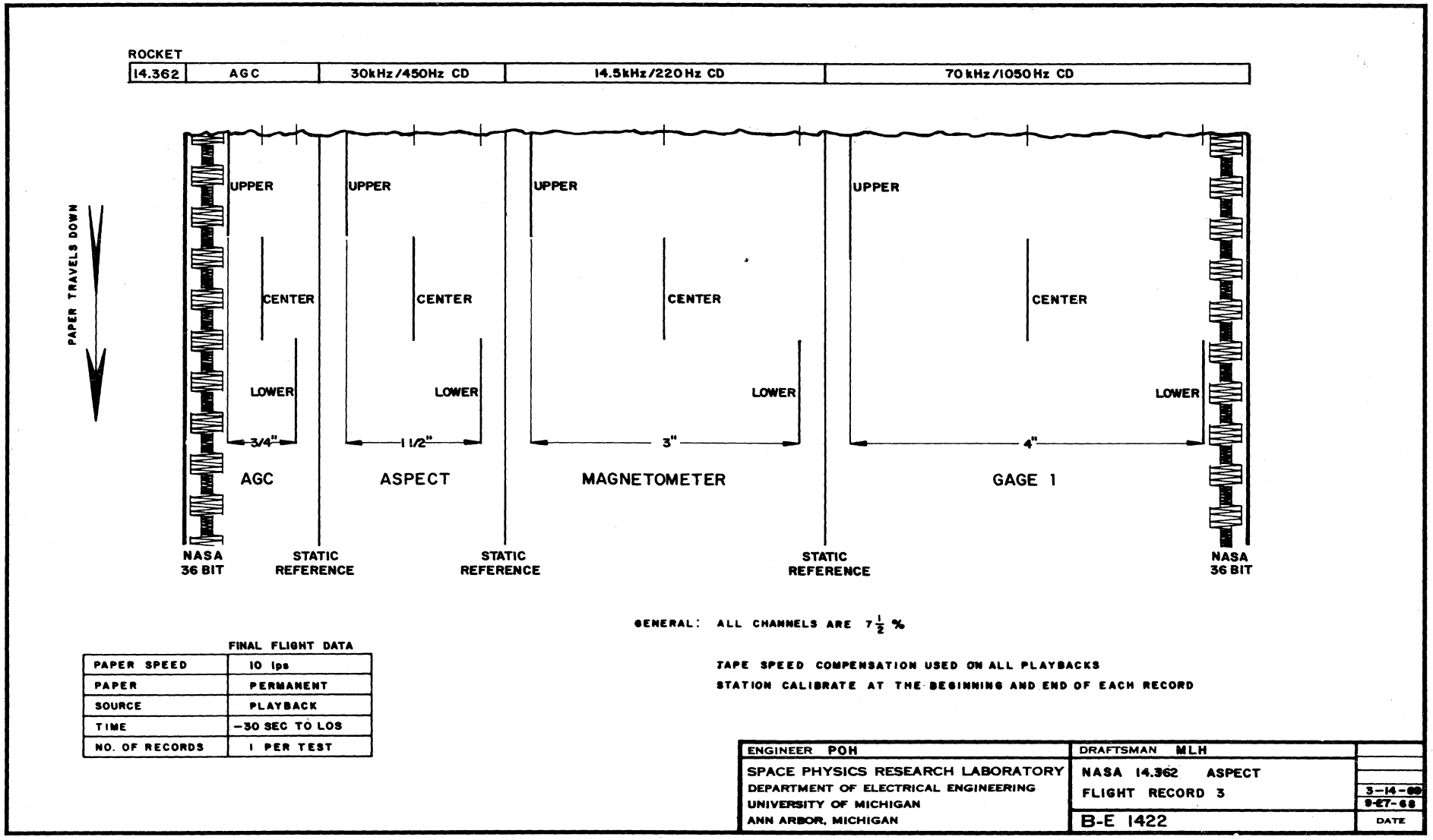

Figure 12. Oscillograph record format, aspect.

5.2. DATA CONDITIONING, ANALOG TO DIGITAL CONVERSION

When the magnetic tape containing analog telemetry data is received at SPRL, it is processed in the Data Conditioning System of the laboratory.

The discriminators in the system are set so that the upper band edge produces an output of -8V and the lower band edge produces a +8V output. The 12-bit successive approximation A/D converter has a resolution of plus or minus half the least significant bit, or $\pm$ 2.4 mV referred to a -10V to +10V full scale signal. Channel-to-channel spacing can be adjusted between 57.3 and 500 μsec; 57.3 μsec is the spacing used for pitot probe data. Three channels are sampled in every pitot probe flight.

Multiplexer scans are triggered by an external signal which is commonly either the 100 kHz reference signal recorded on the tape or the BCD time code carrier. For the pitot probe, the reference signal is divided so as to provide a sampling rate of 100 samples per sec per channel when the data are sampled. The overall data sampling rate capability of the system is 13 kHz, and for pitot probe data the overall sampling rate is 300 samples/sec. The 100 kHz reference is also used to compensate for tape wow and flutter.

The BCD time code can be sampled without missing a data sample, and the sampling is done either on external command signal or at the beginning of each digital tape record. The second procedure is standard when pitot probe data are processed. The BCD time code carrier normally used is one kHz, providing one msec time resolution. During normal processing of pitot probe data, the time taken is that corresponding to the first data sample in each record. Each record of data contains 334 samples per channel. As the converter digitizes one data record, the record is accumulated in one buffer of the PDP-8 computer of the Data Conditioning System until the buffer (with a capacity of 1028 words) is filled. Then the following data record starts filling the second buffer while the first buffer is written onto the digital magnetic tape. The recorded digital tape is a standard seven-track magnetic tape recorded in binary mode at 556 characters/in.

5.3. PROCESSING OF ASPECT DATA

5.3.1. Angle Between the Rocket Vector and the Geomagnetic Field Vector

Throughout the upleg portion of the flight, measurements of the voltage difference ΔV in the magnetometer output and the 0V and 5V calibrations from the magnetometer channel are made at 1-sec intervals. Of these data, the first 20 or 30 sec are selected as calibration data for calculation of the calibration constant. A computer program called MOP (Magnetometer Orientation Program) is used for the calculations, and was written for the IBM 360/67. Inputs to MOP are these:

(1) launch site coordinates,

(2) height of the launch site above the mean radius of the earth,

(3) time from launch and magnetometer data (ΔV and channel calibrations), and

(4) trajectory information (velocity components and altitude versus time).

The program includes subroutines which generate the geomagnetic field model (Breckenridge, 1965). The generation is achieved by means of Legendre polynomials using Gaussian-normalized coefficients derived from spherical harmonics analysis. A calibration constant is calculated (see Equations (40) and (41)) for every second of calibration data. These calibration constants are averaged into one which is then used to calculate the angle between the rocket vector and the geomagnetic field vector (see Equation (39)). An abbreviated flow chart for MOP is given in Figure 13. Output from the program (see Figure 14) follow:

Calibration information:

(1) time from launch (TIME) in sec

(2) altitude (ALTITUDE) in km

(3) angle between the geomagnetic field vector and the velocity vector (ANGLE) in deg

(4) elevation of the geomagnetic field vector (EL B) in deg

(5) azimuth of the geomagnetic field vector (AZ B) in deg

(6) elevation of the velocity vector (EL TRAJ) in deg

(7) azimuth of the velocity (AZ TRAJ) in deg

(8) calibration constant (CAL CONST)

Other information:

(1) relation between voltage and magnetic field (Average Calibration Constant)

(2) time from launch (TIME) in sec

(3) altitude (ALTITUDE) in km

(4) angle between the geomagnetic field vector and the rocket vector, μ_B (ANGLE 2) in deg

(5) supplement to μ_B (ANGLE 1) in deg

(6) elevation of the geomagnetic field vector (EL B) in deg

(7) azimuth of the geomagnetic field vector (AZ B) in deg

(8) elevation of the velocity vector (EL TRAJ) in deg

(9) zenith of the velocity vector (ZEN TRAJ) in deg

(10) azimuth of the velocity vector (AZ TRAJ) in deg

5.3.2. Angle of Attack

Once the angle μ_B between the rocket vector and the geomagnetic field vector, and the angle σ between the sun (moon) vector and the rocket vector are known, the angle of attack is calculated by a computer program called Pitot Aspect Program. The program is written for the IBM 360/67. Inputs to the program are

(1) GMT launch time in hr, min, and sec

(2) latitude and longitude of the launch site in deg

(3) apparent right ascension of the sun (moon) in hr

(4) apparent sidereal time in hr

(5) declination of the sun (moon) in deg

(6) time from launch

(7) angle between the rocket vector and sun (moon) vector in deg

(8) angle between the rocket vector and geomagnetic field vector in deg

The first five are used for the purpose of defining the sun vector. The last three are given at 1-sec intervals over the region of interest.

The program calculates the rocket vector from Equations (47), (48), and (49), and the angle of attack from Equation (50). There are two possible solutions for the rocket vector and for the angle of attack. Output from the program (see Figure 15) are

(1) zenith angle of the sun (moon) in deg

(2) azimuth of the sun (moon) in deg

(3) time from launch (TIME) in sec

First Solution

(4) zenith angle of the rocket vector (ZENITH) in deg

(5) azimuth of the rocket vector (AZIMUTH) in deg

(6) angle of attack (ALPHA) in deg

(7) cosine of the angle of attack (COS ALPHA)

Second Solution

(8) zenith angle of the rocket vector (ZENITH) in deg

(9) azimuth angle of the rocket vector (AZIMUTH) in deg

(10) angle of attack (ALPHA) in deg

(11) cosine of the angle of attack (COS ALPHA)

(12) zenith angle of the velocity vector (VEL ZEN) in deg

(13) azimuth angle of the velocity vector (VEL AZ) in deg

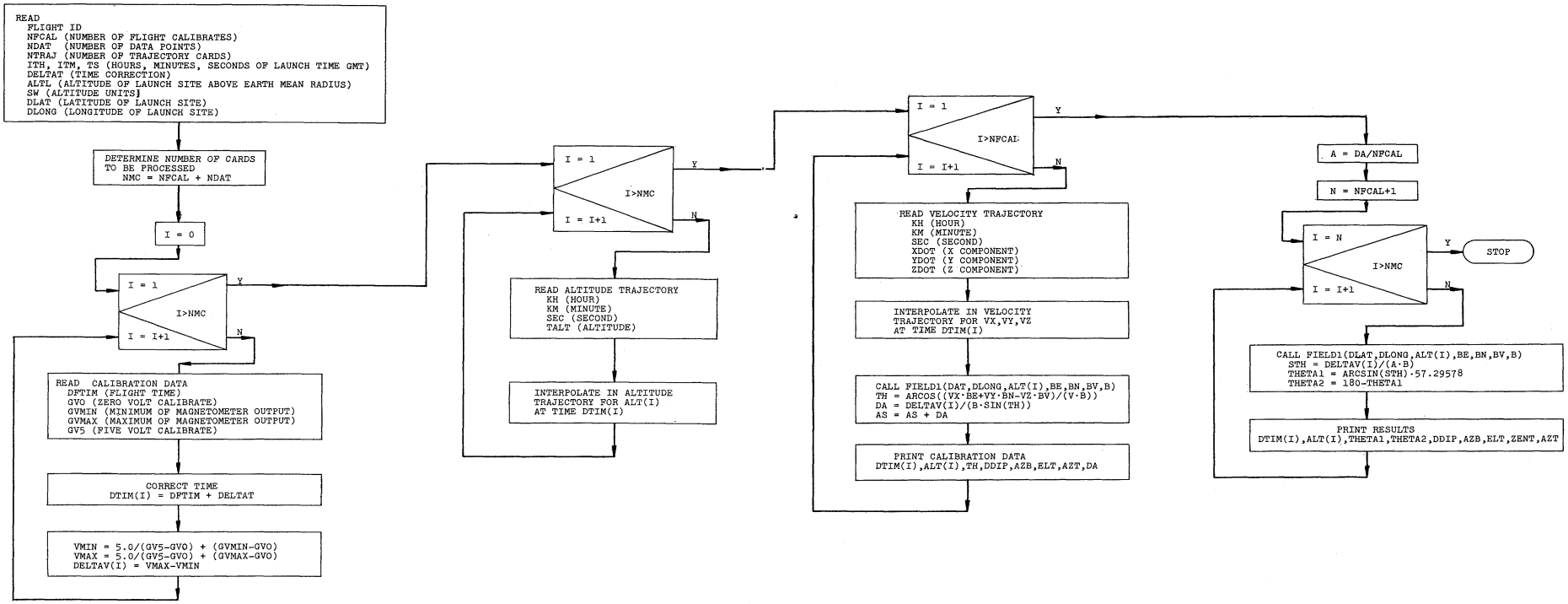

Figure 13. MOP abbreviated flow chart.

CALIBRATION INFORMATION

TIME	ALTITUDE	ANGLE	EL B	AZ B	EL TRAJ	AZ TRAJ	CAL CONST
20.185	11.401	158.959	-69.821	351.526	77.240	95.100	4.8707
21.185	11.787	158.756	-69.821	351.527	76.801	94.906	4.5386
22.185	12.160	158.897	-69.820	351.528	76.681	95.782	4.6515
23.185	12.556	160.279	-69.820	351.529	77.501	101.074	4.8752
24.185	13.113	162.058	-69.819	351.530	78.587	108.840	5.5362
25.185	13.851	163.044	-69.818	351.532	79.029	113.830	5.8502
26.185	14.787	163.497	-69.817	351.534	79.225	116.273	6.0616
27.185	15.958	163.826	-69.816	351.537	79.437	118.162	6.4003
28.185	17.414	164.019	-69.815	351.541	79.466	119.256	6.5895
29.185	19.064	164.225	-69.813	351.545	79.393	120.349	6.7895
30.185	20.708	164.329	-69.811	351.550	79.329	120.877	6.9503
31.185	22.327	164.369	-69.809	351.554	79.258	121.045	7.0289
32.185	23.924	164.421	-69.808	351.558	79.217	121.307	6.8337
33.185	25.501	164.334	-69.806	351.562	79.280	120.896	6.8465
34.185	27.060	164.367	-69.805	351.566	79.237	121.054	6.9221
35.185	28.602	164.434	-69.803	351.570	79.150	121.359	6.7324
36.185	30.128	164.405	-69.801	351.573	79.085	121.159	6.7812
37.185	31.640	164.372	-69.800	351.577	79.045	120.964	6.7725
38.185	33.138	164.354	-69.798	351.581	79.029	120.870	6.7143
39.185	34.623	164.332	-69.797	351.585	78.970	120.724	6.5425

Figure 14. MOP output format.

MAGNETOMETER DATA REDUCTION

FOR NASA 14.386

FROM THE INFLIGHT CALIBRATION THE FOLLOWING RELATION BETWEEN VOLTAGE AND MAGNETIC FIELD HAS BEEN DETERMINED

P-P VOLTAGE= 6.214382 *MAG.FIELD*SIN(ANGLE)

LAUNCH TIME	72299.815
LATITUDE	37.840
LONGITUDE	-75.480

TIME	ALTITUDE	ANGLE1	ANGLE2	EL B	AZ B	EL TRAJ	ZEN TRAJ	AZ TRAJ
40.185	36.095	17.259	162.741	-69.795	351.589	78.825	11.175	120.823
41.185	37.555	17.272	162.728	-69.794	351.592	78.797	11.203	120.637
42.185	39.005	17.140	162.860	-69.792	351.596	78.740	11.260	120.501
43.185	40.444	16.715	163.285	-69.791	351.600	78.549	11.451	120.566
44.185	41.872	16.436	163.564	-69.789	351.603	78.414	11.586	120.421
45.185	43.288	16.302	163.698	-69.788	351.607	78.571	11.429	120.322
46.185	44.697	15.296	164.704	-69.786	351.610	78.612	11.388	120.634
47.185	46.095	15.505	164.495	-69.785	351.614	78.315	11.685	120.757
48.185	47.483	15.370	164.630	-69.783	351.617	78.320	11.680	120.589
49.185	48.861	14.944	165.056	-69.782	351.621	78.238	11.762	120.788
50.185	50.229	15.831	164.169	-69.780	351.624	78.087	11.913	120.488
51.185	51.587	16.429	163.571	-69.779	351.628	78.058	11.942	120.412
52.185	52.935	15.414	164.586	-69.778	351.631	77.937	12.063	121.057
53.185	54.273	14.111	165.889	-69.776	351.634	77.830	12.170	121.536
54.185	55.602	14.558	165.442	-69.775	351.638	77.851	12.149	120.616
55.185	56.921	15.886	164.114	-69.773	351.641	77.711	12.289	120.977
56.185	58.230	17.373	162.627	-69.772	351.644	77.488	12.512	121.871
57.185	59.529	18.128	161.872	-69.771	351.647	77.448	12.552	121.263
58.185	60.818	17.248	162.752	-69.770	351.651	77.413	12.587	121.289
59.185	62.098	16.077	163.923	-69.768	351.654	77.323	12.677	121.387
60.185	63.368	14.764	165.236	-69.767	351.657	77.228	12.772	121.318
61.185	64.628	14.236	165.764	-69.766	351.660	77.129	12.871	121.307
62.185	65.879	14.392	165.608	-69.764	351.663	77.018	12.982	121.380
63.185	67.120	15.286	164.714	-69.763	351.666	76.925	13.075	121.375
64.185	68.352	16.779	163.221	-69.762	351.669	76.807	13.193	121.465
65.185	69.573	17.836	162.164	-69.760	351.672	76.727	13.273	121.387
66.185	70.785	18.750	161.250	-69.759	351.676	76.671	13.329	121.339
67.185	71.988	19.518	160.482	-69.758	351.678	76.565	13.435	121.416
68.185	73.181	19.530	160.470	-69.757	351.681	76.466	13.534	121.384
69.185	74.365	19.391	160.609	-69.756	351.684	76.368	13.632	121.333
70.185	75.540	18.948	161.052	-69.754	351.687	76.286	13.714	121.278
71.185	76.705	18.204	161.796	-69.753	351.690	76.178	13.822	121.321
72.185	77.860	17.914	162.086	-69.752	351.693	76.066	13.934	121.366
73.185	79.006	16.873	163.127	-69.751	351.696	75.957	14.043	121.350
74.185	80.142	16.434	163.566	-69.750	351.698	75.841	14.159	121.350
75.185	81.269	16.063	163.937	-69.748	351.701	75.736	14.264	121.282
76.185	82.386	16.072	163.928	-69.747	351.704	75.616	14.384	121.254
77.185	83.494	16.230	163.770	-69.746	351.707	75.465	14.535	121.340
78.185	84.591	16.538	163.462	-69.745	351.709	75.321	14.679	121.433
79.185	85.679	16.846	163.154	-69.744	351.712	75.191	14.809	121.424
80.185	86.758	17.305	162.695	-69.743	351.715	75.075	14.925	121.471
81.185	87.827	17.916	162.084	-69.742	351.718	74.972	15.028	121.578
82.185	88.886	18.681	161.319	-69.741	351.720	74.858	15.142	121.550
83.185	89.936	19.603	160.397	-69.740	351.723	74.712	15.288	121.590
84.185	90.976	20.224	159.776	-69.738	351.725	74.557	15.443	121.664

Figure 14. (Continued)

85.185	92.007	21.002	158.998	-69.737	351.728	74.499	15.501	121.496
86.185	93.028	21.785	158.215	-69.736	351.730	74.381	15.619	121.480
87.185	94.040	22.573	157.427	-69.735	351.733	74.206	15.794	121.539
88.185	95.043	23.250	156.750	-69.734	351.735	74.095	15.905	121.453
89.185	96.036	23.892	156.108	-69.733	351.738	73.961	16.039	121.499
90.185	97.019	24.696	155.304	-69.732	351.740	73.848	16.152	121.529
91.185	97.993	25.186	154.814	-69.731	351.742	73.707	16.293	121.523
92.185	98.958	25.679	154.321	-69.730	351.745	73.535	16.465	121.553
93.185	99.913	26.335	153.665	-69.729	351.747	73.413	16.587	121.582
94.185	100.859	26.671	153.329	-69.728	351.749	73.279	16.721	121.590
95.185	101.795	26.847	153.153	-69.727	351.751	73.104	16.896	121.631
96.185	102.721	27.023	152.977	-69.726	351.754	72.913	17.087	121.722
97.185	103.638	27.036	152.964	-69.725	351.756	72.750	17.250	121.878
98.185	104.545	27.212	152.788	-69.725	351.758	72.648	17.352	122.001
99.185	105.443	27.063	152.937	-69.724	351.760	72.517	17.483	121.999
100.185	106.332	26.913	153.087	-69.723	351.762	72.398	17.602	122.161
101.185	107.211	26.926	153.074	-69.722	351.765	72.249	17.751	122.228
102.185	108.081	26.614	153.386	-69.721	351.767	72.093	17.907	122.166
103.185	108.941	26.303	153.697	-69.720	351.769	71.935	18.065	122.291
104.185	109.792	25.508	154.492	-69.719	351.771	71.752	18.248	122.332
105.185	110.633	25.198	154.802	-69.718	351.773	71.566	18.434	122.270
106.185	111.465	24.409	155.591	-69.718	351.775	71.335	18.665	122.395
107.185	112.288	23.942	156.058	-69.717	351.777	71.168	18.832	122.372
108.185	113.101	23.318	156.682	-69.716	351.779	71.059	18.941	122.264
109.185	113.905	22.696	157.304	-69.715	351.781	70.884	19.116	122.361
110.185	114.700	21.762	158.238	-69.714	351.783	70.685	19.315	122.340
111.185	115.485	21.146	158.854	-69.713	351.785	70.461	19.539	122.300
112.185	116.261	20.531	159.469	-69.713	351.787	70.236	19.764	122.345
113.185	117.027	19.764	160.236	-69.712	351.788	70.052	19.948	122.321
114.185	117.784	18.999	161.001	-69.711	351.790	69.815	20.185	122.309
115.185	118.532	18.237	161.763	-69.710	351.792	69.582	20.418	122.264
116.185	119.270	17.449	162.551	-69.710	351.794	69.408	20.592	122.235
117.185	120.000	17.150	162.850	-69.709	351.796	69.204	20.796	122.329
118.185	120.720	16.852	163.148	-69.708	351.797	68.973	21.027	122.216
119.185	121.430	16.402	163.598	-69.707	351.799	68.748	21.252	122.046
120.185	122.131	16.408	163.592	-69.707	351.801	68.497	21.503	122.037
121.185	122.823	16.262	163.738	-69.706	351.802	68.224	21.776	122.128
122.185	123.506	16.115	163.885	-69.705	351.804	67.992	22.008	122.195
123.185	124.179	16.730	163.270	-69.705	351.806	67.728	22.272	122.218
124.185	124.843	16.735	163.265	-69.704	351.807	67.372	22.628	122.183
125.185	125.497	17.046	162.954	-69.703	351.809	67.041	22.959	122.156
126.185	126.141	17.818	162.182	-69.703	351.810	66.754	23.246	122.087
127.185	126.777	18.439	161.561	-69.702	351.812	66.462	23.538	121.987
128.185	127.403	18.908	161.092	-69.701	351.813	66.180	23.820	122.040
129.185	128.019	19.689	160.311	-69.701	351.815	65.856	24.144	122.041
130.185	128.626	20.388	159.612	-69.700	351.816	65.472	24.528	121.993
131.185	129.224	21.179	158.821	-69.700	351.818	65.112	24.888	122.135
132.185	129.812	22.134	157.866	-69.699	351.819	64.779	25.221	122.188
133.185	130.391	22.777	157.223	-69.698	351.821	64.453	25.547	122.022
134.185	130.961	23.103	156.897	-69.698	351.822	64.077	25.923	122.008
135.185	131.522	23.911	156.089	-69.697	351.823	63.671	26.329	122.066
136.185	132.073	24.563	155.437	-69.697	351.824	63.306	26.694	122.037
137.185	132.614	25.056	154.944	-69.696	351.826	62.930	27.070	121.875
138.185	133.146	25.551	154.449	-69.696	351.827	62.529	27.471	121.763
139.185	133.670	26.049	153.951	-69.695	351.828	62.157	27.843	121.826
140.185	134.183	26.220	153.780	-69.694	351.830	61.755	28.245	121.871
141.185	134.688	26.556	153.444	-69.694	351.831	61.356	28.644	121.955
142.185	135.183	26.728	153.272	-69.693	351.832	60.926	29.074	122.035
143.185	135.669	27.065	152.935	-69.693	351.833	60.435	29.565	121.986
144.185	136.146	26.928	153.072	-69.693	351.834	59.862	30.138	121.944

Figure 14. (Continued)

145.185	136.613	26.935	153.065	-69.692	351.835	59.354	30.646	122.063
146.185	137.070	26.777	153.223	-69.692	351.836	58.925	31.075	122.090
147.185	137.519	26.784	153.216	-69.691	351.837	58.436	31.564	122.145
148.185	137.958	27.284	152.716	-69.691	351.839	57.894	32.106	122.232
149.185	138.388	27.621	152.379	-69.690	351.840	57.271	32.729	122.305
150.185	138.809	27.628	152.372	-69.690	351.841	56.606	33.394	122.487
151.185	139.220	27.634	152.366	-69.689	351.842	55.959	34.041	122.658
152.185	139.621	27.474	152.526	-69.689	351.843	55.341	34.659	122.689
153.185	140.013	27.646	152.354	-69.689	351.844	54.680	35.320	122.696
154.185	140.396	27.486	152.514	-69.688	351.844	53.882	36.118	122.757
155.185	140.769	26.666	153.334	-69.688	351.845	53.136	36.864	122.822
156.185	141.133	26.343	153.657	-69.687	351.846	52.487	37.513	122.725
157.185	141.487	25.857	154.143	-69.687	351.847	51.786	38.214	122.654
158.185	141.832	25.508	154.492	-69.687	351.848	51.040	38.960	122.811
159.185	142.168	24.859	155.141	-69.686	351.849	50.196	39.804	122.731
160.185	142.494	24.052	155.948	-69.686	351.849	49.264	40.736	122.664
161.185	142.811	23.088	156.912	-69.686	351.850	48.325	41.675	122.801
162.185	143.118	22.291	157.709	-69.685	351.851	47.273	42.727	122.701
163.185	143.416	21.497	158.503	-69.685	351.852	46.339	43.661	122.504
164.185	143.704	20.392	159.608	-69.685	351.852	45.399	44.601	122.573
165.185	143.982	19.451	160.549	-69.685	351.853	44.425	45.575	122.692
166.185	144.252	18.359	161.641	-69.684	351.854	43.358	46.642	122.702
167.185	144.512	17.274	162.726	-69.684	351.854	42.140	47.860	122.662
168.185	144.761	16.503	163.497	-69.684	351.855	40.884	49.116	122.588
169.185	145.001	15.581	164.419	-69.684	351.855	39.709	50.291	122.622
170.185	145.233	14.510	165.490	-69.683	351.856	38.556	51.444	122.623
171.185	145.454	14.206	165.794	-69.683	351.856	37.350	52.650	122.601
172.185	145.666	13.423	166.577	-69.683	351.857	36.193	53.807	122.710
173.185	145.869	12.969	167.031	-69.683	351.857	35.038	54.962	122.737
174.185	146.063	12.819	167.181	-69.683	351.858	33.844	56.156	122.712
175.185	146.248	12.820	167.180	-69.682	351.858	32.732	57.268	122.830
176.185	146.424	13.125	166.875	-69.682	351.859	31.624	58.376	122.967
177.185	146.591	13.734	166.266	-69.682	351.859	30.335	59.665	123.166
178.185	146.750	14.344	165.656	-69.682	351.859	28.984	61.016	123.367
179.185	146.899	14.957	165.043	-69.682	351.860	27.569	62.431	123.296
180.185	147.039	15.725	164.275	-69.682	351.860	26.181	63.819	123.333
181.185	147.170	16.650	163.350	-69.681	351.860	24.809	65.191	123.499
182.185	147.293	17.890	162.110	-69.681	351.861	23.202	66.798	123.513
183.185	147.406	18.670	161.330	-69.681	351.861	21.663	68.337	123.588
184.185	147.510	19.768	160.232	-69.681	351.861	20.105	69.895	123.892
185.185	147.605	20.873	159.127	-69.681	351.861	18.300	71.700	123.997
186.185	147.691	21.668	158.332	-69.681	351.862	16.441	73.559	123.987
187.185	147.767	22.307	157.693	-69.681	351.862	14.599	75.401	123.923
188.185	147.835	23.270	156.730	-69.681	351.862	12.734	77.266	123.759
189.185	147.892	24.403	155.597	-69.681	351.862	10.858	79.142	123.697
190.185	147.941	25.055	154.945	-69.681	351.862	8.867	81.133	123.626
191.185	147.980	25.711	154.289	-69.681	351.862	6.808	83.192	123.666
192.185	148.009	26.040	153.960	-69.681	351.862	4.771	85.229	123.782
193.185	148.029	26.701	153.299	-69.681	351.863	2.805	87.195	123.628
194.185	148.040	27.033	152.967	-69.680	351.863	0.824	89.176	123.429
195.185	148.041	27.532	152.468	-69.680	351.863	-1.206	91.206	123.507

Figure 14. (Concluded)

SOLAR POSITION ZENITH ANGLE 73.8 AZIMUTH 228.1

PITOT ASPECT FOR NASA 14.386

TIME	ZENITH	AZIMUTH	ALPHA	COS ALPHA	ZENITH	AZIMUTH	ALPHA	COS ALPHA	VEL ZEN	VEL AZ
40.0	28.8	134.7	18.1	0.95072	8.7	114.1	2.8	0.99879	11.3	120.4
41.0	30.9	139.4	20.5	0.93655	5.6	121.6	5.7	0.99505	11.3	120.2
42.0	28.7	134.9	18.0	0.95131	8.6	114.8	2.9	0.99874	11.4	120.1
43.0	29.5	137.0	18.7	0.94727	7.5	118.1	4.1	0.99746	11.5	120.1
44.0	29.9	139.2	19.2	0.94443	6.6	124.4	5.1	0.99600	11.7	120.0
45.0	30.5	141.3	20.1	0.93885	5.7	132.1	6.2	0.99420	11.6	119.9
46.0	28.5	138.8	17.9	0.95146	8.0	127.1	3.8	0.99786	11.5	120.1
47.0	28.3	138.8	17.5	0.95350	8.1	127.4	3.8	0.99775	11.8	120.2
48.0	29.3	141.3	18.8	0.94689	6.8	134.3	5.5	0.99546	11.8	120.1
49.0	29.6	143.2	19.2	0.94457	6.5	142.0	6.4	0.99386	11.9	120.2
50.0	29.1	141.0	18.3	0.94927	7.1	133.7	5.4	0.99555	12.0	120.0
51.0	29.5	138.7	18.5	0.94855	7.0	123.6	5.1	0.99605	12.1	119.9
52.0	28.9	139.9	17.8	0.95201	7.4	130.1	5.0	0.99615	12.2	120.4
53.0	28.3	143.0	17.5	0.95373	7.7	141.7	5.8	0.99495	12.3	120.9
54.0	29.5	144.6	18.9	0.94586	6.5	148.1	7.2	0.99213	12.3	120.2
55.0	29.7	142.2	18.7	0.94720	6.4	137.5	6.6	0.99339	12.4	120.3
56.0	31.0	139.5	19.4	0.94308	5.5	121.1	7.1	0.99222	12.6	121.1
57.0	31.1	137.1	19.2	0.94435	6.1	110.6	6.8	0.99294	12.7	120.8
58.0	31.2	138.5	19.4	0.94329	5.6	116.1	7.2	0.99218	12.7	120.7
59.0	30.5	140.7	18.9	0.94586	5.7	129.2	7.2	0.99208	12.8	120.8
60.0	29.2	142.3	17.8	0.95213	6.8	138.5	6.7	0.99310	12.9	120.7
61.0	28.6	143.0	17.2	0.95513	7.4	141.7	6.6	0.99330	13.0	120.7
62.0	28.6	142.6	17.0	0.95618	7.5	140.2	6.5	0.99347	13.1	120.8
63.0	28.8	141.4	17.1	0.95604	7.3	135.5	6.5	0.99367	13.2	120.8
64.0	29.8	139.5	17.6	0.95313	6.6	126.2	6.8	0.99300	13.4	120.8
65.0	31.3	137.6	18.8	0.94674	5.8	111.3	7.8	0.99075	13.4	120.8
66.0	31.6	135.9	18.9	0.94610	6.1	103.0	7.9	0.99048	13.5	120.7
67.0	31.8	134.8	18.9	0.94625	6.4	98.3	8.0	0.99016	13.6	120.8
68.0	31.6	134.0	18.5	0.94857	6.9	97.6	7.8	0.99073	13.7	120.7
69.0	31.3	133.7	18.1	0.95062	7.2	98.6	7.6	0.99119	13.8	120.7
70.0	30.9	133.9	17.6	0.95318	7.4	101.7	7.3	0.99192	13.9	120.6
71.0	29.9	134.1	16.6	0.95853	8.0	107.6	6.5	0.99365	14.0	120.6
72.0	31.2	135.2	17.8	0.95197	6.7	103.5	8.0	0.99035	14.1	120.7
73.0	28.7	135.1	15.3	0.96467	8.6	115.5	5.7	0.99507	14.2	120.7
74.0	27.6	134.8	14.1	0.97008	9.6	118.8	4.7	0.99659	14.3	120.7
75.0	27.0	134.4	13.4	0.97279	10.2	119.5	4.3	0.99721	14.5	120.6
76.0	26.5	133.5	12.7	0.97540	10.8	119.0	3.8	0.99781	14.6	120.6
77.0	26.2	132.7	12.2	0.97736	11.3	118.3	3.5	0.99812	14.7	120.6
78.0	26.2	131.7	11.9	0.97843	11.5	116.7	3.5	0.99818	14.9	120.7
79.0	26.0	130.4	11.4	0.98018	12.1	115.3	3.2	0.99845	15.0	120.7
80.0	25.7	128.9	10.9	0.98182	12.7	113.6	3.0	0.99865	15.1	120.7
81.0	25.8	127.2	10.8	0.98242	13.2	111.1	3.1	0.99849	15.2	120.8
82.0	26.6	126.4	11.4	0.98027	12.9	107.3	4.1	0.99746	15.4	120.8
83.0	26.9	125.0	11.5	0.97981	13.2	104.4	4.6	0.99671	15.5	120.9
84.0	27.6	123.8	11.9	0.97834	13.3	100.9	5.5	0.99543	15.7	120.9
85.0	28.4	122.9	12.7	0.97547	13.3	96.7	6.5	0.99367	15.7	120.8
86.0	29.1	121.7	13.3	0.97329	13.5	93.0	7.3	0.99185	15.8	120.7
87.0	29.6	120.3	13.6	0.97214	14.0	90.3	8.0	0.99015	16.0	120.8
88.0	30.2	119.4	14.1	0.96993	14.3	87.2	8.9	0.98807	16.1	120.7
89.0	30.8	118.6	14.6	0.96787	14.6	84.6	9.6	0.98597	16.3	120.7
90.0	30.9	117.4	14.6	0.96771	15.2	83.7	10.0	0.98486	16.4	120.8
91.0	31.3	116.5	14.9	0.96652	15.6	82.1	10.5	0.98310	16.5	120.8

Figure 15. Pitot aspect program output format.

92.0	31.8	116.1	15.2	0.96499	15.8	80.2	11.1	0.98113	16.7	120.8
93.0	32.0	115.5	15.4	0.96430	16.1	79.2	11.6	0.97974	16.8	120.8
94.0	32.5	115.3	15.7	0.96287	16.2	77.7	12.1	0.97797	17.0	120.8
95.0	32.6	115.0	15.6	0.96297	16.3	77.2	12.3	0.97705	17.1	120.8
96.0	32.7	114.7	15.6	0.96314	16.5	76.8	12.6	0.97603	17.3	120.9
97.0	33.1	115.3	15.8	0.96220	16.2	75.3	13.0	0.97447	17.5	121.1
98.0	33.5	115.8	16.0	0.96105	15.9	73.9	13.4	0.97295	17.6	121.2
99.0	33.6	116.3	16.0	0.96135	15.6	73.6	13.5	0.97257	17.7	121.2
100.0	33.8	117.1	16.1	0.96099	15.2	72.6	13.7	0.97159	17.9	121.3
101.0	34.0	118.1	16.0	0.96110	14.7	71.9	13.9	0.97088	18.0	121.4
102.0	34.1	119.0	16.0	0.96130	14.2	71.2	14.0	0.97019	18.2	121.4
103.0	34.1	120.2	15.8	0.96213	13.5	71.1	14.1	0.96989	18.3	121.5
104.0	34.0	121.0	15.5	0.96360	13.0	71.6	14.1	0.96997	18.5	121.5
105.0	33.8	122.2	15.1	0.96561	12.3	72.8	13.9	0.97058	18.7	121.5
106.0	33.6	123.2	14.7	0.96738	11.8	73.8	13.9	0.97055	18.9	121.6
107.0	33.3	124.4	14.3	0.96909	11.2	75.3	13.9	0.97086	19.1	121.6
108.0	33.0	125.8	13.9	0.97061	10.5	77.4	13.7	0.97152	19.2	121.5
109.0	32.3	126.5	13.1	0.97399	10.2	81.8	13.2	0.97359	19.4	121.5
110.0	31.7	127.5	12.4	0.97665	9.9	85.9	12.9	0.97487	19.6	121.5
111.0	31.2	128.4	11.8	0.97898	9.6	89.8	12.6	0.97575	19.8	121.5
112.0	30.9	129.5	11.3	0.98047	9.3	93.0	12.7	0.97573	20.0	121.5
113.0	30.2	130.3	10.6	0.98287	9.3	98.0	12.3	0.97711	20.2	121.5
114.0	29.7	131.1	10.1	0.98445	9.2	101.7	12.2	0.97744	20.5	121.5
115.0	29.1	131.9	9.5	0.98638	9.3	106.2	12.0	0.97832	20.7	121.4
116.0	28.4	132.3	8.7	0.98843	9.7	110.4	11.5	0.97988	20.9	121.4
117.0	28.0	133.0	8.4	0.98936	9.8	113.4	11.5	0.97995	21.1	121.5
118.0	27.8	133.6	8.2	0.98969	9.7	115.2	11.7	0.97921	21.3	121.4
119.0	27.2	133.6	7.6	0.99126	10.2	117.2	11.4	0.98043	21.5	121.2
120.0	26.6	133.1	6.8	0.99287	10.8	117.9	11.0	0.98163	21.8	121.2
121.0	26.1	132.4	6.0	0.99448	11.5	118.2	10.6	0.98287	22.1	121.3
122.0	25.7	131.7	5.4	0.99558	12.0	118.1	10.4	0.98359	22.3	121.3
123.0	25.4	130.6	4.7	0.99669	12.5	117.2	10.1	0.98438	22.6	121.4
124.0	25.0	129.4	3.9	0.99771	13.1	116.4	9.9	0.98504	22.9	121.4
125.0	24.9	128.1	3.2	0.99840	13.5	114.8	10.0	0.98496	23.2	121.3
126.0	25.2	127.0	2.9	0.99874	13.7	112.8	10.2	0.98408	23.5	121.3
127.0	25.7	126.0	2.8	0.99884	13.6	109.7	10.8	0.98215	23.8	121.2
128.0	26.3	125.0	2.7	0.99889	13.6	106.6	11.5	0.98002	24.1	121.2
129.0	26.9	124.0	2.7	0.99888	13.6	103.6	12.2	0.97757	24.4	121.2
130.0	27.2	122.6	2.5	0.99905	13.9	100.9	12.6	0.97577	24.8	121.2
131.0	27.9	121.6	2.7	0.99890	14.1	97.6	13.4	0.97258	25.2	121.3
132.0	28.7	120.9	3.2	0.99844	14.0	93.9	14.5	0.96818	25.5	121.4
133.0	29.1	119.7	3.3	0.99830	14.5	91.6	15.0	0.96602	25.9	121.2
134.0	29.7	118.9	3.7	0.99797	14.7	88.9	15.8	0.96236	26.2	121.2
135.0	29.9	117.5	3.7	0.99792	15.3	87.7	16.1	0.96076	26.6	121.2
136.0	30.5	116.8	4.1	0.99745	15.5	85.1	16.9	0.95669	27.0	121.2
137.0	30.6	115.6	4.2	0.99733	16.1	84.4	17.2	0.95547	27.4	121.1
138.0	30.7	114.5	4.3	0.99723	16.7	84.0	17.4	0.95438	27.8	121.0
139.0	31.1	114.3	4.4	0.99702	16.7	82.4	18.1	0.95048	28.2	121.0
140.0	31.1	113.4	4.6	0.99683	17.2	82.4	18.3	0.94934	28.6	121.1
141.0	31.3	113.0	4.7	0.99663	17.4	81.7	18.8	0.94672	29.0	121.1
142.0	31.4	112.7	4.8	0.99653	17.6	81.2	19.2	0.94415	29.4	121.2
143.0	31.9	113.2	4.6	0.99681	17.3	79.5	20.2	0.93841	29.9	121.2
144.0	32.4	113.8	4.4	0.99712	17.0	77.8	21.2	0.93216	30.4	121.2
145.0	33.0	114.8	4.0	0.99755	16.4	75.7	22.4	0.92450	31.0	121.2
146.0	33.4	115.3	3.8	0.99784	16.1	74.3	23.3	0.91867	31.4	121.3
147.0	33.9	116.2	3.5	0.99818	15.7	72.3	24.3	0.91106	31.9	121.3
148.0	34.6	117.4	3.1	0.99854	15.1	69.7	25.6	0.90149	32.4	121.4
149.0	35.0	118.3	2.6	0.99893	14.6	68.0	26.8	0.89294	33.0	121.5
150.0	35.3	119.2	2.2	0.99927	14.1	66.2	27.9	0.88365	33.7	121.7
151.0	35.8	120.3	1.7	0.99954	13.6	63.9	29.2	0.87276	34.3	121.8

Figure 15. (Continued)

152.0	36.1	121.3	1.2	0.99977	13.0	62.3	30.3	0.86377	35.0	121.9
153.0	36.5	122.4	0.9	0.99987	12.4	60.1	31.5	0.85304	35.6	121.9
154.0	36.7	123.7	1.1	0.99981	11.7	58.1	32.7	0.84127	36.4	122.0
155.0	36.8	125.0	1.8	0.99950	11.0	57.2	33.8	0.83131	37.2	122.0
156.0	36.8	126.2	2.8	0.99883	10.3	56.3	34.7	0.82217	37.8	122.0
157.0	37.0	127.9	4.0	0.99759	9.3	54.0	35.9	0.80987	38.5	121.9
158.0	36.9	129.4	5.1	0.99597	8.4	53.6	36.9	0.79989	39.3	122.0
159.0	37.0	131.4	6.6	0.99337	7.3	50.5	38.3	0.78475	40.1	122.0
160.0	37.0	133.1	8.1	0.99006	6.3	49.2	39.5	0.77135	41.0	121.9
161.0	36.6	134.7	9.6	0.98603	5.3	50.9	40.5	0.76038	42.0	122.0
162.0	36.1	136.2	11.3	0.98053	4.3	55.4	41.4	0.74975	43.0	122.0
163.0	35.5	137.4	13.0	0.97436	3.6	64.6	42.1	0.74228	43.9	121.8
164.0	34.7	138.4	14.6	0.96755	3.3	80.3	42.5	0.73744	44.9	121.8
165.0	33.9	139.6	16.4	0.95955	3.1	98.5	43.1	0.73064	45.9	122.0
166.0	33.3	140.7	18.1	0.95054	3.2	115.1	43.7	0.72243	46.9	122.0
167.0	32.4	141.7	20.1	0.93934	3.8	128.5	44.3	0.71514	48.1	122.0
168.0	31.3	142.4	22.2	0.92591	4.7	136.8	44.8	0.70978	49.4	121.9
169.0	30.2	142.9	24.2	0.91222	5.8	140.2	45.1	0.70641	50.5	121.9
170.0	29.2	143.1	26.1	0.89788	6.9	141.9	45.3	0.70349	51.7	121.9
171.0	28.3	143.2	28.0	0.88329	7.8	142.4	45.7	0.69862	52.9	121.9
172.0	27.4	142.9	29.6	0.86935	8.6	141.6	46.0	0.69453	54.1	122.0
173.0	26.4	142.3	31.4	0.85352	9.7	140.3	46.1	0.69316	55.2	122.1
174.0	25.5	141.2	33.1	0.83809	10.6	138.2	46.3	0.69079	56.4	122.1
175.0	24.7	139.9	34.6	0.82358	11.5	135.9	46.5	0.68868	57.6	122.2
176.0	24.5	138.6	35.6	0.81299	11.8	133.6	47.1	0.68053	58.7	122.3
177.0	24.5	137.2	36.6	0.80293	12.0	130.8	48.1	0.66820	59.9	122.5
178.0	24.7	135.8	37.5	0.79360	12.0	127.8	49.3	0.65169	61.3	122.7
179.0	24.5	133.5	38.7	0.78009	12.5	124.1	50.2	0.64074	62.7	122.7
180.0	24.6	131.4	39.8	0.76816	12.9	120.4	51.2	0.62696	64.1	122.7
181.0	25.1	129.2	40.6	0.75937	13.1	116.0	52.4	0.60980	65.4	122.9
182.0	25.5	127.0	41.6	0.74785	13.4	111.7	53.9	0.58957	67.0	122.9
183.0	26.0	125.0	42.6	0.73596	13.8	107.7	55.3	0.56902	68.6	123.0
184.0	27.0	123.6	43.1	0.72966	13.7	102.8	57.4	0.53913	70.1	123.2
185.0	27.7	122.1	44.2	0.71725	13.9	98.7	59.4	0.50976	71.9	123.4
186.0	27.9	120.2	45.9	0.69649	14.6	96.4	60.8	0.48719	73.7	123.4
187.0	28.9	119.5	46.8	0.68453	14.6	92.5	63.2	0.45101	75.6	123.4
188.0	29.6	118.3	48.0	0.66921	15.0	89.1	65.2	0.41878	77.4	123.2
189.0	30.5	117.7	49.0	0.65619	15.1	85.4	67.6	0.38135	79.3	123.2
190.0	31.4	117.2	50.1	0.64084	15.2	82.0	70.0	0.34195	81.3	123.1
191.0	32.2	117.3	51.3	0.62512	15.1	78.7	72.8	0.29641	83.3	123.1
192.0	32.7	117.0	52.9	0.60303	15.3	76.9	75.0	0.25866	85.4	123.2
193.0	33.5	117.2	54.1	0.58650	15.1	73.9	77.6	0.21426	87.4	123.1
194.0	34.2	117.6	55.3	0.56861	14.9	71.2	80.2	0.17025	89.3	123.0
195.0	34.8	118.1	56.7	0.54843	14.7	68.8	82.8	0.12485	91.4	123.0

Figure 15. (Concluded)

5.4. PROCESSING OF GAUGE OUTPUT DATA

Figure 16 is a drawing of the timing functions and gauge outputs versus flight time for the two ionization gauges of the pitot probe. Gauge 1 provides the data for the early part of the flight and gauge 2 becomes the main gauge in the high altitude portion of the flight. Gauge output data are as shown in Figure 17. The calibration sequence, composed of five segments (see Figure 8), includes

(1) thermistor output

(2) 0V reference
(3) 5V reference
(4) 2.5V reference

} nominal values (real values are used)

(5) range indicator

The data formats are essential to the automatic processing of the data. The above mentioned information, along with the gauge output data, is contained in one channel for each gauge.

During the flight, a calibration sequence occurs automatically whenever there is a range change. This feature has been included in order to place the calibrations and housekeeping data where the data are lost because of range switches. When the gauge stops changing range, a calibration sequence occurs every 15 sec (nominal) as commanded by an internal free run timer.

The data from both gauges are processed in exactly the same way by means of a main program called PITOT, which has been written for the IBM 360/67. The procedure for processing data from a gauge is as follows.

First, the program is supplied with the following input data:

(1) trajectory information (stored in disc file),

(2) gauge output data from the digital magnetic tape,

(3) gauge calibration table, and

(4) angle of attack versus flight time.

Tables included in the program are

(1) speed of sound from the U. S. Standard Atmosphere, 1962,

(2) geometry correction factor $\eta(\alpha,S)$, and

(3) transition number $K(\rho)$.

The program reads every data point from the digital tape after which a scan is performed which looks for a calibration sequence. When a calibration sequence is recognized by the program, a second order polynomial is fit through the three points. The data points between two calibration sequences are calibrated in terms of voltage with the aid of the fit polynomial. This procedure is repeated until all the data points are in the form of a calibrated voltage. At this point an impact pressure is associated to each data point by means of a calibration table lookup. This pressure is corrected for gauge temperature (gauge 1 only) which is a function of the gauge thermistor output included in the calibration sequence (Simmons, 1964).

The time interval corresponding to 250 meters in altitude is obtained from trajectory information. For this time interval, which varies along the trajectory, a straight line least squares fit of impact pressure versus time is computed. Impact pressure is then determined at the time of interest, which corresponds to an even quarter km point.

Mach number is then approximated by using velocity information from the trajectory data and the speed of sound is obtained from the U. S. Standard Atmosphere, 1962. Values of ρ_1 and ρ_2 are calculated by using Equations (4) and (13), respectively. For those times which are included within the table of angle of attack versus time given, the program will obtain an angle of attack by interpolation. The velocity ratio S is calculated from the approximated Mach number.

The geometry correction factor η is calculated by double entry interpolation in the geometry correction factor tables. After η and $\cos\alpha$ are obtained, they are applied to ρ_2 (see Equation (15)), and atmospheric density is obtained according to the free molecular flow theory.

At this point atmospheric density has been computed according to continuum flow theory, ρ_1, and according to free molecular flow theory, ρ_{fmf}. Atmospheric density in the transition region is then calculated by using Equation (16). An iterative procedure is used in this computation.

An abbreviated flow chart for PITOT is given in Figure 18. The printed output of the program has the format shown in Figure 19, and includes

(1) time from launch (TIME) in sec

(2) altitude (ALTITUDE) in km

(3) velocity (VELOCITY) in m/sec

(4) impact pressure corrected for gauge temperature (PRESSURE) in mmHg

(5) atmospheric density according to continuum flow theory (RHO 1) in kg/m^3

(6) ρ_2 according to Equation (13) (RHO 2) in kg/m^3

(7) angle of attack of the probe (ALPHA) in deg

(8) geometry and angle of attack correction factor $1/\eta \cos\alpha$ (CORR)

(9) atmospheric density according to free molecular flow theory (RHO2*CORR) in kg/m^3

(10) transition number (K)

(11) atmospheric density

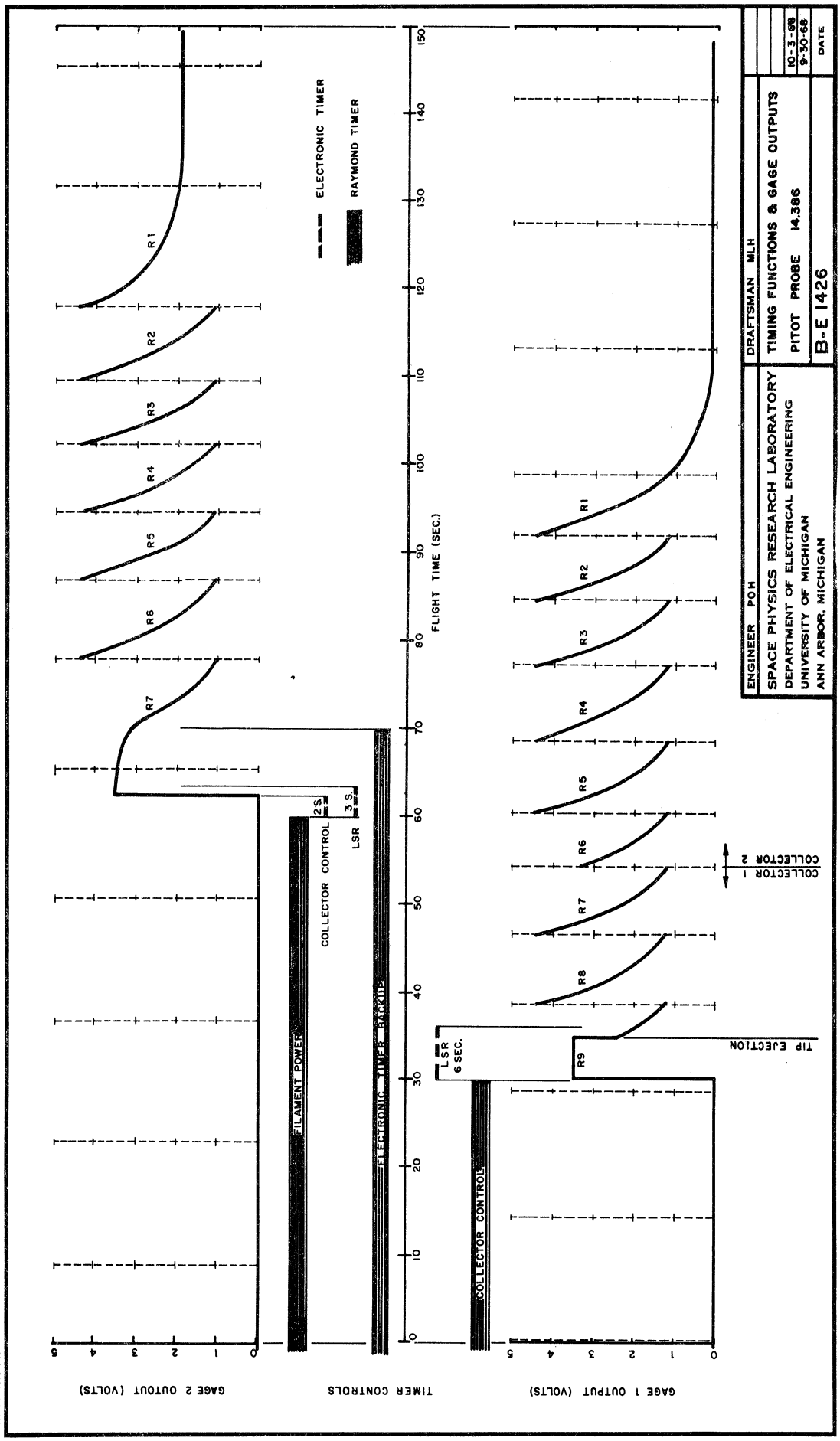

Figure 16. Timing functions and gauge output versus time.

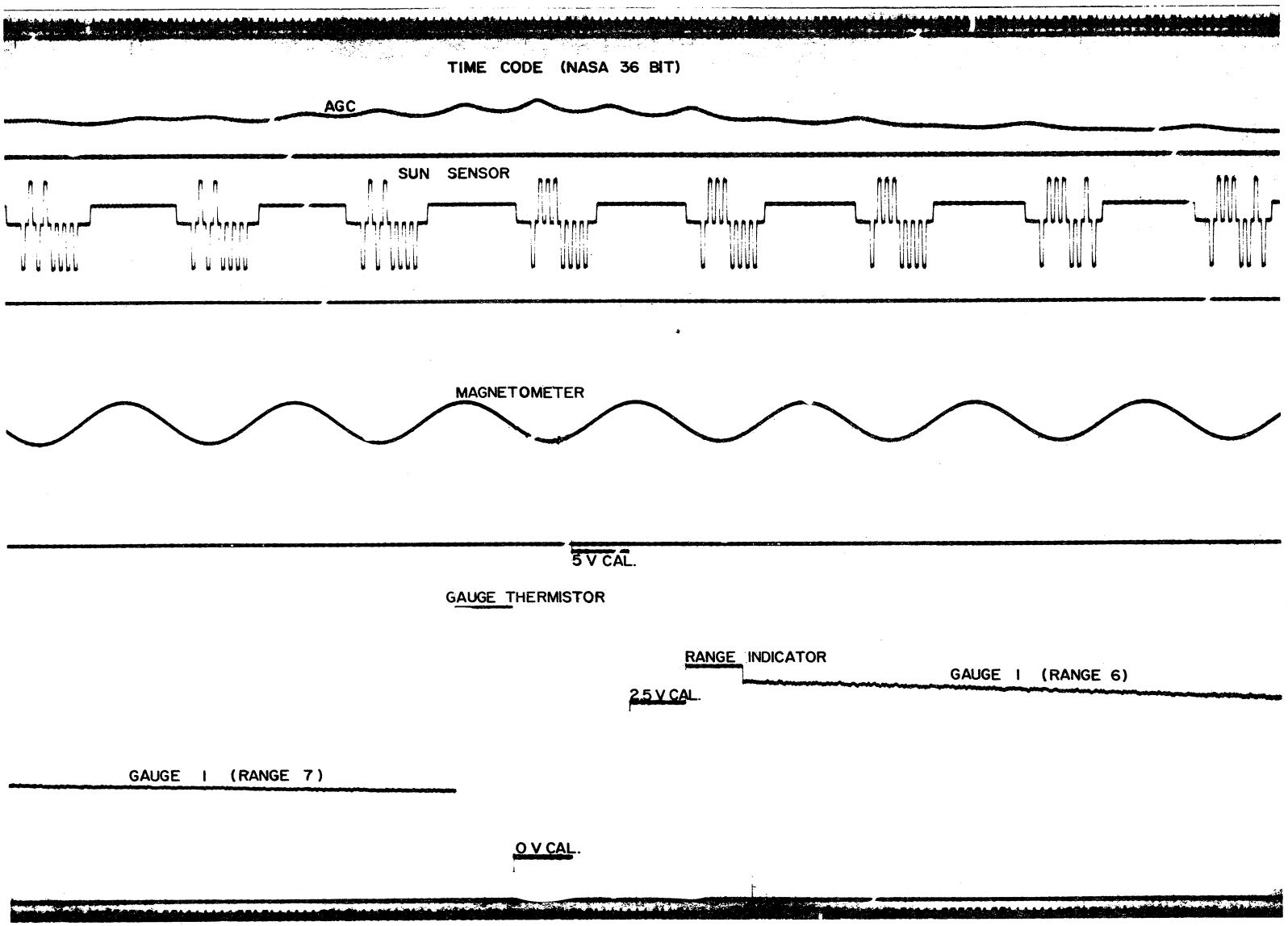

Figure 17. Analog oscillograph record of flight data.

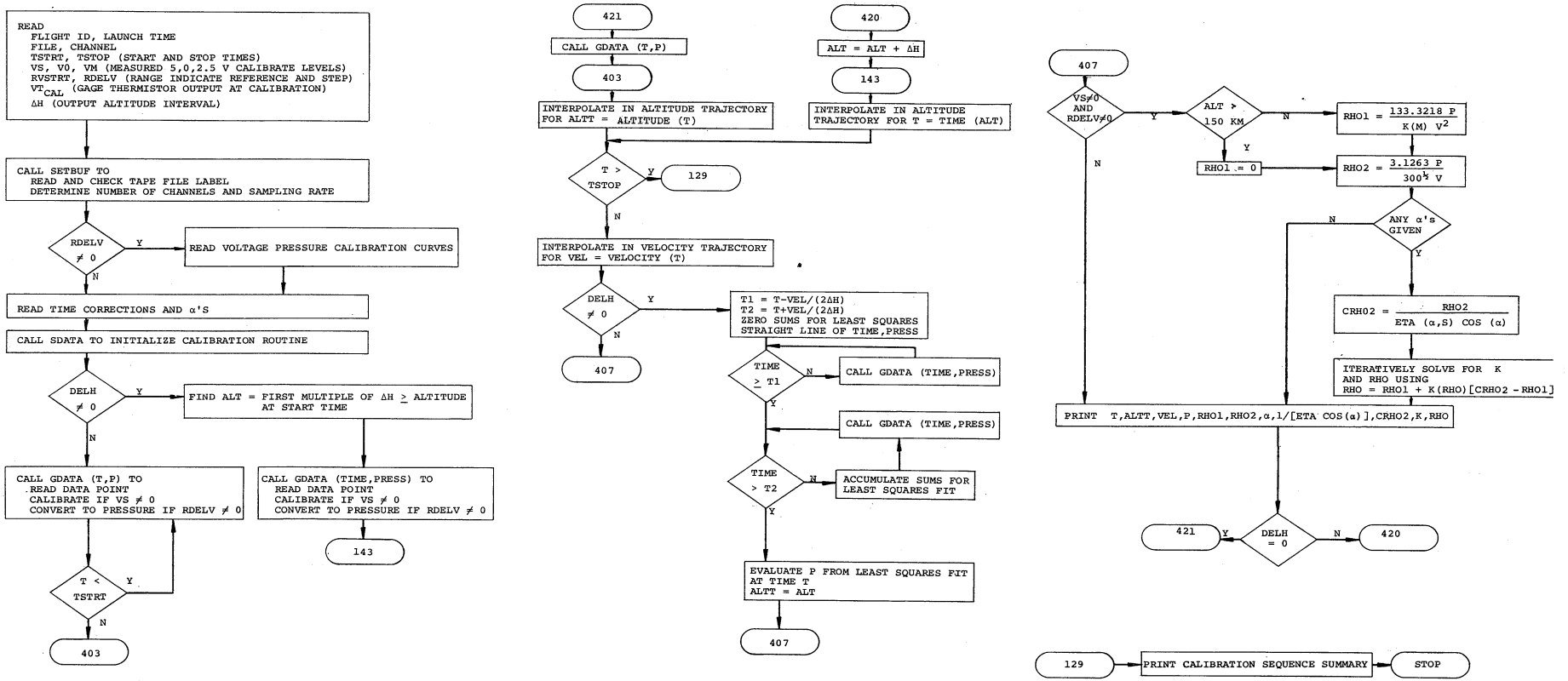

Figure 18. PITOT abbreviated flow chart.

SPACE PHYSICS RESEARCH LABORATORY
THE UNIVERSITY OF MICHIGAN
ANN ARBOR, MICHIGAN
17:46.11 DECEMBER 18,1969

NASA 14.386 GAGE 1 F
LAUNCH TIME: 20: 4:59.815 Z

INPUT FILE 1 CHANNEL INDEX 1
TAPE ID: SPRL NASA 14.386 12/12/69 8020 F1 08 Q

CALIBRATE LEVELS: 5.003 0.004 2.503

VTCAL: 3.700

RANGE 1 INDICATE: 0.500
STEP BETWEEN RANGES: 0.500

RANGE: 2

VOLTAGE	PRESSURE	VOLTAGE	PRESSURE	VOLTAGE	PRESSURE	VOLTAGE	PRESSURE	VOLTAGE	PRESSURE
0.900	8.300E-03	2.200	2.060E-02	3.500	3.420E-02	4.750	4.780E-02		

RANGE: 3

VOLTAGE	PRESSURE	VOLTAGE	PRESSURE	VOLTAGE	PRESSURE	VOLTAGE	PRESSURE	VOLTAGE	PRESSURE
0.890	3.550E-02	2.190	9.100E-02	3.490	1.460E-01	4.740	1.980E-01		

RANGE: 4

VOLTAGE	PRESSURE	VOLTAGE	PRESSURE	VOLTAGE	PRESSURE	VOLTAGE	PRESSURE	VOLTAGE	PRESSURE
0.900	1.510E-01	2.190	3.750E-01	3.500	6.000E-01	4.750	8.180E-01		

RANGE: 5

VOLTAGE	PRESSURE	VOLTAGE	PRESSURE	VOLTAGE	PRESSURE	VOLTAGE	PRESSURE	VOLTAGE	PRESSURE
0.890	6.200E-01	2.190	1.520E 00	3.490	2.420E 00	4.740	3.300E 00		

RANGE: 6

VOLTAGE	PRESSURE	VOLTAGE	PRESSURE	VOLTAGE	PRESSURE	VOLTAGE	PRESSURE	VOLTAGE	PRESSURE
0.900	2.480E 00	2.200	6.110E 00	3.500	9.850E 00	4.750	1.360E 01		

RANGE: 7

VOLTAGE	PRESSURE	VOLTAGE	PRESSURE	VOLTAGE	PRESSURE	VOLTAGE	PRESSURE	VOLTAGE	PRESSURE
0.890	7.200E 00	2.190	1.750E 01	3.490	2.800E 01	4.740	3.810E 01		

RANGE: 8

VOLTAGE	PRESSURE	VOLTAGE	PRESSURE	VOLTAGE	PRESSURE	VOLTAGE	PRESSURE	VOLTAGE	PRESSURE
0.900	2.870E 01	2.000	6.390E 01	3.100	9.940E 01	4.750	1.530E 02		

RANGE: 9

VOLTAGE	PRESSURE	VOLTAGE	PRESSURE	VOLTAGE	PRESSURE	VOLTAGE	PRESSURE	VOLTAGE	PRESSURE
0.890	1.170E 02	1.790	2.410E 02	2.690	3.710E 02	3.590	5.100E 02		

TIME CORRECTIONS

0.0	0.0	500.000	0.0

Figure 19. PITOT output format.

TIME	ALTITUDE	VELOCITY	PRESSURE	RHO1	RHO2	ALPHA	CORR	RHO2*CORR	K	RHO
36.101	30.000	1547.9	2.946E 02	1.758E-02	3.435E-02					
36.265	30.250	1545.4	2.827E 02	1.693E-02	3.302E-02					
36.431	30.500	1543.1	2.683E 02	1.611E-02	3.139E-02					
36.596	30.750	1540.7	2.556E 02	1.539E-02	2.994E-02					
36.762	31.000	1538.4	2.461E 02	1.487E-02	2.887E-02					
36.927	31.250	1536.0	2.364E 02	1.433E-02	2.778E-02					
37.093	31.500	1533.7	2.267E 02	1.378E-02	2.668E-02					
37.258	31.750	1531.4	2.167E 02	1.321E-02	2.554E-02					
37.425	32.000	1529.2	2.069E 02	1.265E-02	2.442E-02					
37.592	32.250	1526.9	1.974E 02	1.210E-02	2.333E-02					
37.759	32.500	1524.7	1.895E 02	1.165E-02	2.244E-02					
37.926	32.750	1522.5	1.825E 02	1.125E-02	2.164E-02					
38.093	33.000	1520.3	1.773E 02	1.097E-02	2.106E-02					
38.260	33.250	1518.1	1.697E 02	1.052E-02	2.018E-02					
38.429	33.500	1515.9	1.626E 02	1.011E-02	1.937E-02					
38.597	33.750	1513.7	1.551E 02	9.671E-03	1.849E-02					
38.765	34.000	1511.6	1.463E 02	9.147E-03	1.747E-02					
38.934	34.250	1509.4	1.397E 02	8.758E-03	1.670E-02					
39.441	35.000	1503.1	1.258E 02	7.952E-03	1.511E-02					
39.611	35.250	1501.0	1.220E 02	7.732E-03	1.467E-02					
39.781	35.500	1499.0	1.177E 02	7.476E-03	1.417E-02					
39.950	35.750	1496.9	1.129E 02	7.194E-03	1.361E-02					
40.120	36.000	1494.9	1.091E 02	6.972E-03	1.318E-02					
40.291	36.250	1492.9	1.008E 02	6.457E-03	1.219E-02					
40.462	36.500	1491.0	1.002E 02	6.435E-03	1.213E-02					
40.633	36.750	1489.1	9.548E 01	6.145E-03	1.157E-02					
40.805	37.000	1487.2	9.119E 01	5.884E-03	1.107E-02					
40.976	37.250	1485.3	8.792E 01	5.687E-03	1.068E-02					
41.147	37.500	1483.4	8.482E 01	5.500E-03	1.032E-02					
41.319	37.750	1481.6	8.198E 01	5.329E-03	9.988E-03					
41.492	38.000	1479.7	7.874E 01	5.130E-03	9.605E-03					
41.664	38.250	1477.8	7.524E 01	4.915E-03	9.189E-03					
41.836	38.500	1476.0	7.227E 01	4.732E-03	8.837E-03					
42.009	38.750	1474.1	6.877E 01	4.514E-03	8.421E-03					
42.181	39.000	1472.2	6.613E 01	4.351E-03	8.108E-03					
42.355	39.250	1470.4	6.357E 01	4.193E-03	7.804E-03					
42.529	39.500	1468.6	6.078E 01	4.018E-03	7.470E-03					
42.703	39.750	1466.8	5.840E 01	3.870E-03	7.186E-03					
42.876	40.000	1465.0	5.611E 01	3.727E-03	6.913E-03					
43.050	40.250	1463.2	5.411E 01	3.603E-03	6.675E-03					
43.224	40.500	1461.4	5.187E 01	3.462E-03	6.406E-03					
43.399	40.750	1459.6	5.010E 01	3.352E-03	6.196E-03					
43.575	41.000	1457.7	4.738E 01	3.177E-03	5.866E-03					
43.750	41.250	1455.9	4.510E 01	3.032E-03	5.591E-03					
43.925	41.500	1454.1	4.344E 01	2.927E-03	5.392E-03					
44.100	41.750	1452.3	4.206E 01	2.842E-03	5.228E-03					
44.276	42.000	1450.5	4.048E 01	2.741E-03	5.038E-03					
44.452	42.250	1448.7	3.898E 01	2.646E-03	4.857E-03					
44.629	42.500	1446.9	3.752E 01	2.553E-03	4.681E-03					
44.805	42.750	1445.1	3.626E 01	2.473E-03	4.529E-03					
44.982	43.000	1443.3	3.482E 01	2.380E-03	4.354E-03					

Figure 19. (Continued)

TIME	ALTITUDE	VELOCITY	PRESSURE	RHO1	RHO2	ALPHA	CORR	RHO2*CORR	K	RHO
45.158	43.250	1441.5	3.357E C1	2.300E-03	4.203E-03					
45.335	43.500	1439.7	3.242E 01	2.227E-03	4.065E-03					
45.690	44.000	1436.2	3.035E C1	2.095E-03	3.814E-03					
45.867	44.250	1434.4	2.930E C1	2.027E-03	3.686E-03					
46.045	44.500	1432.7	2.828E C1	1.961E-03	3.563E-03					
46.222	44.750	1430.9	2.752E C1	1.913E-03	3.472E-03					
46.401	45.000	1429.2	2.613E C1	1.820E-03	3.300E-03					
46.580	45.250	1427.5	2.574E C1	1.797E-03	3.254E-03					
46.759	45.500	1425.7	2.496E C1	1.747E-03	3.160E-03					
46.938	45.750	1424.0	2.408E C1	1.690E-03	3.052E-03					
47.117	46.000	1422.2	2.319E C1	1.631E-03	2.944E-03					
47.296	46.250	1420.5	2.228E C1	1.571E-03	2.831E-03					
47.477	46.500	1418.7	2.161E C1	1.527E-03	2.749E-03					
47.657	46.750	1417.0	2.097E 01	1.486E-03	2.672E-03					
47.837	47.000	1415.2	2.033E C1	1.443E-03	2.593E-03					
48.017	47.250	1413.4	1.955E 01	1.391E-03	2.496E-03					
48.197	47.500	1411.7	1.888E C1	1.347E-03	2.414E-03					
48.379	47.750	1409.9	1.816E C1	1.299E-03	2.325E-03					
48.560	48.000	1408.1	1.762E C1	1.263E-03	2.259E-03					
48.742	48.250	1406.3	1.705E C1	1.225E-03	2.188E-03					
48.923	48.500	1404.6	1.634E C1	1.177E-03	2.100E-03					
49.104	48.750	1402.8	1.563E C1	1.129E-03	2.011E-03					
49.286	49.000	1401.0	1.508E C1	1.092E-03	1.943E-03					
49.469	49.250	1399.2	1.455E C1	1.056E-03	1.877E-03					
49.652	49.500	1397.5	1.398E C1	1.017E-03	1.805E-03					
49.835	49.750	1395.7	1.343E C1	9.793E-04	1.736E-03					
50.018	50.000	1393.9	1.303E C1	9.528E-04	1.687E-03					
50.201	50.250	1392.1	1.270E C1	9.308E-04	1.646E-03					
50.385	50.500	1390.3	1.233E C1	9.065E-04	1.601E-03					
50.569	50.750	1388.6	1.196E 01	8.815E-04	1.555E-03					
50.753	51.000	1386.8	1.154E C1	8.525E-04	1.502E-03					
50.937	51.250	1385.0	1.114E 01	8.248E-04	1.452E-03					
51.121	51.500	1383.2	1.079E C1	8.009E-04	1.408E-03					
51.306	51.750	1381.4	1.045E C1	7.780E-04	1.366E-03					
51.491	52.000	1379.7	1.013E 01	7.556E-04	1.325E-03					
51.677	52.250	1377.9	9.767E 00	7.306E-04	1.279E-03					
51.862	52.500	1376.1	9.470E 00	7.101E-04	1.242E-03					
52.048	52.750	1374.4	9.117E 00	6.854E-04	1.197E-03					
52.233	53.000	1372.6	8.782E 00	6.619E-04	1.155E-03					
52.420	53.250	1370.8	8.487E 00	6.412E-04	1.117E-03					
52.607	53.500	1369.1	8.168E 00	6.188E-04	1.077E-03					
52.981	54.000	1365.5	7.576E 00	5.769E-04	1.001E-03					
53.168	54.250	1363.7	7.357E 00	5.616E-04	9.737E-04					
53.356	54.500	1361.9	7.101E 00	5.436E-04	9.411E-04					
53.544	54.750	1360.1	6.874E 00	5.276E-04	9.122E-04					
53.732	55.000	1358.2	6.585E 00	5.068E-04	8.751E-04					
53.920	55.250	1356.4	6.312E 00	4.871E-04	8.400E-04					
54.108	55.500	1354.5	6.088E 00	4.711E-04	8.113E-04					
54.297	55.750	1352.7	5.899E 00	4.577E-04	7.872E-04					
54.487	56.000	1350.9	5.698E 00	4.433E-04	7.614E-04					
54.676	56.250	1349.1	5.518E 00	4.304E-04	7.382E-04					

Figure 19. (Continued)

TIME	ALTITUDE	VELOCITY	PRESSURE	RHO1	RHO2	ALPHA	CORR	RHO2*CORR	K	RHO
54.866	56.500	1347.2	5.325E CO	4.165E-04	7.135E-04					
55.055	56.750	1345.4	5.154E CO	4.041E-04	6.914E-04					
55.245	57.000	1343.6	4.983E CO	3.903E-04	6.667E-04					
55.436	57.250	1341.8	4.797E CO	3.782E-04	6.453E-04					
55.627	57.500	1340.1	4.639E CO	3.667E-04	6.248E-04					
55.818	57.750	1338.3	4.501E CO	3.567E-04	6.070E-04					
56.009	58.000	1336.5	4.569E CO	3.631E-04	6.170E-04					
56.200	58.250	1334.7	4.221E CO	3.363E-04	5.709E-04					
56.393	58.500	1332.9	4.091E CO	3.269E-04	5.540E-04					
56.585	58.750	1331.0	3.942E CO	3.158E-04	5.345E-04					
56.778	59.000	1329.2	3.775E CO	3.033E-04	5.127E-04					
56.971	59.250	1327.3	3.635E CO	2.928E-04	4.943E-04					
57.163	59.500	1325.5	3.530E CO	2.852E-04	4.807E-04					
57.357	59.750	1323.6	3.442E CO	2.788E-04	4.694E-04					
57.551	60.000	1321.8	3.327E CO	2.703E-04	4.543E-04					
57.744	60.250	1319.9	3.211E CO	2.615E-04	4.391E-04					
57.938	60.500	1318.1	3.114E CO	2.544E-04	4.264E-04					
58.132	60.750	1316.2	3.024E CO	2.478E-04	4.148E-04					
58.327	61.000	1314.3	2.931E CO	2.408E-04	4.025E-04					
58.522	61.250	1312.5	2.789E CO	2.298E-04	3.836E-04					
58.913	61.750	1308.8	2.655E CO	2.200E-04	3.652E-04					
59.109	62.000	1306.9	2.561E CO	2.127E-04	3.537E-04					
59.305	62.250	1305.0	2.463E CO	2.052E-04	3.407E-04					
59.502	62.500	1303.2	2.297E CO	1.919E-04	3.181E-04					
59.696	62.750	1301.3	2.285E CO	1.915E-04	3.169E-04					
59.895	63.000	1299.4	2.206E CO	1.854E-04	3.064E-04					
60.092	63.250	1297.6	2.135E CO	1.799E-04	2.970E-04					
60.290	63.500	1295.7	2.060E CO	1.741E-04	2.869E-04					
60.488	63.750	1293.9	1.993E CO	1.690E-04	2.781E-04					
60.686	64.000	1292.0	1.919E CO	1.632E-04	2.681E-04					
60.885	64.250	1290.2	1.856E CO	1.583E-04	2.597E-04					
61.083	64.500	1288.3	1.795E CO	1.535E-04	2.514E-04					
61.282	64.750	1286.5	1.715E CO	1.471E-04	2.407E-04					
61.482	65.000	1284.6	1.658E CO	1.426E-04	2.329E-04					
61.682	65.250	1282.7	1.609E CO	1.388E-04	2.264E-04					
61.882	65.500	1280.8	1.555E CO	1.345E-04	2.191E-04					
62.082	65.750	1278.9	1.501E CO	1.302E-04	2.118E-04					
62.282	66.000	1277.1	1.451E CO	1.263E-04	2.051E-04					
62.484	66.250	1275.1	1.403E CO	1.225E-04	1.986E-04					
62.685	66.500	1273.2	1.357E CO	1.189E-04	1.924E-04					
62.887	66.750	1271.3	1.313E CO	1.153E-04	1.865E-04					
63.088	67.000	1269.4	1.269E CO	1.118E-04	1.804E-04					
63.290	67.250	1267.5	1.224E CO	1.081E-04	1.742E-04					
63.493	67.500	1265.6	1.177E CO	1.043E-04	1.678E-04					
63.696	67.750	1263.6	1.134E CO	1.008E-04	1.620E-04					
63.899	68.000	1261.7	1.089E CO	9.714E-05	1.558E-04					
64.102	68.250	1259.8	1.036E CO	9.264E-05	1.484E-04					
64.306	68.500	1257.8	9.887E-01	8.873E-05	1.419E-04					
64.511	68.750	1255.9	9.462E-01	8.517E-05	1.360E-04					
64.716	69.000	1254.0	9.089E-01	8.208E-05	1.308E-04					
64.921	69.250	1252.1	8.773E-01	7.946E-05	1.265E-04					

Figure 19. (Continued)

TIME	ALTITUDE	VELOCITY	PRESSURE	RHO1	RHO2	ALPHA	CORR	RHO2*CORR	K	RHO
65.125	69.500	1250.1	8.517E-01	7.739E-05	1.230E-04					
65.331	69.750	1248.2	8.207E-01	7.479E-05	1.187E-04					
65.537	70.000	1246.3	7.946E-01	7.265E-05	1.151E-04					
65.743	70.250	1244.4	7.686E-01	7.049E-05	1.115E-04					
65.950	70.500	1242.5	7.333E-01	6.746E-05	1.065E-04					
66.363	71.000	1238.6	6.972E-01	6.454E-05	1.016E-04					
66.571	71.250	1236.7	6.602E-01	6.131E-05	9.636E-05					
66.779	71.500	1234.8	6.346E-01	5.912E-05	9.277E-05					
66.987	71.750	1232.9	6.126E-01	5.724E-05	8.968E-05					
67.195	72.000	1231.0	5.918E-01	5.548E-05	8.678E-05					
67.404	72.250	1229.1	5.659E-01	5.321E-05	8.311E-05					
67.614	72.500	1227.1	5.401E-01	5.095E-05	7.944E-05					
67.823	72.750	1225.2	5.317E-01	5.031E-05	7.833E-05					
68.033	73.000	1223.3	5.144E-01	4.884E-05	7.590E-05					
68.243	73.250	1221.3	4.954E-01	4.718E-05	7.321E-05					
68.454	73.500	1219.4	4.779E-01	4.566E-05	7.073E-05					
68.665	73.750	1217.4	4.594E-01	4.403E-05	6.811E-05					
68.876	74.000	1215.4	4.424E-01	4.255E-05	6.570E-05					
69.088	74.250	1213.5	4.078E-01	3.934E-05	6.065E-05					
69.300	74.500	1211.5	3.861E-01	3.738E-05	5.753E-05					
69.512	74.750	1209.5	3.664E-01	3.558E-05	5.468E-05					
69.725	75.000	1207.6	3.411E-01	3.324E-05	5.098E-05					
69.938	75.250	1205.6	3.159E-01	3.089E-05	4.730E-05					
70.151	75.500	1203.6	2.978E-01	2.921E-05	4.466E-05	3.255	0.951	4.249E-05	0.0	2.921E-05
70.365	75.750	1201.6	2.842E-01	2.797E-05	4.268E-05	3.190	0.951	4.061E-05	0.0	2.797E-05
70.580	76.000	1199.6	2.728E-01	2.694E-05	4.104E-05	3.126	0.952	3.906E-05	0.0	2.694E-05
70.795	76.250	1197.7	2.606E-01	2.581E-05	3.927E-05	3.062	0.952	3.737E-05	0.0	2.581E-05
71.009	76.500	1195.7	2.466E-01	2.451E-05	3.722E-05	2.997	0.952	3.544E-05	0.0	2.451E-05
71.224	76.750	1193.7	2.334E-01	2.328E-05	3.529E-05	2.933	0.952	3.360E-05	0.0	2.328E-05
71.441	77.000	1191.7	2.241E-01	2.243E-05	3.395E-05	2.868	0.952	3.233E-05	0.0	2.243E-05
71.657	77.250	1189.7	2.160E-01	2.169E-05	3.277E-05	2.803	0.952	3.121E-05	0.0	2.169E-05
71.873	77.500	1187.7	2.080E-01	2.096E-05	3.162E-05	2.738	0.953	3.012E-05	0.0	2.096E-05
72.090	77.750	1185.7	2.001E-01	2.023E-05	3.046E-05	2.678	0.953	2.902E-05	0.0	2.023E-05
72.307	78.000	1183.6	1.920E-01	1.948E-05	2.928E-05	2.623	0.953	2.791E-05	0.0	1.948E-05
72.525	78.250	1181.6	1.829E-01	1.862E-05	2.794E-05	2.569	0.953	2.663E-05	0.0	1.862E-05
72.743	78.500	1179.6	1.742E-01	1.779E-05	2.665E-05	2.514	0.953	2.541E-05	0.0	1.779E-05
73.180	79.000	1175.5	1.618E-01	1.665E-05	2.484E-05	2.405	0.954	2.369E-05	0.001	1.665E-05
73.400	79.250	1173.5	1.563E-01	1.613E-05	2.404E-05	2.350	0.954	2.292E-05	0.001	1.614E-05
73.620	79.500	1171.4	1.512E-01	1.567E-05	2.330E-05	2.295	0.954	2.223E-05	0.002	1.568E-05
73.840	79.750	1169.4	1.459E-01	1.517E-05	2.252E-05	2.240	0.954	2.148E-05	0.003	1.519E-05
74.060	80.000	1167.3	1.377E-01	1.437E-05	2.129E-05	2.197	0.954	2.032E-05	0.005	1.440E-05
74.281	80.250	1165.3	1.309E-01	1.371E-05	2.028E-05	2.186	0.954	1.935E-05	0.006	1.375E-05
74.502	80.500	1163.2	1.291E-01	1.357E-05	2.003E-05	2.175	0.955	1.912E-05	0.006	1.360E-05
74.724	80.750	1161.2	1.250E-01	1.318E-05	1.943E-05	2.164	0.954	1.855E-05	0.007	1.322E-05
74.946	81.000	1159.1	1.208E-01	1.278E-05	1.881E-05	2.153	0.954	1.795E-05	0.009	1.283E-05
75.168	81.250	1157.0	1.163E-01	1.235E-05	1.814E-05	2.142	0.954	1.731E-05	0.011	1.240E-05
75.392	81.500	1155.0	1.119E-01	1.193E-05	1.749E-05	2.130	0.954	1.669E-05	0.013	1.199E-05
75.615	81.750	1152.9	1.068E-01	1.142E-05	1.671E-05	2.119	0.954	1.594E-05	0.016	1.149E-05
75.839	82.000	1150.8	1.010E-01	1.084E-05	1.584E-05	2.108	0.954	1.510E-05	0.018	1.092E-05
76.063	82.250	1148.7	9.669E-02	1.042E-05	1.519E-05	2.109	0.954	1.449E-05	0.021	1.050E-05
76.288	82.500	1146.6	9.207E-02	9.953E-06	1.449E-05	2.143	0.953	1.382E-05	0.023	1.004E-05

Figure 19. (Continued)

TIME	ALTITUDE	VELOCITY	PRESSURE	RHO1	RHO2	ALPHA	CORR	RHO2*CORR	K	RHO
76.513	82.750	1144.5	8.867E-02	9.619E-06	1.398E-05	2.177	0.953	1.333E-05	0.025	9.711E-06
76.739	83.000	1142.4	8.594E-02	9.357E-06	1.358E-05	2.211	0.953	1.294E-05	0.026	9.451E-06
76.965	83.250	1140.3	8.286E-02	9.055E-06	1.312E-05	2.245	0.953	1.250E-05	0.028	9.151E-06
77.191	83.500	1138.2	8.003E-02	8.777E-06	1.269E-05	2.279	0.952	1.209E-05	0.030	8.876E-06
77.418	83.750	1136.1	7.738E-02	8.518E-06	1.229E-05	2.313	0.952	1.171E-05	0.032	8.620E-06
77.646	84.000	1134.0	7.492E-02	8.277E-06	1.193E-05	2.347	0.952	1.135E-05	0.034	8.381E-06
77.874	84.250	1131.9	7.252E-02	8.041E-06	1.156E-05	2.381	0.952	1.101E-05	0.036	8.147E-06
78.102	84.500	1129.8	6.972E-02	7.759E-06	1.114E-05	2.431	0.952	1.060E-05	0.038	7.867E-06
78.331	84.750	1127.6	6.674E-02	7.455E-06	1.068E-05	2.499	0.951	1.016E-05	0.041	7.566E-06
78.560	85.000	1125.5	6.347E-02	7.116E-06	1.018E-05	2.568	0.951	9.680E-06	0.044	7.229E-06
78.790	85.250	1123.3	5.955E-02	6.701E-06	9.569E-06	2.637	0.951	9.098E-06	0.048	6.817E-06
79.020	85.500	1121.2	5.567E-02	6.288E-06	8.962E-06	2.706	0.951	8.518E-06	0.053	6.406E-06
79.250	85.750	1119.1	5.179E-02	5.872E-06	8.354E-06	2.775	0.950	7.938E-06	0.058	5.992E-06
79.482	86.000	1116.9	4.852E-02	5.522E-06	7.841E-06	2.845	0.950	7.450E-06	0.063	5.644E-06
79.714	86.250	1114.8	4.601E-02	5.256E-06	7.449E-06	2.914	0.950	7.075E-06	0.067	5.378E-06
79.946	86.500	1112.6	4.438E-02	5.089E-06	7.199E-06	2.984	0.950	6.836E-06	0.070	5.211E-06
80.178	86.750	1110.4	4.311E-02	4.962E-06	7.008E-06	3.170	0.949	6.651E-06	0.072	5.084E-06
80.645	87.250	1106.1	3.948E-02	4.579E-06	6.442E-06	3.619	0.948	6.110E-06	0.080	4.701E-06
80.879	87.500	1103.9	3.757E-02	4.375E-06	6.144E-06	3.844	0.948	5.824E-06	0.084	4.497E-06
81.113	87.750	1101.7	3.607E-02	4.216E-06	5.909E-06	4.068	0.948	5.600E-06	0.088	4.337E-06
81.348	88.000	1099.5	3.480E-02	4.084E-06	5.713E-06	4.294	0.947	5.412E-06	0.091	4.204E-06
81.584	88.250	1097.3	3.332E-02	3.926E-06	5.481E-06	4.521	0.947	5.191E-06	0.094	4.045E-06
81.820	88.500	1095.1	3.181E-02	3.762E-06	5.243E-06	4.747	0.947	4.964E-06	0.098	3.880E-06
82.056	88.750	1092.9	3.066E-02	3.641E-06	5.063E-06	4.974	0.947	4.793E-06	0.101	3.757E-06
82.293	89.000	1090.7	3.011E-02	3.590E-06	4.984E-06	5.201	0.946	4.716E-06	0.103	3.706E-06
82.531	89.250	1088.5	2.877E-02	3.444E-06	4.771E-06	5.430	0.946	4.514E-06	0.107	3.557E-06
82.769	89.500	1086.2	2.754E-02	3.309E-06	4.576E-06	5.659	0.946	4.328E-06	0.111	3.422E-06
83.008	89.750	1084.0	2.648E-02	3.195E-06	4.410E-06	5.887	0.946	4.170E-06	0.115	3.308E-06
83.246	90.000	1081.8	2.538E-02	3.074E-06	4.234E-06	6.116	0.946	4.004E-06	0.119	3.185E-06
83.487	90.250	1079.6	2.450E-02	2.980E-06	4.096E-06	6.347	0.945	3.872E-06	0.123	3.089E-06
83.727	90.500	1077.3	2.346E-02	2.865E-06	3.930E-06	6.578	0.945	3.715E-06	0.127	2.973E-06
83.967	90.750	1075.1	2.257E-02	2.768E-06	3.789E-06	6.809	0.945	3.582E-06	0.131	2.875E-06
84.208	91.000	1072.9	2.159E-02	2.658E-06	3.633E-06	7.039	0.945	3.433E-06	0.136	2.764E-06
84.450	91.250	1070.6	2.060E-02	2.547E-06	3.473E-06	7.272	0.945	3.282E-06	0.142	2.651E-06
84.693	91.500	1068.4	1.978E-02	2.455E-06	3.342E-06	7.505	0.945	3.158E-06	0.147	2.558E-06
84.936	91.750	1066.1	1.883E-02	2.346E-06	3.188E-06	7.738	0.945	3.011E-06	0.154	2.448E-06
85.179	92.000	1063.8	1.808E-02	2.262E-06	3.067E-06	7.832	0.944	2.897E-06	0.160	2.363E-06
85.423	92.250	1061.7	1.723E-02	2.164E-06	2.929E-06	7.876	0.944	2.767E-06	0.167	2.265E-06
85.668	92.500	1059.5	1.667E-02	2.102E-06	2.840E-06	7.920	0.944	2.682E-06	0.172	2.202E-06
85.913	92.750	1057.3	1.599E-02	2.025E-06	2.731E-06	7.964	0.944	2.578E-06	0.178	2.123E-06
86.157	93.000	1055.1	1.541E-02	1.958E-06	2.636E-06	8.008	0.944	2.488E-06	0.185	2.056E-06
86.404	93.250	1052.9	1.492E-02	1.904E-06	2.558E-06	8.053	0.944	2.414E-06	0.191	2.001E-06
86.651	93.500	1050.6	1.427E-02	1.828E-06	2.452E-06	8.097	0.944	2.314E-06	0.199	1.925E-06
86.898	93.750	1048.4	1.364E-02	1.755E-06	2.349E-06	8.142	0.944	2.216E-06	0.208	1.851E-06
87.145	94.000	1046.1	1.294E-02	1.671E-06	2.232E-06	8.186	0.943	2.105E-06	0.219	1.766E-06

Figure 19. (Continued)

COMMUTATOR VALUES

TIME	CHL 1	CHL 4	CHL 5
35.275	4.153	2.503	4.448
39.365	4.142	2.503	4.077
45.675	4.113	2.503	3.462
52.896	4.092	2.503	3.102
58.846	4.076	2.503	2.493
66.387	4.047	2.503	2.148
73.127	4.027	2.503	1.528
80.587	4.002	2.503	1.157

ERROR RETURN

Figure 19. (Continued)

SPACE PHYSICS RESEARCH LABORATORY
THE UNIVERSITY OF MICHIGAN
ANN ARBOR, MICHIGAN
17:46.11 DECEMBER 18,1969

NASA 14.386 GAGE 1 F
LAUNCH TIME: 20: 4:59.815 Z

INPUT FILE 1 CHANNEL INDEX 1
TAPE ID: SPRL NASA 14.386 12712769 8020 F1 08 Q

CALIBRATE LEVELS: 5.003 0.004 2.503

VTCAL: 3.700

RANGE 1 INDICATE: 0.500
STEP BETWEEN RANGES: 0.500

RANGE: 2

VOLTAGE	PRESSURE	VOLTAGE	PRESSURE	VOLTAGE	PRESSURE	VOLTAGE	PRESSURE	VOLTAGE	PRESSURE
0.900	8.300E-03	2.200	2.060E-02	3.500	3.420E-02	4.750	4.780E-02		

RANGE: 3

VOLTAGE	PRESSURE	VOLTAGE	PRESSURE	VOLTAGE	PRESSURE	VOLTAGE	PRESSURE	VOLTAGE	PRESSURE
0.890	3.550E-02	2.190	9.100E-02	3.490	1.460E-01	4.740	1.980E-01		

RANGE: 4

VOLTAGE	PRESSURE	VOLTAGE	PRESSURE	VOLTAGE	PRESSURE	VOLTAGE	PRESSURE	VOLTAGE	PRESSURE
0.900	1.510E-01	2.190	3.750E-01	3.500	6.000E-01	4.750	8.180E-01		

RANGE: 5

VOLTAGE	PRESSURE	VOLTAGE	PRESSURE	VOLTAGE	PRESSURE	VOLTAGE	PRESSURE	VOLTAGE	PRESSURE
0.890	6.200E-01	2.190	1.520E 00	3.490	2.420E 00	4.740	3.300E 00		

RANGE: 6

VOLTAGE	PRESSURE	VOLTAGE	PRESSURE	VOLTAGE	PRESSURE	VOLTAGE	PRESSURE	VOLTAGE	PRESSURE
0.900	2.480E 00	2.200	6.110E 00	3.500	9.850E 00	4.750	1.360E 01		

RANGE: 7

VOLTAGE	PRESSURE	VOLTAGE	PRESSURE	VOLTAGE	PRESSURE	VOLTAGE	PRESSURE	VOLTAGE	PRESSURE
0.890	7.200E 00	2.190	1.750E 01	3.490	2.800E 01	4.740	3.810E 01		

RANGE: 8

VOLTAGE	PRESSURE	VOLTAGE	PRESSURE	VOLTAGE	PRESSURE	VOLTAGE	PRESSURE	VOLTAGE	PRESSURE
0.900	2.870E 01	2.000	6.390E 01	3.100	9.940E 01	4.750	1.530E 02		

RANGE: 9

VOLTAGE	PRESSURE	VOLTAGE	PRESSURE	VOLTAGE	PRESSURE	VOLTAGE	PRESSURE	VOLTAGE	PRESSURE
0.890	1.170E 02	1.790	2.410E 02	2.690	3.710E 02	3.590	5.100E 02		

TIME CORRECTIONS

0.0 0.0 500.000 0.0

Figure 19. (Continued)

TIME	ALTITUDE	VELOCITY	PRESSURE	RHO1	RHO2	ALPHA	CORR	RHO2*CORR	K	RHO
81.348	88.000	1099.5	3.462E-02	4.062E-06	5.683E-06	4.294	0.947	5.384E-06	0.091	4.183E-06
81.584	88.250	1097.3	3.349E-02	3.945E-06	5.509E-06	4.521	0.947	5.217E-06	0.094	4.065E-06
81.820	88.500	1095.1	3.233E-02	3.824E-06	5.329E-06	4.747	0.947	5.046E-06	0.096	3.942E-06
82.056	88.750	1092.9	3.122E-02	3.708E-06	5.156E-06	4.974	0.947	4.881E-06	0.100	3.824E-06
82.293	89.000	1090.7	3.020E-02	3.601E-06	4.998E-06	5.201	0.946	4.730E-06	0.102	3.717E-06
82.531	89.250	1088.5	2.883E-02	3.451E-06	4.781E-06	5.430	0.946	4.523E-06	0.106	3.565E-06
82.769	89.500	1086.2	2.759E-02	3.315E-06	4.584E-06	5.659	0.946	4.336E-06	0.111	3.428E-06
83.008	89.750	1084.0	2.654E-02	3.203E-06	4.419E-06	5.887	0.946	4.180E-06	0.115	3.315E-06
83.246	90.000	1081.8	2.561E-02	3.102E-06	4.272E-06	6.116	0.946	4.040E-06	0.118	3.213E-06
83.487	90.250	1079.6	2.464E-02	2.998E-06	4.120E-06	6.347	0.945	3.896E-06	0.122	3.107E-06
83.727	90.500	1077.3	2.363E-02	2.885E-06	3.958E-06	6.578	0.945	3.742E-06	0.126	2.993E-06
83.967	90.750	1075.1	2.262E-02	2.773E-06	3.797E-06	6.809	0.945	3.589E-06	0.131	2.880E-06
84.208	91.000	1072.9	2.172E-02	2.674E-06	3.654E-06	7.039	0.945	3.453E-06	0.136	2.779E-06
84.450	91.250	1070.6	2.081E-02	2.573E-06	3.509E-06	7.272	0.945	3.316E-06	0.140	2.677E-06
84.693	91.500	1068.4	1.996E-02	2.477E-06	3.372E-06	7.505	0.945	3.185E-06	0.146	2.580E-06
84.936	91.750	1066.1	1.896E-02	2.362E-06	3.209E-06	7.738	0.945	3.032E-06	0.152	2.464E-06
85.179	92.000	1063.8	1.809E-02	2.263E-06	3.069E-06	7.832	0.944	2.899E-06	0.159	2.365E-06
85.423	92.250	1061.7	1.732E-02	2.176E-06	2.945E-06	7.876	0.944	2.782E-06	0.166	2.277E-06
85.668	92.500	1059.5	1.629E-02	2.054E-06	2.775E-06	7.920	0.944	2.620E-06	0.176	2.154E-06
85.913	92.750	1057.3	1.533E-02	1.941E-06	2.617E-06	7.964	0.944	2.471E-06	0.187	2.040E-06
86.157	93.000	1055.1	1.505E-02	1.912E-06	2.574E-06	8.008	0.944	2.430E-06	0.190	2.010E-06
86.404	93.250	1052.9	1.447E-02	1.847E-06	2.481E-06	8.053	0.944	2.341E-06	0.197	1.944E-06
86.651	93.500	1050.6	1.389E-02	1.780E-06	2.386E-06	8.097	0.944	2.252E-06	0.205	1.876E-06
86.898	93.750	1048.4	1.330E-02	1.711E-06	2.289E-06	8.142	0.944	2.160E-06	0.214	1.807E-06
87.145	94.000	1046.1	1.279E-02	1.652E-06	2.207E-06	8.186	0.943	2.082E-06	0.222	1.747E-06
87.394	94.250	1043.8	1.242E-02	1.611E-06	2.147E-06	8.231	0.943	2.025E-06	0.227	1.705E-06
87.644	94.500	1041.5	1.147E-02	1.495E-06	1.989E-06	8.276	0.943	1.875E-06	0.250	1.590E-06
87.893	94.750	1039.2	1.090E-02	1.425E-06	1.892E-06	8.321	0.943	1.785E-06	0.264	1.520E-06
88.142	95.000	1036.9	1.036E-02	1.362E-06	1.804E-06	8.366	0.943	1.701E-06	0.279	1.456E-06
88.394	95.250	1034.6	9.868E-03	1.302E-06	1.722E-06	8.411	0.943	1.623E-06	0.294	1.396E-06
88.645	95.500	1032.2	9.314E-03	1.234E-06	1.629E-06	8.456	0.943	1.535E-06	0.311	1.328E-06
88.897	95.750	1029.9	9.074E-03	1.208E-06	1.590E-06	8.502	0.942	1.499E-06	0.318	1.300E-06
89.149	96.000	1027.6	8.640E-03	1.155E-06	1.518E-06	8.547	0.942	1.430E-06	0.337	1.248E-06
89.403	96.250	1025.3	8.252E-03	1.108E-06	1.453E-06	8.593	0.942	1.369E-06	0.354	1.200E-06
89.657	96.500	1022.9	7.877E-03	1.062E-06	1.390E-06	8.638	0.942	1.309E-06	0.371	1.154E-06
89.911	96.750	1020.6	7.553E-03	1.023E-06	1.336E-06	8.684	0.942	1.258E-06	0.386	1.114E-06
90.166	97.000	1018.3	7.270E-03	9.885E-07	1.289E-06	8.760	0.942	1.214E-06	0.401	1.079E-06
90.422	97.250	1015.9	6.981E-03	9.535E-07	1.240E-06	8.852	0.942	1.168E-06	0.419	1.043E-06
90.679	97.500	1013.6	6.693E-03	9.181E-07	1.192E-06	8.944	0.942	1.123E-06	0.436	1.007E-06
90.935	97.750	1011.2	6.427E-03	8.856E-07	1.147E-06	9.037	0.942	1.081E-06	0.455	9.744E-07
91.192	98.000	1008.9	6.163E-03	8.528E-07	1.103E-06	9.129	0.942	1.039E-06	0.474	9.410E-07
91.451	98.250	1006.6	5.908E-03	8.213E-07	1.059E-06	9.222	0.942	9.982E-07	0.493	9.085E-07
91.710	98.500	1004.2	5.664E-03	7.908E-07	1.018E-06	9.316	0.942	9.593E-07	0.515	8.775E-07
91.969	98.750	1001.8	5.441E-03	7.631E-07	9.803E-07	9.409	0.942	9.238E-07	0.536	8.492E-07
92.229	99.000	999.5	5.218E-03	7.351E-07	9.424E-07	9.502	0.942	8.881E-07	0.557	8.203E-07
92.491	99.250	997.0	5.011E-03	7.092E-07	9.071E-07	9.597	0.943	8.550E-07	0.579	7.936E-07
92.752	99.500	994.6	4.809E-03	6.837E-07	8.727E-07	9.691	0.943	8.227E-07	0.607	7.680E-07
93.014	99.750	992.2	4.617E-03	6.596E-07	8.400E-07	9.785	0.943	7.919E-07	0.633	7.434E-07
93.277	100.000	989.7	4.425E-03	6.349E-07	8.069E-07	9.880	0.943	7.608E-07	0.660	7.181E-07
93.541	100.250	987.3	4.233E-03	6.103E-07	7.738E-07	9.975	0.943	7.297E-07	0.691	6.928E-07
93.806	100.500	984.9	4.039E-03	5.850E-07	7.402E-07	10.070	0.943	6.981E-07	0.732	6.678E-07

Figure 19. (Continued)

TIME	ALTITUDE	VELOCITY	PRESSURE	RHO1	RHO2	ALPHA	CORR	RHO2*CORR	K	RHO
94.070	100.750	982.4	3.840E-03	5.589E-07	7.056E-07	10.165	0.943	6.655E-07	0.777	6.418E-07
94.336	101.000	980.0	3.643E-03	5.325E-07	6.709E-07	10.261	0.943	6.329E-07	0.831	6.159E-07
94.603	101.250	977.6	3.435E-03	5.045E-07	6.342E-07	10.357	0.944	5.983E-07	0.891	5.881E-07
94.870	101.500	975.1	3.391E-03	5.004E-07	6.277E-07	10.453	0.944	5.923E-07	0.902	5.834E-07
95.137	101.750	972.7	3.004E-03	4.454E-07	5.575E-07	10.514	0.944	5.261E-07	1.000	5.261E-07
95.406	102.000	970.2	2.811E-03	4.186E-07	5.229E-07	10.541	0.944	4.934E-07	1.000	4.934E-07
95.676	102.250	967.8	2.633E-03	3.941E-07	4.911E-07	10.568	0.944	4.634E-07	1.000	4.634E-07
95.946	102.500	965.3	2.479E-03	3.728E-07	4.636E-07	10.595	0.944	4.375E-07	1.000	4.375E-07
96.348	102.750	961.6	2.203E-03	3.337E-07	4.135E-07	10.635	0.944	3.903E-07	1.000	3.903E-07
96.489	103.000	960.3	2.139E-03	3.248E-07	4.020E-07	10.649	0.944	3.794E-07	1.000	3.794E-07
96.762	103.250	957.8	2.002E-03	3.054E-07	3.772E-07	10.676	0.944	3.560E-07	1.000	3.560E-07
97.034	103.500	955.3	1.856E-03	2.846E-07	3.507E-07	10.703	0.944	3.310E-07	1.000	3.310E-07
97.308	103.750	952.7	1.711E-03	2.637E-07	3.242E-07	10.731	0.944	3.060E-07	1.000	3.060E-07
97.584	104.000	950.2	1.587E-03	2.458E-07	3.016E-07	10.758	0.944	2.846E-07	1.000	2.846E-07
97.860	104.250	947.7	1.480E-03	2.303E-07	2.819E-07	10.786	0.944	2.660E-07	1.000	2.660E-07
98.135	104.500	945.1	1.393E-03	2.179E-07	2.661E-07	10.814	0.944	2.511E-07	1.000	2.511E-07
98.413	104.750	942.6	1.320E-03	2.074E-07	2.527E-07	10.841	0.944	2.385E-07	1.000	2.385E-07
98.691	105.000	940.0	1.257E-03	1.985E-07	2.414E-07	10.869	0.944	2.278E-07	1.000	2.278E-07
98.970	105.250	937.5	1.215E-03	1.929E-07	2.339E-07	10.897	0.944	2.208E-07	1.000	2.208E-07
99.249	105.500	934.9	1.159E-03	1.850E-07	2.238E-07	10.925	0.944	2.114E-07	1.000	2.114E-07
99.530	105.750	932.3	1.158E-03	1.858E-07	2.242E-07	10.953	0.944	2.118E-07	1.000	2.118E-07
99.811	106.000	929.7	1.079E-03	1.739E-07	2.094E-07	10.981	0.945	1.978E-07	1.000	1.978E-07
100.093	106.250	927.1	1.042E-03	1.688E-07	2.028E-07	10.983	0.945	1.916E-07	1.000	1.916E-07
100.376	106.500	924.5	1.010E-03	1.645E-07	1.972E-07	10.932	0.944	1.862E-07	1.000	1.862E-07
100.660	106.750	921.9	9.762E-04	1.599E-07	1.911E-07	10.881	0.944	1.805E-07	1.000	1.805E-07
100.945	107.000	919.3	9.488E-04	1.562E-07	1.863E-07	10.830	0.944	1.759E-07	1.000	1.759E-07
101.229	107.250	916.7	9.190E-04	1.521E-07	1.810E-07	10.779	0.944	1.709E-07	1.000	1.709E-07
101.517	107.500	914.0	8.757E-04	1.457E-07	1.729E-07	10.727	0.944	1.633E-07	1.000	1.633E-07
101.804	107.750	911.4	8.487E-04	1.420E-07	1.681E-07	10.675	0.944	1.587E-07	1.000	1.587E-07
102.092	108.000	908.7	8.200E-04	1.379E-07	1.629E-07	10.623	0.944	1.537E-07	1.000	1.537E-07
102.381	108.250	906.1	7.892E-04	1.334E-07	1.572E-07	10.571	0.944	1.484E-07	1.000	1.484E-07
102.672	108.500	903.4	7.592E-04	1.290E-07	1.517E-07	10.519	0.944	1.432E-07	1.000	1.432E-07
102.963	108.750	900.8	7.340E-04	1.255E-07	1.471E-07	10.467	0.944	1.388E-07	1.000	1.388E-07
103.254	109.000	898.2	7.565E-04	1.300E-07	1.520E-07	10.414	0.944	1.434E-07	1.000	1.434E-07
103.548	109.250	895.5	6.863E-04	1.186E-07	1.383E-07	10.361	0.943	1.305E-07	1.000	1.305E-07
103.842	109.500	892.9	6.606E-04	1.147E-07	1.336E-07	10.308	0.943	1.260E-07	1.000	1.260E-07
104.136	109.750	890.2	6.348E-04	1.109E-07	1.287E-07	10.256	0.943	1.214E-07	1.000	1.214E-07
104.432	110.000	887.5	6.107E-04	1.072E-07	1.242E-07	10.202	0.943	1.171E-07	1.000	1.171E-07
104.729	110.250	884.9	5.869E-04	1.037E-07	1.197E-07	10.149	0.943	1.129E-07	1.000	1.129E-07
105.026	110.500	882.2	5.626E-04	9.990E-08	1.151E-07	10.093	0.943	1.085E-07	1.000	1.085E-07
105.325	110.750	879.5	5.294E-04	9.455E-08	1.086E-07	10.009	0.943	1.024E-07	1.000	1.024E-07
105.626	111.000	876.8	5.039E-04	9.043E-08	1.037E-07	9.925	0.943	9.777E-08	1.000	9.777E-08
105.926	111.250	874.2	4.717E-04	8.514E-08	9.739E-08	9.841	0.942	9.178E-08	1.000	9.178E-08
106.227	111.500	871.5	4.374E-04	7.935E-08	9.060E-08	9.756	0.942	8.537E-08	1.000	8.537E-08
106.531	111.750	868.7	4.061E-04	7.411E-08	8.437E-08	9.671	0.942	7.948E-08	1.000	7.948E-08
106.835	112.000	866.0	3.732E-04	6.846E-08	7.779E-08	9.586	0.942	7.327E-08	1.000	7.327E-08
107.139	112.250	863.2	3.435E-04	6.339E-08	7.183E-08	9.501	0.942	6.764E-08	1.000	6.764E-08
107.446	112.500	860.4	3.161E-04	5.865E-08	6.632E-08	9.415	0.942	6.245E-08	1.000	6.245E-08
107.753	112.750	857.6	2.919E-04	5.449E-08	6.144E-08	9.329	0.941	5.784E-08	1.000	5.784E-08
108.061	113.000	854.8	2.700E-04	5.065E-08	5.700E-08	9.243	0.941	5.365E-08	1.000	5.365E-08
108.370	113.250	852.0	2.511E-04	4.741E-08	5.320E-08	9.156	0.941	5.006E-08	1.000	5.006E-08

Figure 19. (Continued)

TIME	ALTITUDE	VELOCITY	PRESSURE	RHO1	RHO2	ALPHA	CORR	RHO2*CORR	K	RHO
108.681	113.500	849.3	2.344E-04	4.448E-08	4.982E-08	9.069	0.941	4.687E-08	1.000	4.687E-08
108.992	113.750	846.6	2.201E-04	4.203E-08	4.694E-08	8.982	0.941	4.415E-08	1.000	4.415E-08
109.304	114.000	843.8	2.081E-04	3.993E-08	4.450E-08	8.895	0.940	4.186E-08	1.000	4.186E-08
109.619	114.250	841.0	1.958E-04	3.781E-08	4.203E-08	8.807	0.940	3.952E-08	1.000	3.952E-08
109.934	114.500	838.2	1.864E-04	3.619E-08	4.014E-08	8.719	0.940	3.773E-08	1.000	3.773E-08
110.249	114.750	835.4	1.769E-04	3.457E-08	3.823E-08	8.635	0.940	3.594E-08	1.000	3.594E-08
110.567	115.000	832.6	1.688E-04	3.316E-08	3.660E-08	8.552	0.940	3.440E-08	1.000	3.440E-08
110.886	115.250	829.7	1.612E-04	3.186E-08	3.506E-08	8.470	0.940	3.295E-08	1.000	3.295E-08
111.204	115.500	826.9	1.547E-04	3.075E-08	3.378E-08	8.387	0.940	3.174E-08	1.000	3.174E-08
111.526	115.750	824.0	1.484E-04	2.968E-08	3.250E-08	8.303	0.940	3.054E-08	1.000	3.054E-08
111.849	116.000	821.2	1.429E-04	2.875E-08	3.141E-08	8.219	0.940	2.953E-08	1.000	2.953E-08
112.171	116.250	818.3	1.376E-04	2.787E-08	3.036E-08	8.136	0.940	2.853E-08	1.000	2.853E-08
112.497	116.500	815.4	1.330E-04	2.709E-08	2.945E-08	8.051	0.940	2.769E-08	1.000	2.769E-08
113.040	116.750	810.5	1.269E-04	2.612E-08	2.825E-08	7.910	0.940	2.656E-08	1.000	2.656E-08
113.149	117.000	809.5	1.256E-04	2.590E-08	2.801E-08	7.881	0.940	2.634E-08	1.000	2.634E-08
113.479	117.250	806.6	1.213E-04	2.517E-08	2.713E-08	7.795	0.940	2.551E-08	1.000	2.551E-08
113.809	117.500	803.7	1.176E-04	2.454E-08	2.640E-08	7.710	0.940	2.483E-08	1.000	2.483E-08
114.140	117.750	800.8	1.137E-04	2.390E-08	2.564E-08	7.624	0.940	2.411E-08	1.000	2.411E-08
114.473	118.000	797.8	1.103E-04	2.330E-08	2.496E-08	7.537	0.941	2.347E-08	1.000	2.347E-08
114.808	118.250	794.9	1.071E-04	2.277E-08	2.431E-08	7.450	0.941	2.287E-08	1.000	2.287E-08
115.142	118.500	791.9	1.040E-04	2.225E-08	2.370E-08	7.376	0.941	2.229E-08	1.000	2.229E-08
115.480	118.750	788.9	1.010E-04	2.176E-08	2.310E-08	7.320	0.941	2.173E-08	1.000	2.173E-08
115.819	119.000	785.9	9.817E-05	2.128E-08	2.255E-08	7.264	0.941	2.121E-08	1.000	2.121E-08
116.157	119.250	782.9	9.538E-05	2.083E-08	2.199E-08	7.207	0.941	2.069E-08	1.000	2.069E-08
116.500	119.500	779.9	9.292E-05	2.041E-08	2.151E-08	7.150	0.941	2.024E-08	1.000	2.024E-08
116.842	119.750	776.8	9.049E-05	2.002E-08	2.103E-08	7.093	0.941	1.979E-08	1.000	1.979E-08
117.185	120.000	773.8	8.813E-05	1.962E-08	2.056E-08	7.036	0.941	1.935E-08	1.000	1.935E-08
117.532	120.250	770.7	8.559E-05	1.919E-08	2.005E-08	6.978	0.941	1.887E-08	1.000	1.887E-08
117.880	120.500	767.7	8.340E-05	1.881E-08	1.961E-08	6.920	0.942	1.846E-08	1.000	1.846E-08
118.228	120.750	764.6	8.120E-05	1.845E-08	1.917E-08	6.911	0.942	1.805E-08	1.000	1.805E-08
118.579	121.000	761.5	7.915E-05	1.808E-08	1.876E-08	6.929	0.942	1.768E-08	1.000	1.768E-08
118.931	121.250	758.3	7.707E-05	1.774E-08	1.835E-08	6.947	0.942	1.729E-08	1.000	1.729E-08
119.284	121.500	755.2	7.497E-05	1.734E-08	1.792E-08	6.964	0.943	1.690E-08	1.000	1.690E-08
119.641	121.750	752.1	7.335E-05	1.709E-08	1.761E-08	6.982	0.943	1.661E-08	1.000	1.661E-08
119.997	122.000	748.9	7.129E-05	1.670E-08	1.718E-08	7.000	0.944	1.622E-08	1.000	1.622E-08
120.356	122.250	745.8	6.954E-05	1.641E-08	1.683E-08	7.085	0.944	1.589E-08	1.000	1.589E-08
120.717	122.500	742.6	6.777E-05	1.607E-08	1.647E-08	7.172	0.945	1.556E-08	1.000	1.556E-08
121.079	122.750	739.5	6.622E-05	1.583E-08	1.616E-08	7.259	0.945	1.528E-08	1.000	1.528E-08
121.444	123.000	736.3	6.454E-05	1.551E-08	1.582E-08	7.346	0.946	1.496E-08	1.000	1.496E-08
121.810	123.250	733.1	6.299E-05	1.525E-08	1.551E-08	7.434	0.946	1.467E-08	1.000	1.467E-08
122.177	123.500	729.8	6.141E-05	1.495E-08	1.519E-08	7.522	0.947	1.438E-08	1.000	1.438E-08
122.548	123.750	726.6	5.995E-05	1.470E-08	1.489E-08	7.611	0.947	1.411E-08	1.000	1.411E-08
122.919	124.000	723.4	5.849E-05	1.442E-08	1.459E-08	7.701	0.948	1.383E-08	1.000	1.383E-08
123.292	124.250	720.2	5.710E-05	1.419E-08	1.431E-08	7.790	0.948	1.357E-08	1.000	1.357E-08
123.668	124.500	717.0	5.575E-05	1.393E-08	1.404E-08	7.880	0.949	1.332E-08	1.000	1.332E-08
124.045	124.750	713.7	5.430E-05	1.367E-08	1.373E-08	7.971	0.949	1.304E-08	1.000	1.304E-08
124.425	125.000	710.4	5.317E-05	1.346E-08	1.351E-08	8.062	0.950	1.284E-08	1.000	1.284E-08

Figure 19. (Continued)

COMMUTATOR VALUES

TIME	CHL 1	CHL 4	CHL 5
48.786	3.522	2.503	3.402
68.147	3.459	2.503	3.346
78.777	3.462	2.503	2.947
87.458	3.459	2.503	2.412
96.318	3.454	2.503	1.993
103.349	3.455	2.503	1.458
113.020	3.456	2.503	1.063

ERROR RETURN

Figure 19. (Continued)

SPACE PHYSICS RESEARCH LABORATORY
THE UNIVERSITY OF MICHIGAN
ANN ARBOR, MICHIGAN
17:47.15 DECEMBER 18,1969

14.386 HOUSEKEEPING
LAUNCH TIME: 20: 4:59.815 Z

INPUT FILE 1 CHANNEL INDEX 3
TAPE ID: SPRL NASA 14.386 12/12/69 8020 FI OB Q

CALIBRATE LEVELS: 5.003 0.004

NO TEMPERATURE CORRECTION WILL BE MADE

COMMUTATOR VALUES

TIME	CHL 1	CHL 4	CHL 5
47.355	0.005	4.974	4.505
61.136	0.007	4.969	3.845
74.957	0.008	4.973	3.224
88.778	0.027	4.976	2.873
102.609	0.006	4.970	2.753
116.460	0.001	4.968	2.726
130.341	0.007	4.972	2.779
144.242	0.005	4.967	2.863
158.152	0.005	4.968	2.972
172.113	0.010	4.967	3.068
186.104	-0.002	4.975	3.180
200.115	-0.002	4.964	3.272
214.166	0.010	4.970	3.379
228.246	0.013	4.966	3.467
242.357	-0.005	4.970	3.552
256.498	0.004	4.978	3.646
270.649	0.009	4.974	3.715
284.839	0.018	4.975	3.784
299.050	0.010	4.967	3.832
313.291	0.008	4.970	3.908
327.592	0.009	4.972	3.963
341.932	-0.001	4.971	3.994

ERROR RETURN

Figure 19. (Concluded)

5.5. OBTAINING FINAL DATA

An atmospheric density profile for the whole flight can be obtained from the density data given by the PITOT program. At high altitudes the profile consists of atmospheric density calculated by using free molecular flow theory. As we trace down the altitude profile, we enter the transition region, and we use the corresponding values of atmospheric density. At the end of the transition region and down to the bottom of the density profile, the value of atmospheric density used is that calculated from continuum flow theory. From the resulting atmospheric density profile, values of density and altitude are recorded at 0.5 km intervals.

A value for atmospheric temperature at the highest altitude is estimated with the aid of an atmospheric model or the U. S. Standard Atmosphere, 1962. The estimated temperature is used as the starting temperature for the density integration. Atmospheric temperature and pressure profiles are calculated by means of a computer program written for the IBM 360/67 of the MTS, called FLOP. Inputs to FLOP (Final Listed Output and Plot) are

(1) altitude and density in km and kg/m^3, respectively, and from high to low altitudes, and

(2) starting temperature or reference temperature in °K.

After integrating the atmospheric density profile (Equation (28)), atmospheric temperature and pressure are calculated by means of Equations (30) and (31), respectively.

Finally, the ratios of atmospheric density and pressure to the corresponding values given by the U. S. Standard Atmosphere, 1962 are calculated, and the difference between the calculated atmospheric temperature and the temperature given by the U. S. Standard Atmosphere, 1962 is determined.

An abbreviated flow chart of the program is given in Figure 20. The output from the program is shown in Figure 21.

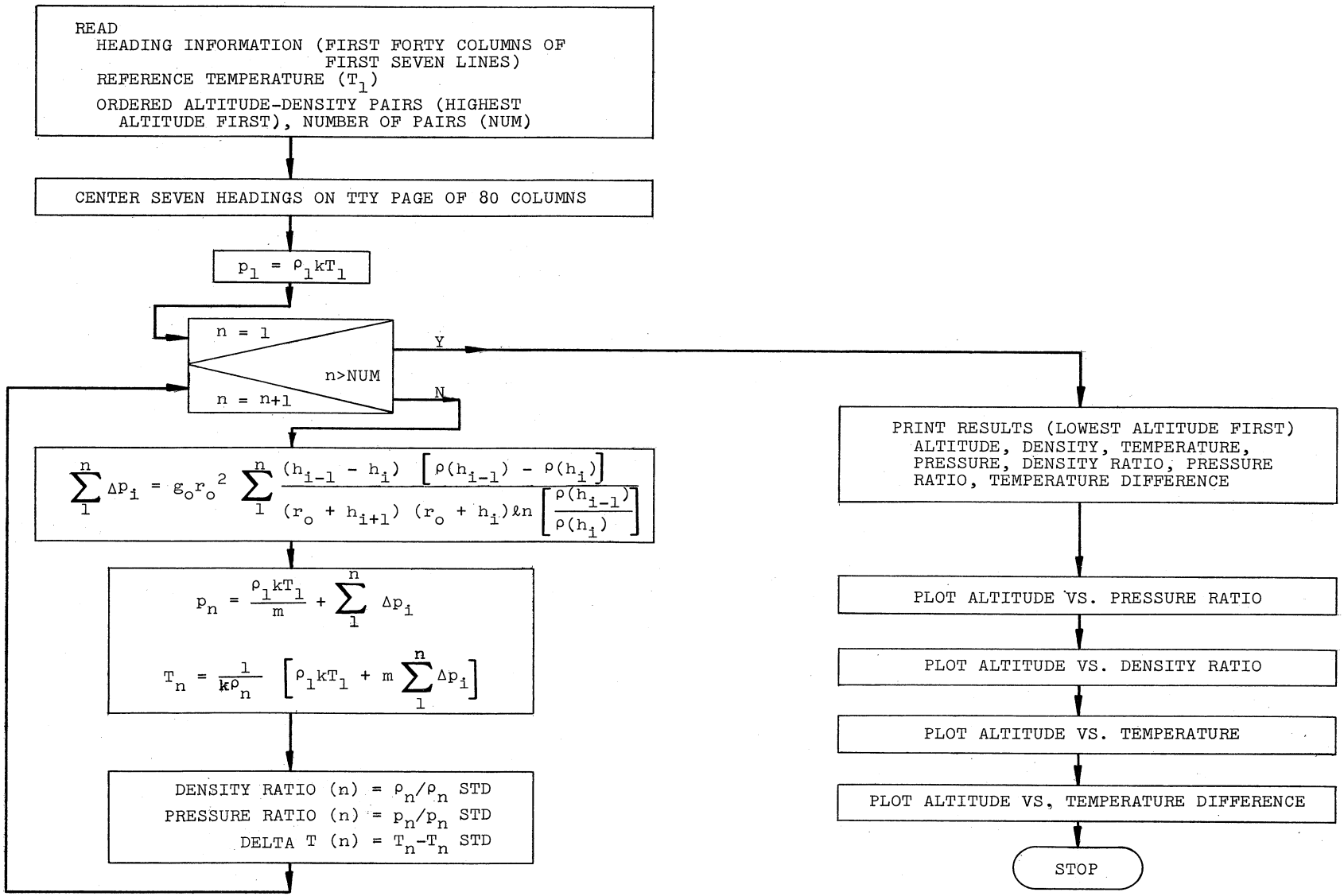

Figure 20. FLOP abbreviated flow chart.

SPACE PHYSICS RESEARCH LABORATORY
THE UNIVERSITY OF MICHIGAN
ANN ARBOR, MICHIGAN
12:00.55 DECEMBER 17,1969

NASA 14.386
19 NOVEMBER 1968
15:04:59.815 EST
20:04:59.815 GMT
WALLOPS ISLAND, VIRGINIA
LAT. 37 DEG 50 MIN N
LONG. 75 DEG 29 MIN W

PRESSURE RATIO = P/P STD.
DENSITY RATIO = RHO/RHO STD.
DELTA T = T-T STD.

ALTITUDE KM	DENSITY KG/CU-M	TEMP. K	PRESSURE TORR	DENSITY RATIO	PRESSURE RATIO	DELTA T
30.0	1.76E-02	222.1	8.42E 00	0.96	0.94	-4.4
30.5	1.62E-02	223.6	7.80E 00	0.95	0.94	-3.4
31.0	1.49E-02	225.5	7.24E 00	0.94	0.94	-2.0
31.5	1.38E-02	225.9	6.72E 00	0.95	0.94	-2.1
32.0	1.26E-02	229.7	6.23E 00	0.93	0.93	1.2
32.5	1.16E-02	231.9	5.79E 00	0.93	0.94	2.3
33.0	1.10E-02	227.2	5.38E 00	0.95	0.93	-3.8
33.5	1.00E-02	232.2	5.00E 00	0.93	0.93	-0.1
34.0	9.20E-03	234.8	4.65E 00	0.93	0.93	1.1
34.5	8.47E-03	237.4	4.33E 00	0.93	0.94	2.3
35.0	7.95E-03	235.5	4.03E 00	0.94	0.94	-1.0
35.5	7.48E-03	232.9	3.75E 00	0.95	0.94	-5.0
36.0	6.96E-03	232.8	3.49E 00	0.96	0.93	-6.5
36.5	6.45E-03	233.6	3.25E 00	0.96	0.93	-7.0
37.0	5.90E-03	237.8	3.02E 00	0.95	0.93	-4.2
37.5	5.50E-03	237.6	2.81E 00	0.95	0.93	-5.9
38.0	5.12E-03	237.7	2.62E 00	0.95	0.93	-7.1
38.5	4.72E-03	240.3	2.44E 00	0.95	0.93	-5.9
39.0	4.35E-03	243.1	2.28E 00	0.94	0.92	-4.5
39.5	4.01E-03	246.2	2.13E 00	0.93	0.92	-2.8
40.0	3.73E-03	247.2	1.99E 00	0.93	0.92	-3.2
40.5	3.46E-03	248.9	1.86E 00	0.93	0.92	-2.8
41.0	3.19E-03	252.4	1.73E 00	0.92	0.92	-0.7
41.5	2.93E-03	257.3	1.62E 00	0.91	0.92	2.8
42.0	2.74E-03	257.7	1.52E 00	0.92	0.92	1.8
42.5	2.54E-03	260.4	1.42E 00	0.91	0.93	3.2
43.0	2.37E-03	261.7	1.34E 00	0.91	0.92	3.1
43.5	2.21E-03	263.2	1.25E 00	0.91	0.92	3.2
44.0	2.10E-03	259.7	1.17E 00	0.93	0.92	-1.7
44.5	1.97E-03	259.4	1.10E 00	0.94	0.93	-3.4
45.0	1.86E-03	257.4	1.03E 00	0.94	0.92	-6.8
45.5	1.75E-03	256.3	9.66E-01	0.95	0.92	-9.3
46.0	1.63E-03	257.7	9.05E-01	0.95	0.92	-9.2

Figure 21. FLOP output format.

ALTITUDE KM	DENSITY KG/CU-M	TEMP. K	PRESSURE TORR	DENSITY RATIO	PRESSURE RATIO	DELTA T
46.5	1.53E-03	257.2	8.48E-01	0.96	0.92	-11.1
47.0	1.44E-03	255.9	7.94E-01	0.96	0.91	-13.8
47.5	1.35E-03	255.6	7.43E-01	0.96	0.91	-15.0
48.0	1.26E-03	256.4	6.96E-01	0.95	0.91	-14.2
48.5	1.17E-03	258.7	6.52E-01	0.94	0.90	-11.9
49.0	1.09E-03	260.2	6.11E-01	0.94	0.90	-10.4
49.5	1.01E-03	263.4	5.73E-01	0.93	0.90	-7.2
50.0	9.51E-04	262.4	5.37E-01	0.92	0.90	-8.2
50.5	9.03E-04	259.1	5.04E-01	0.94	0.90	-11.5
51.0	8.51E-04	257.6	4.72E-01	0.94	0.89	-13.0
51.5	8.00E-04	256.7	4.42E-01	0.94	0.89	-13.9
52.0	7.52E-04	255.7	4.14E-01	0.94	0.89	-14.9
52.5	7.10E-04	253.6	3.88E-01	0.94	0.88	-17.0
53.0	6.64E-04	253.8	3.63E-01	0.94	0.88	-15.7
53.5	6.15E-04	256.6	3.40E-01	0.92	0.88	-11.9
54.0	5.76E-04	256.6	3.18E-01	0.91	0.87	-11.0
54.5	5.44E-04	254.4	2.98E-01	0.91	0.87	-12.2
55.0	5.09E-04	254.5	2.79E-01	0.91	0.87	-11.1
55.5	4.73E-04	256.5	2.61E-01	0.90	0.87	-8.1
56.0	4.43E-04	256.5	2.45E-01	0.89	0.87	-7.1
56.5	4.17E-04	255.2	2.29E-01	0.89	0.87	-7.4
57.0	3.90E-04	255.5	2.15E-01	0.88	0.86	-6.2
57.5	3.68E-04	253.5	2.01E-01	0.89	0.86	-7.2
58.0	3.45E-04	253.1	1.88E-01	0.88	0.86	-6.6
58.5	3.25E-04	251.4	1.76E-01	0.88	0.86	-7.3
59.0	3.04E-04	251.4	1.65E-01	0.88	0.86	-6.3
59.5	2.87E-04	249.1	1.54E-01	0.88	0.86	-7.7
60.0	2.70E-04	247.5	1.44E-01	0.88	0.86	-8.3
60.5	2.53E-04	246.8	1.35E-01	0.88	0.85	-8.0
61.0	2.40E-04	243.0	1.26E-01	0.89	0.85	-10.8
61.5	2.27E-04	239.7	1.17E-01	0.89	0.85	-13.1
62.0	2.13E-04	238.1	1.09E-01	0.89	0.85	-12.9
62.5	1.99E-04	237.6	1.02E-01	0.88	0.84	-11.5
63.0	1.86E-04	236.8	9.49E-02	0.87	0.84	-10.3
63.5	1.74E-04	235.9	8.84E-02	0.87	0.83	-9.3
64.0	1.63E-04	234.5	8.23E-02	0.87	0.83	-8.7
64.5	1.53E-04	232.5	7.66E-02	0.86	0.83	-8.7
65.0	1.43E-04	231.5	7.13E-02	0.86	0.83	-7.8
65.5	1.35E-04	228.0	6.63E-02	0.86	0.83	-9.3
66.0	1.27E-04	225.1	6.16E-02	0.86	0.83	-10.3
66.5	1.19E-04	222.9	5.71E-02	0.86	0.82	-10.5
67.0	1.11E-04	221.7	5.30E-02	0.85	0.82	-9.7
67.5	1.05E-04	217.2	4.91E-02	0.86	0.82	-12.3
68.0	9.70E-05	217.7	4.55E-02	0.85	0.82	-9.8
68.5	8.87E-05	220.5	4.21E-02	0.83	0.81	-5.1
69.0	8.23E-05	220.3	3.91E-02	0.82	0.81	-3.3
69.5	7.70E-05	218.2	3.62E-02	0.82	0.81	-3.5
70.0	7.24E-05	214.9	3.35E-02	0.83	0.81	-4.8
70.5	6.74E-05	213.5	3.10E-02	0.82	0.81	-4.2
71.0	6.32E-05	210.4	2.86E-02	0.83	0.81	-5.4
71.5	5.92E-05	207.4	2.64E-02	0.83	0.80	-6.4

Figure 21. (Continued)

ALTITUDE KM	DENSITY KG/CU-M	TEMP. K	PRESSURE TORR	DENSITY RATIO	PRESSURE RATIO	DELTA T
72.0	5.54E-05	204.4	2.44E-02	0.83	0.80	-7.5
72.5	5.20E-05	200.5	2.25E-02	0.84	0.80	-9.4
73.0	4.87E-05	196.8	2.06E-02	0.84	0.80	-11.2
73.5	4.56E-05	192.9	1.90E-02	0.85	0.79	-13.1
74.0	4.20E-05	192.1	1.74E-02	0.84	0.79	-12.0
74.5	3.73E-05	198.6	1.60E-02	0.80	0.79	-3.5
75.0	3.30E-05	206.7	1.47E-02	0.76	0.79	6.5
75.5	2.92E-05	215.9	1.36E-02	0.72	0.79	17.7
76.0	2.69E-05	217.0	1.26E-02	0.72	0.80	20.8
76.5	2.45E-05	220.7	1.16E-02	0.71	0.80	26.4
77.0	2.25E-05	222.9	1.08E-02	0.70	0.81	30.6
77.5	2.10E-05	221.6	1.00E-02	0.71	0.82	31.2
78.0	1.94E-05	222.5	9.30E-03	0.71	0.83	34.1
78.5	1.78E-05	225.2	8.63E-03	0.70	0.85	38.7
79.0	1.67E-05	222.8	8.01E-03	0.71	0.86	38.3
79.5	1.57E-05	219.8	7.43E-03	0.72	0.87	37.2
80.0	1.47E-05	217.5	6.89E-03	0.74	0.89	36.9
80.5	1.37E-05	216.1	6.38E-03	0.75	0.90	35.5
81.0	1.28E-05	214.1	5.90E-03	0.77	0.91	33.5
81.5	1.19E-05	213.0	5.46E-03	0.79	0.93	32.4
82.0	1.09E-05	215.2	5.05E-03	0.79	0.94	34.6
82.5	1.01E-05	214.9	4.68E-03	0.80	0.95	34.3
83.0	9.44E-06	212.8	4.33E-03	0.82	0.97	32.2
83.5	8.85E-06	209.8	4.00E-03	0.84	0.98	29.2
84.0	8.40E-06	203.9	3.69E-03	0.88	0.99	23.3
84.5	7.90E-06	199.7	3.40E-03	0.91	1.00	19.1
85.0	7.20E-06	201.7	3.13E-03	0.90	1.01	21.1
85.5	6.42E-06	208.5	2.88E-03	0.88	1.02	27.9
86.0	5.64E-06	219.6	2.67E-03	0.85	1.04	39.0
86.5	5.21E-06	220.5	2.47E-03	0.86	1.05	39.9
87.0	4.83E-06	220.5	2.29E-03	0.88	1.07	39.9
87.5	4.52E-06	218.5	2.13E-03	0.90	1.09	37.9
88.0	4.18E-06	219.0	1.97E-03	0.91	1.11	38.4
88.5	3.91E-06	216.9	1.83E-03	0.94	1.13	36.3
89.0	3.67E-06	214.0	1.69E-03	0.96	1.14	33.4
89.5	3.43E-06	211.7	1.56E-03	0.99	1.16	31.1
90.0	3.18E-06	211.1	1.45E-03	1.00	1.18	30.5
90.5	2.97E-06	208.9	1.34E-03	1.03	1.19	26.8
91.0	2.77E-06	206.8	1.23E-03	1.07	1.21	23.2
91.5	2.57E-06	205.6	1.14E-03	1.09	1.22	20.5
92.0	2.36E-06	206.6	1.05E-03	1.10	1.22	20.0
92.5	2.19E-06	205.4	9.69E-04	1.13	1.23	17.3
93.0	2.07E-06	200.3	8.93E-04	1.18	1.24	10.7
93.5	1.93E-06	197.6	8.22E-04	1.21	1.24	6.5
94.0	1.77E-06	198.2	7.56E-04	1.21	1.25	5.6
94.5	1.59E-06	203.1	6.96E-04	1.20	1.25	9.1
95.0	1.46E-06	203.9	6.41E-04	1.21	1.26	8.4
95.5	1.34E-06	204.8	5.91E-04	1.22	1.26	7.8
96.0	1.24E-06	204.1	5.45E-04	1.23	1.26	5.7
96.5	1.15E-06	202.9	5.03E-04	1.25	1.27	3.0
97.0	1.08E-06	198.9	4.63E-04	1.28	1.27	-2.5

Figure 21. (Continued)

ALTITUDE KM	DENSITY KG/CU-M	TEMP. K	PRESSURE TORR	DENSITY RATIO	PRESSURE RATIO	DELTA T
97.5	1.01E-06	195.6	4.25E-04	1.31	1.26	-7.2
98.0	9.40E-07	193.0	3.91E-04	1.34	1.26	-11.3
98.5	8.78E-07	189.5	3.58E-04	1.36	1.25	-16.2
99.0	8.20E-07	185.7	3.28E-04	1.39	1.24	-21.5
99.5	7.68E-07	181.2	3.00E-04	1.42	1.23	-27.4
100.0	7.15E-07	177.5	2.73E-04	1.44	1.21	-32.5
100.5	6.67E-07	173.1	2.49E-04	1.46	1.19	-39.3
101.0	6.15E-07	170.5	2.26E-04	1.48	1.17	-44.4
101.5	5.60E-07	169.9	2.05E-04	1.47	1.14	-47.3
102.0	5.00E-07	172.8	1.86E-04	1.43	1.12	-46.8
102.5	4.40E-07	178.7	1.69E-04	1.37	1.10	-43.3
103.0	3.84E-07	187.0	1.55E-04	1.31	1.08	-37.4
103.5	3.31E-07	199.2	1.42E-04	1.22	1.07	-27.6
104.0	2.86E-07	212.7	1.31E-04	1.15	1.07	-16.5
104.5	2.52E-07	223.8	1.21E-04	1.10	1.06	-7.7
105.0	2.31E-07	226.9	1.13E-04	1.09	1.05	-7.0
105.5	2.13E-07	228.8	1.05E-04	1.09	1.05	-7.4
106.0	1.99E-07	227.8	9.77E-05	1.11	1.04	-10.8
106.5	1.87E-07	225.4	9.08E-05	1.12	1.04	-15.5
107.0	1.75E-07	223.8	8.44E-05	1.14	1.03	-19.4
107.5	1.65E-07	220.3	7.83E-05	1.15	1.02	-25.2
108.0	1.54E-07	219.0	7.26E-05	1.17	1.02	-28.8
108.5	1.44E-07	217.1	6.73E-05	1.17	1.01	-33.0
109.0	1.34E-07	216.2	6.24E-05	1.18	1.00	-36.2
109.5	1.25E-07	214.7	5.78E-05	1.18	0.98	-40.0
110.0	1.17E-07	212.3	5.35E-05	1.19	0.97	-44.7
110.5	1.08E-07	212.8	4.95E-05	1.19	0.95	-48.9
111.0	9.74E-08	218.6	4.59E-05	1.17	0.94	-47.8
111.5	8.52E-08	232.2	4.26E-05	1.10	0.93	-38.9
112.0	7.30E-08	253.2	3.98E-05	1.02	0.92	-22.6
112.5	6.25E-08	277.9	3.74E-05	0.94	0.92	-2.6
113.0	5.40E-08	303.9	3.53E-05	0.88	0.92	18.7
113.5	4.71E-08	330.7	3.36E-05	0.82	0.92	40.9
114.0	4.19E-08	354.3	3.20E-05	0.79	0.93	59.8
114.5	3.73E-08	380.5	3.06E-05	0.75	0.94	81.3
115.0	3.42E-08	397.8	2.93E-05	0.74	0.95	94.0
115.5	3.17E-08	412.1	2.81E-05	0.73	0.96	103.7
116.0	2.94E-08	427.2	2.71E-05	0.73	0.97	114.2
116.5	2.78E-08	434.9	2.60E-05	0.73	0.98	117.3
117.0	2.61E-08	446.2	2.51E-05	0.74	1.00	124.0
117.5	2.47E-08	454.5	2.42E-05	0.74	1.01	127.7
118.0	2.33E-08	464.9	2.33E-05	0.75	1.02	133.6
118.5	2.22E-08	471.1	2.25E-05	0.76	1.03	135.3
119.0	2.11E-08	478.8	2.18E-05	0.77	1.05	138.4
119.5	2.01E-08	485.7	2.10E-05	0.77	1.06	140.7
120.0	1.93E-08	489.1	2.03E-05	0.79	1.08	139.6
120.5	1.85E-08	493.4	1.97E-05	0.81	1.09	134.6
121.0	1.76E-08	501.8	1.90E-05	0.83	1.10	133.6
121.5	1.70E-08	502.8	1.84E-05	0.86	1.11	125.3
122.0	1.62E-08	510.7	1.78E-05	0.88	1.12	123.9
122.5	1.56E-08	513.6	1.73E-05	0.90	1.13	117.5
123.0	1.50E-08	517.4	1.67E-05	0.93	1.14	112.0
123.5	1.45E-08	518.5	1.62E-05	0.95	1.14	103.9
124.0	1.39E-08	524.2	1.57E-05	0.97	1.15	100.3
124.5	1.33E-08	531.0	1.52E-05	0.98	1.16	97.8
125.0	1.28E-08	535.0	1.47E-05	1.00	1.17	92.6

Figure 21. (Continued)

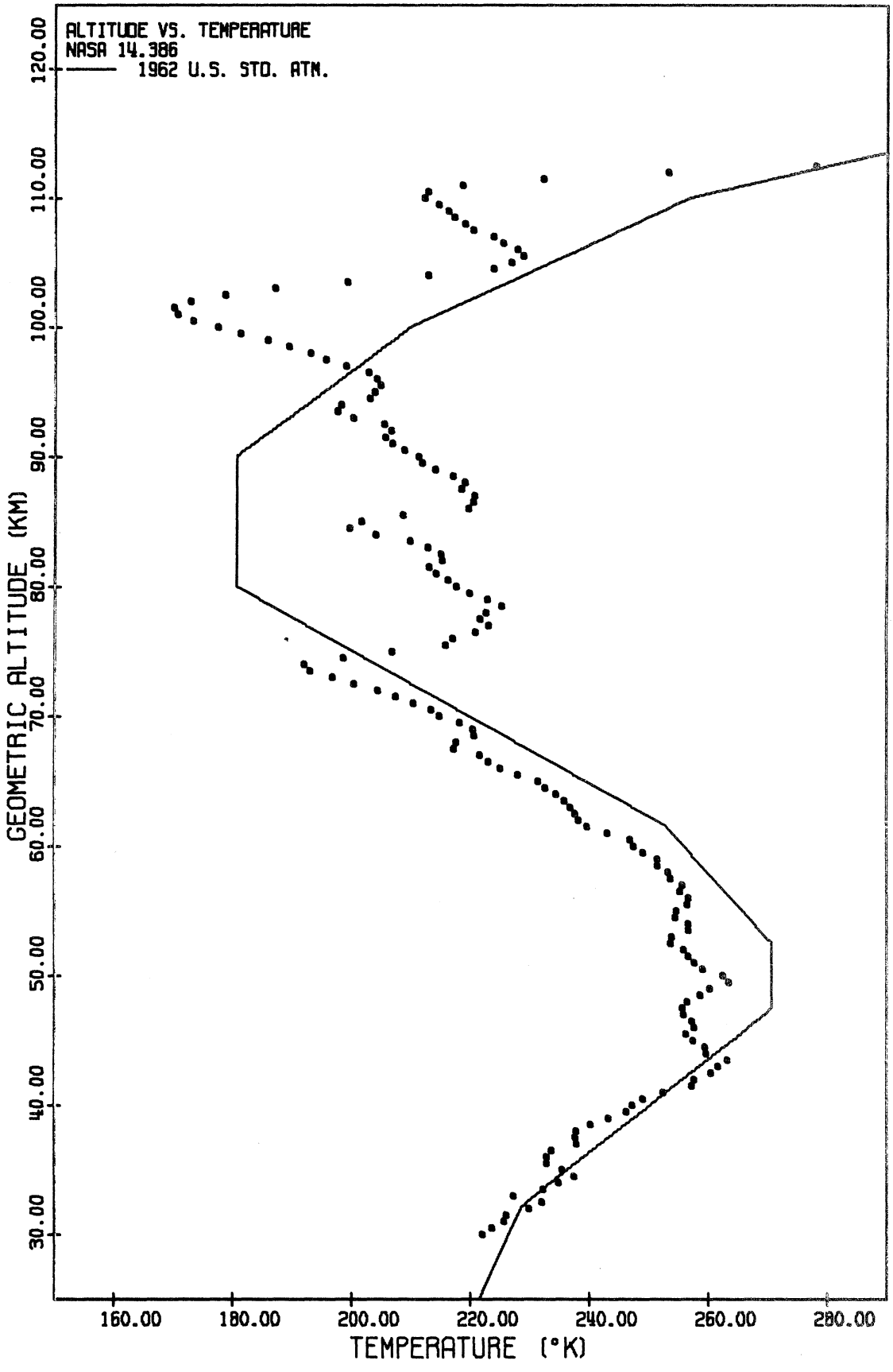

Figure 21. (Continued)

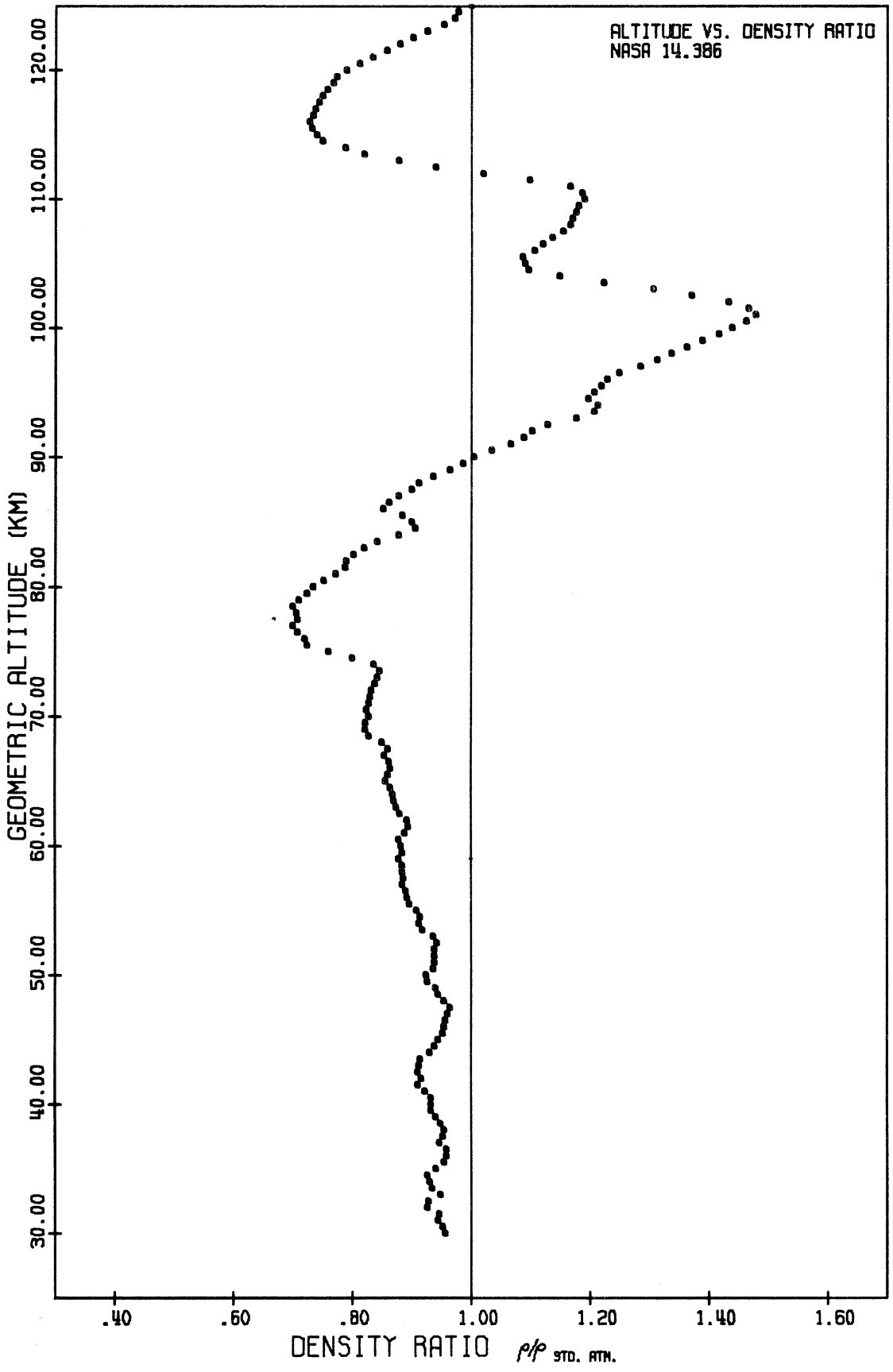

Figure 21. (Continued)

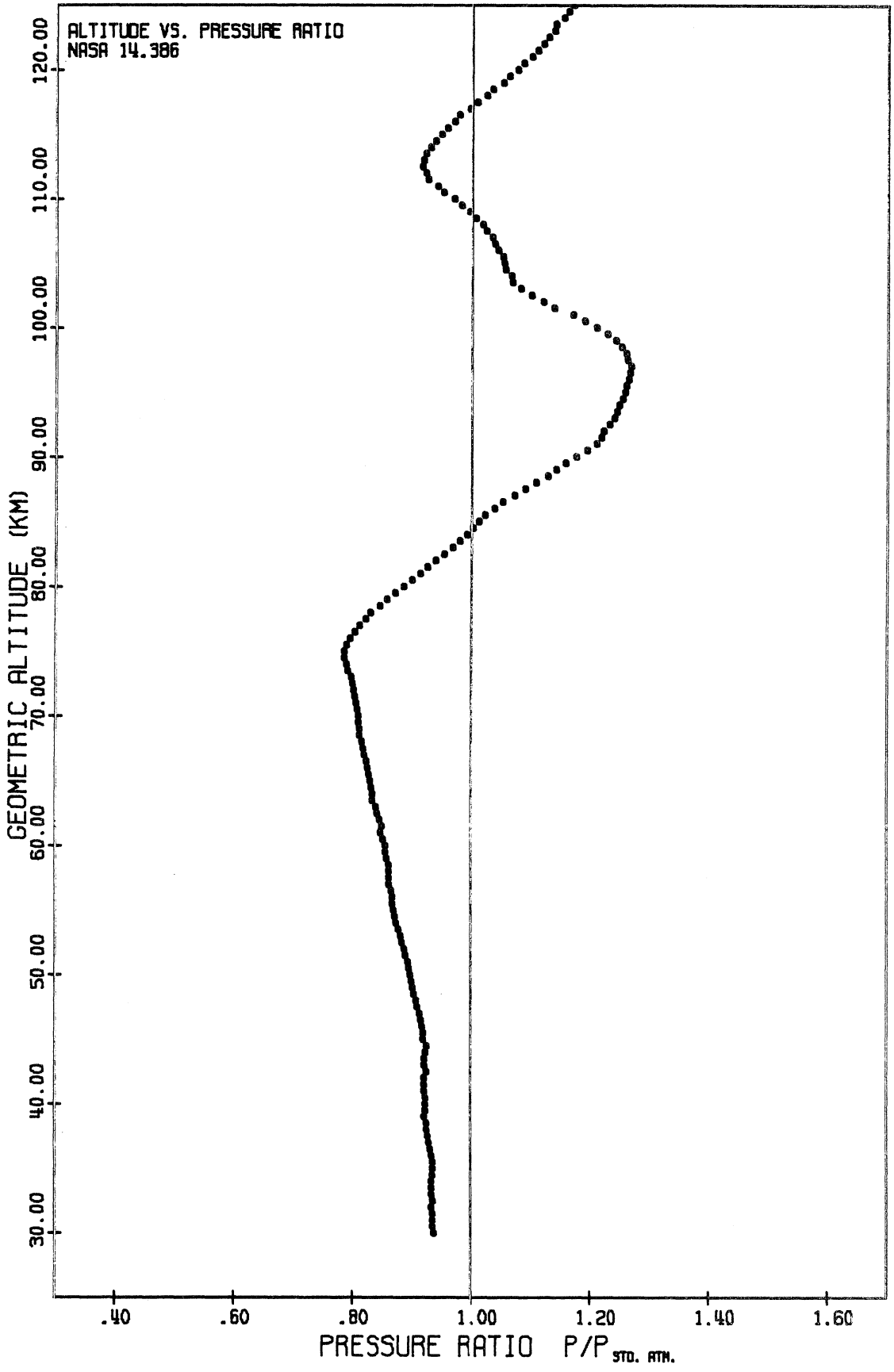

Figure 21. (Continued)

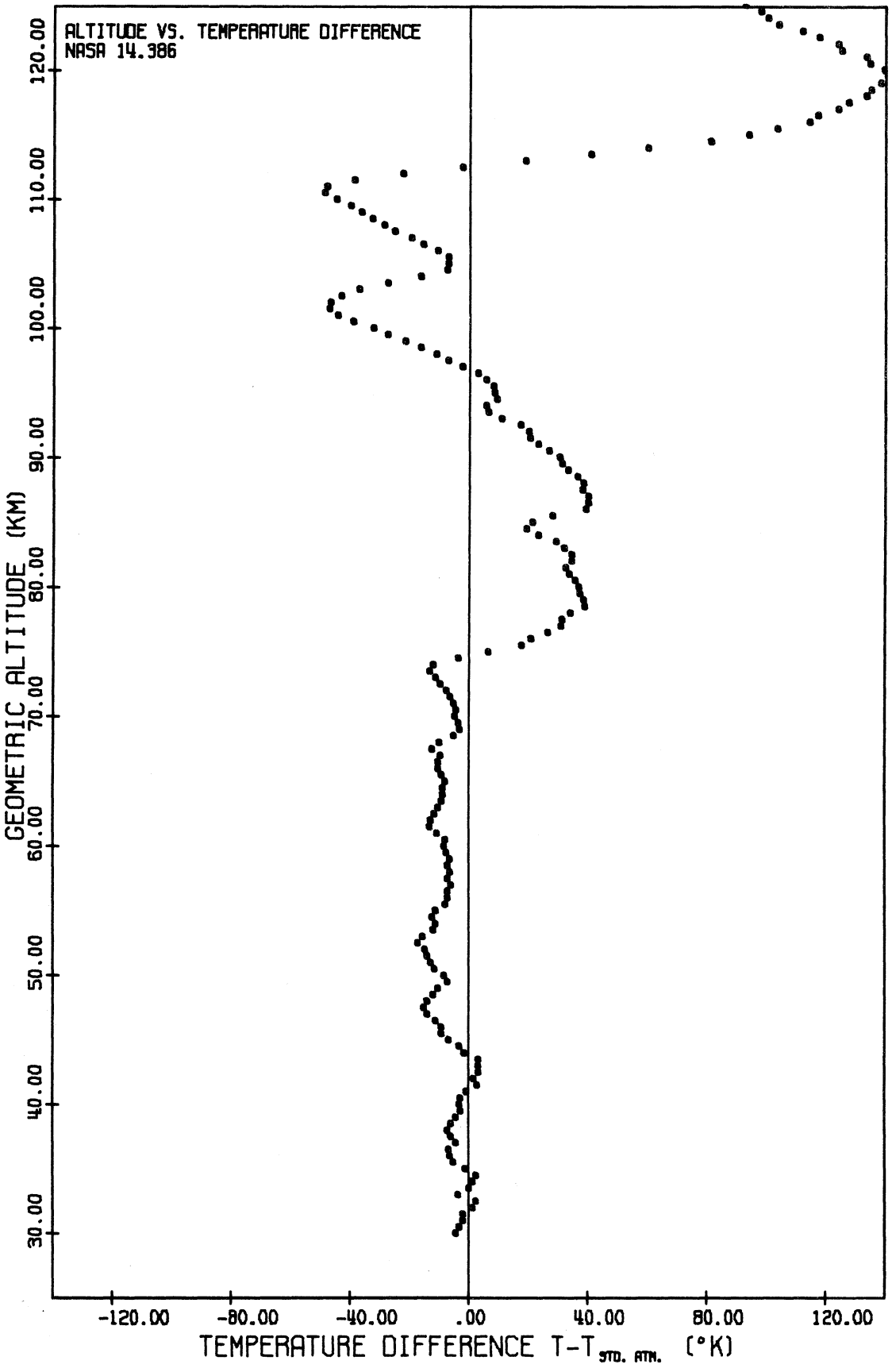

Figure 21. (Concluded)

6. REFERENCES

Ainsworth, J. E., D. F. Fox, and H. E. LaGow, "Upper Atmosphere Structure Measurement Made with the Pitot-Static Tube," Journal of Geophysical Research, 66, No. 10, pp. 3191-3212, 1961.

Breckenridge, Sally, "Evaluation of the Main Geomagnetic Field by Means of Spherical Harmonic Analysis," University of Michigan Internal Note and Program, October 28, 1965.

Cain, Joseph C., W. E. Daniels, Shirley J. Hendricks, and Duane C. Jensen, "An Evaluation of the Main Geomagnetic Field, 1940-1962," Journal of Geophysical Research, 70, No. 15, pp. 3647-3674, August 1, 1965.

Caldwell, Jack, The Space Physics Research Laboratory Data Conditioning System, University of Michigan Engineering Report No. 1, 05776-1-E, January 1966.

Handy, P. O., Design of a Radioactive Ionization Gauge for Upper Atmosphere Measurements, University of Michigan Instrumentation Report 05776-1-I, February 1970.

Horvath, J. J., R. W. Simmons, and L. H. Brace, Theory and Implementation of the Pitot-Static Technique for Upper Atmospheric Measurements, University of Michigan Scientific Report NS-1, 03554, 04673-1-S, March 1962.

Pearl, J. C. and U. Vogel, Application of the Green's Function to Analysis of Internal Flows of Rarefied Gases. University of Michigan Scientific Report, 02770, to be published in 1970.

Range Commanders Council, Telemetry Standards (Revised March 1966), White Sands Missile Range, New Mexico, Document 106-66 (AD 635857), April 1966.

Simmons, R. W., An Introduction to the Theory and Data Reduction Method for the Pitot-Static Technique of Upper Atmosphere Measurement, University of Michigan Scientific Report No. RS-1, 05776-1-S, March 1964.

U. S. Standard Atmosphere, 1962, U. S. Government Printing Office, Washington, D. C., December 1962.

Wainwright, J. B. and K. W. Rogers, Impact Pressure Probe Response Characteristics in High Speed Flows, with Transition Knudsen Numbers, NASA Contractor Report CR-61119, NASA-George C. Marshall Space Flight Center, Huntsville, Alabama, February 18, 1966.